METTL3 DEPENDENT M^6A REGULATES CHROMATIN MODIFIERS IN EPITHELIAL DEVELOPMENT

Alexandra Marie Maldonado López

A DISSERTATION

In

Cell and Molecular Biology

Presented to the Faculties of the University of Pennsylvania

in

Partial Fulfillment of the Requirements for the

Degree of Doctor of Philosophy

2023

Supervisor of Dissertation

Brian C. Capell, M.D., Ph.D.
Assistant Professor of Dermatology

Graduate Group Chairperson

Daniel S. Kessler, Ph.D.
Associate Professor of Cell and Developmental Biology

Dissertation Committee

Kathryn E. Hamilton, Ph.D., Assistant Professor of Pediatrics
Fange (Kathy) Liu, Ph.D., Assistant Professor of Biochemistry and Biophysics
Lan Lin, Ph.D., Assistant Professor of Pathology and Laboratory Medicine
John T. Seykora, M.D., Ph.D., Professor of Dermatology

To my parents.

"Porque soy de papi y mami."

ACKNOWLEDGMENTS

I am grateful for this space to say thank you to all the people who have been an integral part of my Ph.D. journey. Firstly, I want to express my gratitude to my thesis mentor, Dr. Brian Capell, whom I met during my interviews and who welcomed me into his lab since my first rotation. Thank you for giving me the opportunity to pioneer research that had not been done in the lab before, which helped me develop into a full-fledged scientist, brimming with confidence. In the lab, I made great friends who provided me with the opportunity to express my frustrations and share the great moments I encountered over the years. Special thanks to lab members Eun Kyung, Carina, Nina, and Gina for always making me laugh and for helping me with experiments when I needed it the most.

I would also like to acknowledge my best friends from high school who I love, the Mag5. They have been with me in every step of my life and career for the last 10 years, teaching me key traits. Valeria taught me how to be vocal, Evangimel taught me to be reasonable, Edig taught me about perseverance, and Ramiro taught me what it's like to be bold. They all taught me with patience, laughter, and love the true meaning of friendship. We have been through great times and some hard ones too, but we have always stood together no matter what. They are the siblings I never had by blood, but they are the most special people to me.

During this journey, I met the best thing that this Ph.D. has given me – my boyfriend and best friend, Raúl. He has been my rock in these last few years and has helped me flesh out my scientific ideas, as well as understand mathematical and scRNA-seq analysis concepts. Apart from

the academic and scientific standpoint, thank you for teaching me how to be more confident in myself and for loving me and respecting me for who I am. He has shown me to live life to the fullest, embracing silliness, and experiencing pure happiness without a care in the world. He just makes me happy and the love that I hold for him is out of this world. I do not know what the future holds, but I do know that I want it to be by Raúl's side.

Last but not least, I want to thank the people to whom this dissertation is dedicated – my parents, Julio and Marisol. They have loved me so much and have had my back in every single decision I have made, to the extent that they even get worried when I am worried, and I know they won't stop doing it. They have raised this little girl to be a wonderful human being, full of all their great qualities. With maturity, I have come to fully appreciate every sacrifice they made and understand the profound impact of their teachings. They are not just my parents; they are my best friends who have been there for me literally from day one. I do not even have the words to describe how grateful I am for them; I just love them so much that every single thing I do is for them.

ABSTRACT

METTL3 DEPENDENT M^{6}A REGULATES CHROMATIN MODIFIERS IN EPITHELIAL DEVELOPMENT

Alexandra Marie Maldonado López

Brian C. Capell

N6-methyladenosine (m^{6}A) is the most abundant modification on mammalian messenger RNAs (mRNAs). It is catalyzed co-transcriptionally by methyltransferase-like protein 3 (METTL3), which is part of the METTL3-METTL14 writer complex. To understand the role of m^{6}A in a self-renewing epithelial tissue, we deleted *Mettl3* in epidermal progenitors *in vivo* (*Mettl3*-eKO). *Mettl3*-eKO mice present dysfunctional development and self-renewal of the epidermis and non-lingual epithelium, which includes loss of hair follicle morphogenesis and impaired cell adhesion and polarity associated with oral ulcerations. We show that METTL3 promotes the m^{6}A-mediated instability and degradation of mRNAs of critical histone modifying enzymes. Depletion of METTL3 results in the loss of m^{6}A on these chromatin modifying transcripts, thus increasing their mRNA abundance, protein expression and associated modifications. This upregulation in epigenetic writers results in widespread gene expression abnormalities that lead to the gross phenotypic abnormalities in the epidermis and tongue. Altogether, these results identified an additional layer of gene regulation within epithelial tissues, revealing an essential role for m^{6}A in the regulation of chromatin modifiers (a crosstalk between epitranscriptomics and epigenetics), and highlighting a critical role for METTL3-catalyzed m^{6}A

in proper epithelial development and self-renewal that lays the foundation for novel clinical approaches to maintain skin homeostasis and treat benign and malignant skin diseases.

TABLE OF CONTENTS

LIST OF TABLES

LIST OF FIGURES

CHAPTER 1: INTRODUCTION

This chapter includes work adapted from a previously published manuscript: Maldonado López, A., & Capell, B. C. (2021). The METTL3-m^{6}A Epitranscriptome: Dynamic Regulator of Epithelial Development, Differentiation, and Cancer. *Genes*, *12*(7), 1019. https://doi.org/10.3390/genes12071019.

1.1. Epitranscriptomics: A New Layer of Gene Regulation

"RNA epigenetics" or "epitranscriptomics" is the study of reversible RNA chemical modifications (*1-4*). The first RNA modifications were initially described in the 1950s, with the first one being pseudouridine (*5*). In the 1970s, the most abundant modification on messenger RNAs (mRNAs) called *N6*-methyladenosine (m^{6}A) was discovered in the 1970s (*1*). Subsequently over the years, approximately 150 RNA modifications have been described (Fig. 1), the majority found on noncoding ribosomal RNA (rRNA) and transfer RNA (tRNA). Readers are referred to the following recent excellent reviews for further information on other modifications (*3, 6-8*). More than 150 RNA post-transcriptional modifications have been identified to date, which are widely distributed on various types of RNA, including mRNA, tRNA, rRNA, small non-coding RNA (sncRNA), and lncRNA. The variety and breadth of these numerous modifications and numerous types of RNA underscores the vast potential they have for the regulation of biology and disease. Despite this, these RNA modifications were initially viewed as passive structural features since they were originally discovered since their underlying functional effects were unknown. But in 2011 that view was dramatically transformed by the discovery of protein, known as fat mass

and obesity-associated protein (FTO) was shown to demethylate m^6A (*9*). This discovery made it clear that these modifications might in fact be reversible and dynamic.

These reversible RNA chemical modifications now are thought to form an "epitranscriptomic code", that enable and/or enhance RNA-dependent reactions as well as change RNA structure-function relationships. Taking all this together, RNA epigenetics (or epitranscriptomics) offers a new layer of regulation to control gene expression in a spatiotemporal manner like DNA and histone epigenetics. Recently, epitranscriptomic modifications have now been shown to play important roles in numerous critical physiological aspects of tissue development and disease. Despite this, there are many unknowns in this relatively new field, and while the initial insights into the role of the epitranscriptome have been exciting, much remains to be discovered.

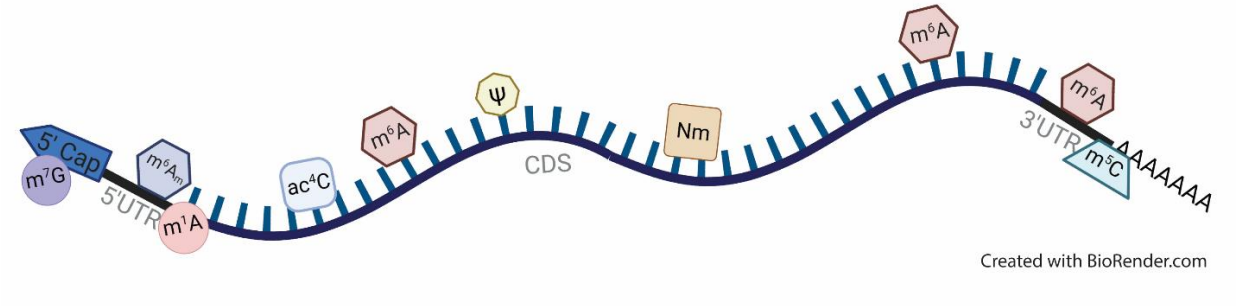

Figure 1. mRNA chemical modifications.

Distribution of chemical modifications on mRNA from 5'cap (left) to poly-A tail (right): 7-methylguanosine (m^7G), *N6*,2'-O-dimethyladenosine (m^6A_m), *N1*-methyladenosine (m^1A), *N4*-acetylcytidine (ac^4C), *N6*-methyladenosine (m^6A), pseudouridine (ψ), 2'-O-methylation (Nm), and

5-methylcytosine (m^5C). 5'UTR is 5' untranslated region, CDS stands for coding sequence, and 3'UTR means 3' untranslated region.

1.2. *N6*-methyladenosine (m^6A) in mRNA

Amongst RNA modifications, *N*6-methyladenosine (m^6A) is the most abundant chemical modification of messenger RNAs (mRNAs) and is enriched in long internal exons, in the 3' untranslated region (UTR) and near stop codons in human and mouse transcriptomes (*10*). m^6A is catalyzed co-transcriptionally on nascent pre-mRNA by an evolutionarily conserved, multicomponent writer complex with one known catalytic component, methyltransferase-like 3 (METTL3). METTL3-mediated m^6A has been shown to regulate various aspects of mRNA metabolism, including both its stability and degradation by phase separation (*11*), as well as its translation (*12-14*).

N-6-methyladenosine (m^6A) is an mRNA reversible chemical modification that is conserved across single-cell organisms such as archaea, bacteria, and yeast, as well as in multicellular eukaryotes including plants and vertebrates, and even among viral RNAs. In vertebrates, approximately 25% of mRNAs contain at least one m^6A modification (*11, 15, 16*). In mammals, m^6A is catalyzed in the nucleus typically at the consensus sequence motif DRACH (D = A/G/U, R = A/G, H = A/C/U), and is enriched transcriptome-wide near stop codons and the 3' untranslated region (UTR), as well as within internal exons (*1*). These internal exons are consistent of being co-transcriptionally written (*13, 17, 18*). Additionally, slower rates of transcription result in increased levels of m^6A, suggesting that m^6A deposition relies on the dynamics of the

transcribing RNA polymerase II (*13*). Collectively, these findings have shown that m^6A methylation occurs co-transcriptionally.

m^6A methylation has been shown to affect diverse aspects of mRNA. m^6A has been shown to either affect transcript turnover by either promoting mRNA degradation or translation by increasing its stability, depending upon the cellular context described more in section 1.2.3 (*1*). Furthermore, the amount of m^6A can also impact transcript turnover as highly m^6A modified transcripts display a slightly lower translational efficiency than unmodified transcripts (*13, 19*). In addition to affecting mRNA stability, m^6A may affect mRNA splicing, though evidence in mammalian systems is limited (*1, 20-22*). All these affected mRNA aspects are due to a set of enzymes that control m^6A. Just like epigenetics, epitranscriptomics has a series of "writers" which are the methyltransferases that deposit the methyl chemical modifications in the RNAs), "readers" which are the RNA binding proteins that decide the fate of the transcription turnover, and "erasers" which are the demethylases that take out the methyl mark from the RNA.

1.2.1. Writers of m^6A

m^6A in mRNA is deposited co-transcriptionally by a large multicomponent writer complex within the nucleus formed by Methyltransferase-like 3 (METTL3), Methyltransferase-like 14 (METTL14) and an adaptor. METTL3 and METTL14 form a heterodimeric complex (METTL3/14 heterodimer) that is responsible for the vast majority of m^6A modifications on mRNA (*1, 23*). Though, both METTL3 and METTL14 contain methyltransferase domains, several structural studies have demonstrated that only METTL3 contains a binding site for the methylation substrate S-adenosylmethionine (SAM) (*24-26*). By METTL3 being the only catalytically active

subunit, METTL14 serves as an allosteric adaptor of METTL3, essential for stabilizing the conformation and substrate RNA binding of METTL3 (*27*). Interestingly, METTL3 expression has been shown to correlate with global levels of m^6A across both human and mouse tissues, supporting its role as the major m^6A methyltransferase (*10*).

Beyond METTL3, m^6A methylation on other types of RNA are catalyzed by other **e**nzymes (*28*). METTL16 carries out m^6A on U6 small nuclear RNA (snRNA) as well as on methionine adenosyltransferase 2A (MAT2A) (*29*). An m^6A modification at the A1832 position of the 18S rRNA is written by METTL5 (*30*). Similarly, called ZCCHC4 methylates A4220 on 28S rRNA (*31*). The functional significance of these modifications is only beginning to be understood.

The METTL3/14 heterodimer binds to different adaptors that do not possess methyltransferase activity that facilitates the functions of the complex. For example, Wilms tumor-associated protein (WTAP) binds to the METTL3/14 heterodimer and is required for optimal localization by binding to chromatin and transcription factors at specific promoters (*32, 33*). Another adaptor protein, called VIRMA (Vir-like m^6A methyltransferase associated) or KIAA1429, is critical for the deposition of m^6A at 3' untranslated regions (UTRs) and near the stop codon (*34*). The ZC3H13 (zinc finger CCCH-type containing 13) adaptor plays a role in the nuclear localization of the writer complex by bridging with WTAP (*25, 35*), while RBM15/15B (RNA binding motif protein 15/15B) binds to U-rich regions and can promote the methylation of certain mRNAs (*36, 37*). Collectively, these diverse complex members endow the METTL3/14 writer complex with an expanded array of unique abilities to enhance its functions.

1.2.2. Erasers of m^6A

Even though the discovery of an eraser (FTO) in 2011 skyrocketed the epitranscriptomics field because the active demethylation of m^6A was thought to potentially be an essential part of m^6A function, more recent findings suggest that it may occur on a limited basis and in a limited number of tissues under physiological conditions. As mentioned, the first discovered m^6A eraser was a nuclear enzyme named FTO (fat mass and obesity-associated protein) (*9*), which reportedly removes the methyl group in m^6A. FTO's protein sequence demonstrated homology to the ALKB family of dioxygenases, which can demethylate both DNA and RNA, providing a clue to FTO possibly having a role in demethylation (*38*). However, subsequent studies suggest that FTO might demethylate m^6A in a very non-specific and inefficient fashion. One pivotal study demonstrated that FTO displayed much higher catalytic activity for demethylating another mRNA modification found in the 5'UTR called *N6*,*2′*-O-dimethyladenosine (m^6A_m) (*39*). Additionally, the majority of FTO-mediated demethylation of m^6A_m likely occurs on snRNAs and not mRNAs (*40*).

There is another known m^6A eraser called ALKBH5 that has no activity towards m^6A_m (*39*). ALKBH5 is also localized in the nucleus where it does its demethylation activity (*41*). Interestingly, Alkbh5-knockout mice appear generally normal, even though ALKBH5 is thought to play an important role in spermatogenesis and germ cell development in the testes (*41*). Consistent with ALKBH5 playing a more critical role in demethylating m^6A in comparison to FTO, expression levels of ALKBH5 are more highly negatively correlated with m^6A levels in comparison to FTO (*10*).

1.2.3. Readers of m^6A

The effects of m^6A methylation on mRNA and its transcription turnover are attributed to the different readers that bind to it. The first discovered m^6A readers were members of the YTH domain-containing proteins. The ~150aa YTH domain is demonstrated to bind RNA in a m^6A-dependent manner. In mammals, there are five YTH domain-containing enzymes, the YTHDCs (YTH domain-containing) and the YTHDFs (YTH domain family) readers. The nuclear m^6A readers are the YTHDCs. YTHDC1 regulates mRNA splicing by interacting with a variety of splicing regulators such as SRSF3 (*42*), and facilitates nuclear export (*43*). Particularly, YTHDC1 has been reported to preferentially bind ncRNAs rather than mRNAs (*36*). In contrast, YTHDC2, which is highly expressed in the testes, has been shown to post-transcriptional control pathway that switches cells from mitotic to meiotic gene expression programs by promoting both mRNA degradation and translation (*1, 44*).

On the other hand, YTHDF proteins bind m^6A in the cytoplasm, and affect mRNA stability, translation, and/or localization. YTHDF1 has been proposed to bind to eIF3 to promote translation (*45*), while YTHDF2 contributes to the mRNA destabilizing effect of m^6A and promotes the degradation of the mRNA (*46*). YTHDF3 has been shown to promote both the degradation and translation of m^6A-marked mRNAs (*47*). Even though it seems that m^6A-mediated transcript regulation is context-dependent of the YTHDF readers, emerging evidence suggests that all YTHDF proteins may primarily serve to promote mRNA degradation (*48, 49*). A lesser known YTHDF2 function is that of phase separation. Mechanistically, this occurs when the YTHDF-bound, m^6A modified mRNAs undergo phase separation into liquid droplets (liquid-liquid phase

separation or LLPS) such as stress granules and P-bodies that are then processed (*11*). Once these stress granules are formed, they can inhibit the translation of mRNAs that are m^6A hypermethylated (*11*) instead of facilitating translation of mRNAs during embryonic development and spermatogenesis when phase separation done by non-m^6A reader proteins (*50, 51*).

Beyond YTH domain-containing proteins, there are additional nuclear and cytoplasmic readers. In the nucleus there are Heterogeneous nuclear ribonucleoprotein (hnRNP) G and C (HNRNPG/HNRNPC) that bind m^6A to regulate mRNA alternative splicing and nuclear export (*18, 52, 53*) and HNRNPA2B1 which binds to m^6A in pre-miRNAs to regulate their processing (*54*). In the cytoplasm, the insulin-like growth factor-2 mRNA-binding protein (IGF2BP) family are unique m^6A readers because they do not promote mRNA degradation, but they stabilize mRNAs (*55*). There are three different readers from this family (IGF2BP1, 2, 3) proteins, form granule-like messenger ribonucleoprotein (mRNP) complexes located in the perinuclear region that determine mRNA fate (*56*).

Together, these emerging findings highlight the complexity of RNA epigenetic regulation (Fig. 2) and how it may contribute to cellular phenotypes, as well as the need for further study to clarify these distinct findings.

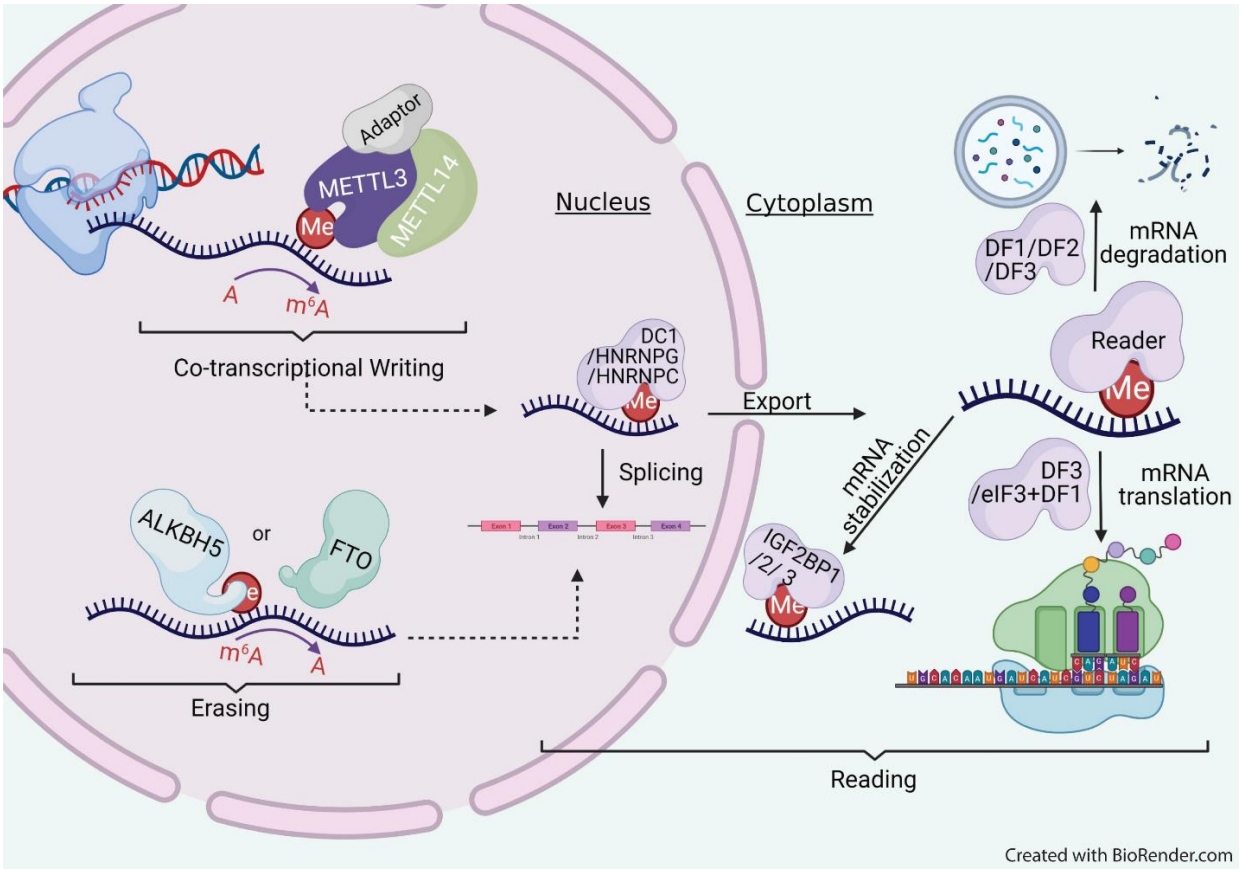

Figure 2. The m^{6}A epitranscriptome.

METTL3 catalyzes m^{6}A methylation (Me) co-transcriptionally within the nucleus which is facilitated by its interacting partner, METTL14, and several adaptor proteins that enhance its activity. A modification upon a mRNA derives in large part by the effects of reader proteins, and ultimately may lead to mRNA splicing, export, degradation, or translation. For example, while YTHDC1 (DC1) exists in the nucleus to promote nuclear export and the HNRNPG/C promote splicing, YTHDF readers can preferentially promote degradation or translation (i.e., YTHDF1 and YTHDF3, or "DF1" and DF3" here). Additionally in the cytoplasm the IGF2BP family stabilizes mRNAs. Alternatively, m^{6}A can also be demethylated by ALKBH5 and FTO in the nucleus.

1.2.4. m^6A epitranscriptomics and epigenetics

Recently, there has been a surge of studies linking epitranscriptomics with epigenetics (*57*). As mentioned above, m^6A methylation occurs co-transcriptionally. The m^6A writer complex can be recruited to DNA by both transcription factors (i.e., CEBPZ) (*58*), as well as chromatin modifications such as histone H3 lysine 36 trimethylation (H3K36me3), a modification that is associated with active transcription (*17*). H3K36me3 was recently shown to be recognized and bound directly by METTL14, which in turn, binds to an adjacent RNA polymerase II to deposit m^6A co-transcriptionally (*17*).

A critical way that epitranscriptomics regulates histone modifiers is by depositing m^6A in their transcripts and destabilizing them. A study showed that the loss of *Mettl14* murine neural stem cells was associated with developmental abnormalities, including reduced proliferation and premature differentiation. Levels of H3K27ac and H3K27me3 were significantly upregulated in the mice compared with controls, and showed increased expression of Cbp and P300, showing minimal m^6A enrichment of *Cbp* and *Ep300* transcripts when *Mettl3* was floxed out (*59*). Additionally, another study found that loss of YTHDF2 led to enhanced stability of the histone demethylase *KDM6B* transcript, thus increasing KDM6B translation and decreasing H3K27me3 levels (*60*).

Intriguingly, loss of METTL3 or METTL14 increased global levels of H3K9me2. This upregulation was reversed by inducing the expression of wild-type METTL3, but not the catalytically inactive METTL3. m^6A itself was shown to be important for recruiting histone demethylase KDM3B to demethylate the repressive histone modification H3K9me2 (*61*).

Beyond these direct effects on mRNA stability, a recent study also identified a role for m^6A methylation on chromosome associated regulatory RNAs (carRNAs). For example, inhibiting m^6A methylate by deleting *Mettl3* in mouse embryonic stem cells (mESC) leads to increased chromatin accessibility and nascent transcription (*62*).

1.3. The Self-Renewing Epitheliums of the Epidermis and the Tongue

1.3.1. Self-Renewing Epithelium

Epithelia are tissues consisting of sheets of similar cells bound closely together, and depending on their predominant function, it can be described further as barrier, secretory, or absorptive, but often all three functions coexist (*63*). Epithelia are found throughout the body in different areas such as the lining of internal and external surfaces as well as be present in either dry or wet environments, such as the surface of the skin and the intestinal track. These epithelial linings form the major barriers between the internal and external environments. Depending on the region of the body, there are different types of epithelia characterized as stratified, transitional, or glandular, where the cells can vary in shape and amount of stratification (*64*). Here we are focusing on the stratified epithelia, which comes in both cornified, and non-cornified types. The stratified non-cornified epithelia is found in the epithelium of the oral cavity. On the other hand, the stratified-cornified epithelia have epithelial cells that are cornified and dead, called corneocytes, and are found in the epidermis (*65*).

The cutaneous and oral stratified epithelia are just examples of tissues that are constantly self-renewing through a stepwise differentiation program. Since changes in gene expression occur during the self-renewal of all epithelial tissues, the epidermis and the tongue provide a great model

in which to study the role of epitranscriptomics in both homeostasis and disease states. Additionally, due to the dynamic dramatic alterations in gene expression the epithelia does through as the cells differentiate, RNA epigenetic mechanisms may play important roles in their physiology.

1.3.2. The epidermis

The skin is constituted of different layers by having a dynamic self-renewal process that depends on the presence of epidermal keratinocyte stem cells that start in the basal layer and progress upwards to become terminally differentiated cells which make up a barrier against water loss, injury, and microbes (*66*). Keratin genes produce the intermediate filaments of keratinocytes that account for about 80% of the total protein content in differentiated cells of stratified epithelia and change with stratification and the state of differentiation. Keratin 14 (K14) is highly expressed in the basal cells of stratified epithelia and is correlated with proliferative activity of keratinocytes. Additionally, these basal stem-like progenitor cells adhere to the basement membrane and through a continuous regenerative process, go on to replace the "suprabasal" cells above them (*67*). In this replacement stage is where we start to see less of K14 and more of Keratin 10 (K10), which is highly expressed in the post-proliferative cells of the suprabasal epidermis (*65, 68, 69*). From the basal layer, the suprabasal layer is the spinous layer, followed by the granular layer which contains glycolipids. If the skin comes from the palms or soles (which is thicker and hairless) we find the stratum lucidum (*70*). With further differentiation, at the cornified layer, the surface epithelial cell eventually sheds off and the process continues (*71, 72*). This epidermal differentiation process

(Fig. 3) in humans is estimated that takes over every 40–56 days (*73*, *74*), whereas in mice the estimated epidermal turnover time is 8–10 days (*75*, *76*).

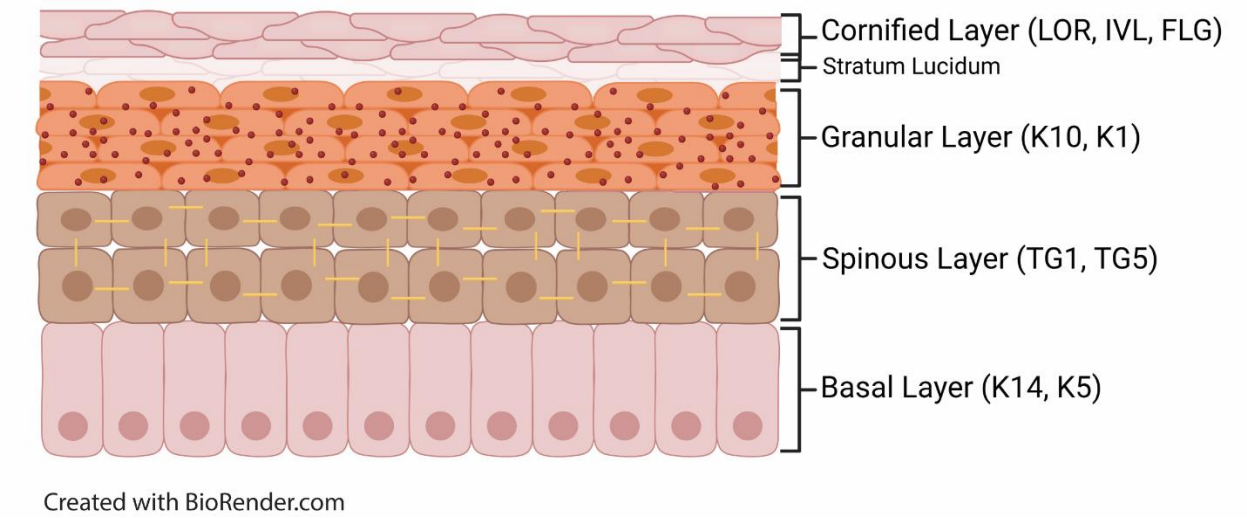

Figure 3. Epidermal differentiation process.

The epidermis consists of layers (indicated on the right) of different stages of keratinocyte differentiation distinguished by expression markers. The process of terminal differentiation of the epidermis starts with cells of the basal layer that proliferate and provide new cells that will differentiate towards the surface of the skin until they reach the cornified layer and are eventually shed during desquamation.

1.3.2. Continued…

Dysregulation of the highly coordinated differentiation process of the epidermis (*77*), can promote hyperplasia, abnormal differentiation, and both neoplastic and inflammatory diseases such as cutaneous squamous cell carcinoma and psoriasis (*78*). While significant progress has been made in discovering many of the pathways involved in driving these

differentiation processes across epithelial tissues, such as WNT, Notch, Sonic Hedgehog (Shh), and BMP signaling (*67, 71, 72*), as well as the master epithelial transcription factor p63 (*64, 79*), the role for epigenetic regulation, and particularly that of epitranscriptomics, is poorly understood.

1.3.3. Filiform Papillae part of the non-taste epithelium

The tongue is a muscular organ that is principally involved in digestion, taste perception, speech and breathing (*80*). On the tongue's surface there is the lingual epithelium which consists of a non-taste epithelium. In the non-taste epithelium there is fungiform papillae surrounded by mechanosensory filiform papillae in the front part of the dorsal lingual epithelium (*81*). Non-taste epithelium takes 5–7 days to be renewed. This non-taste epithelium, Keratin 5/Keratin 14 basal progenitors (*82*) differentiate into Keratin 13 keratinocytes, that make up the suprabasal epithelial layers of the filiform papillae (Fig. 4) (*83, 84*). This turnover takes 5-7 days (*85, 86*).

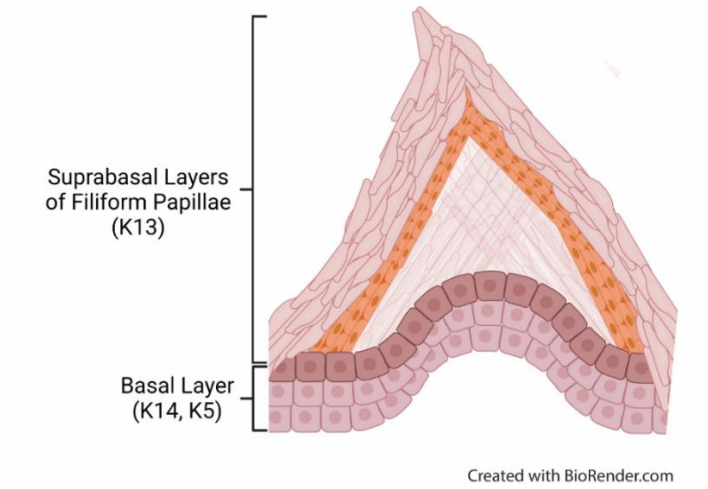

Figure 4. Filiform papillae differentiation process.

The non-taste epithelium filiform papillae consist of layers (indicated on the left) of different stages of epithelial differentiation distinguished by expression markers. The process of terminal

differentiation of the filiform papillae starts with cells of the basal layer that proliferate and provide new cells that will differentiate towards the surface of the non-taste epithelium.

1.3.4. m^{6}A in the epidermis

Studies understanding m^{6}A's roles during epithelial homeostasis and differentiation have been very limited. One study demonstrated that deletion of *Mettl14* in the mouse epidermis impaired the m^{6}A-dependent association between the long non-coding RNA (lncRNA) *Pvt1* and Myc which is shown to be critical for the promotion of epidermal stemness and wound healing capabilities (*87*). A recent study using a mouse model with a *Mettl3* conditional knockout in the epidermis demonstrated broad developmental defects including a significant failure of hair morphogenesis and premature interfollicular differentiation processes due to impaired WNT signaling. The mRNAs encoding several WNT regulators were significantly downregulated by *Mettl3* knockout (*88*). Lastly, one study showed that METTL3 was upregulated in cutaneous squamous cell carcinoma (cSCC) samples. When *METTL3* is knockdowned *in vivo* and *in vitro*, it impairs cSCC's colony forming ability *in vitro* and tumorigenicity was diminished *in vivo* by decreasing the m^{6}A levels and the expression of ΔNp63 (*89*).

These significant epidermal phenotypic abnormalities demonstrate the critical role for m^{6}A in epidermal homeostasis, as well as the need for future studies to answer all the outstanding questions at the intersection of the epitranscriptome and normal epidermal functions.

1.3.5. m^6A in the tongue

A mouse model with a *Mettl3* conditional knockout in the epidermis, also knocks out *Mettl3* in the oral epithelium due to the use of the *K14* promoter for the conditional knockout. This knockout was demonstrated to manifest developmental defects in the tongue such as loss of filiform papillae attributed to altered Wnt signaling (*88*). Another study was conducted using a similar *Mettl3* conditional knockout in dorsal lingual epithelium. *Mettl3* deletion leads to morphological abnormalities in filiform papillae with increased thickness of the epithelium as well as irregular cell alignment due to reduced m^6A of Lats1 (kinase that phosphorylates and inactivates the transcriptional coactivators Yap and Taz) which further inhibited the Hippo pathway(*90*). Another study showed that overexpressing *Mettl3* promoted taste bud recovery from radiation damage by increasing the proliferation of taste bud progenitor cells, although it could not protect mice from epithelial injury due to irradiation (*90*).

1.4. Thesis Objectives and Roadmap for Subsequent Chapters

Together, this literature review can be summarized into three general observations: 1) Epitranscriptomics, or RNA epigenetics, is a new layer of gene regulation in a spatial- and time-dependent manner. More specifically, m^6A has been shown to affect diverse aspects of mRNA biology, including both its degradation and translation, depending upon the cellular context. 2) The epidermis and the non-lingual epithelium are tissues that are constantly self-renewing through a stepwise differentiation program coordinated through spatiotemporal gene regulation, disruption of which can lead to a diseased state. 3) The m^6A epitranscriptome has been recently shown to share a great deal of crosstalk with histone epigenetics through both direct interactions with

chromatin modifiers as well as through the regulation of chromatin modifier mRNA expression in different cellular contexts. Whether this type of epitranscriptomic-epigenetic interplay exists during epithelial development and homeostasis, or cancer are unknown. These observations provide the overarching objective of this thesis to determine the presence and potential role of m^6A epitranscriptomic-epigenetic crosstalk in the complex biology of self-renewing epithelial tissues.

Therefore, in chapter 2 we examine the consequence of loss of m^6A through Mettl3 depletion in the epidermis in mice *in vivo*. We characterize developmental abnormalities in self-renewing tissues such as the epidermis and the tongue that arise from a dysregulation of keratinization and extracellular matrix transcripts. This data leads us to uncover a potentially fundamental role of the m^6A epitranscriptome during epithelial development and differentiation. In chapter 3, we dive deeper to discover the epitranscriptomic mechanisms that contribute to these phenotypic defects. Here, we find that METTL3-dependent m^6A directly regulates chromatin modifiers by promoting the destabilization and, consequently, the degradation of their mRNA transcripts in epidermal progenitors. Finally, in chapter 4 we summarize the impact and broader implications of this thesis work as well as discuss unanswered questions remain and how they provoke potential new research directions to address and add more knowledge to the m^6A epitranscriptomic field as it interfaces with epithelial biology and disease.

CHAPTER 2: DYSREGULATION OF EPITHELIAL HOMEOSTASIS WITH METTL3 DEPLETION

This chapter includes work adapted from a previously published manuscript: Maldonado López, A.M., Ko, E.K., Huang, S., Pacella G., Kuprasertkul, N., D'souza, C., Reyes Hueros, R.A., Shen, H., Stoute, J., Elashal, H., Sinkfield, M., Anderson, A., Prouty, S., Li, H., Seykora, J.T., Liu, K.F., Capell, B. C. (2023) Mettl3-catalyzed m6A regulates histone modifier and modification expression in self-renewing somatic tissue. *Science Advances* DOI: 10.1126/sciadv.adg5234.

2.1. Introduction

To better understand the role of the m^6A epitranscriptome in the epidermis and the tongue, we created mice with an epithelial-specific deletion of *Mettl3* by crossing mice floxed for *Mettl3* with mice carrying a keratin 14 (*K14*)-Cre (*91-93*) (*K14*-Cre; $Mettl3^{fl/fl}$ or "*Mettl3*-eKO") (Fig. 5), as a whole-body deletion of *Mettl3* is embryonic lethal (*94*).

A complete absence of m^6A due to *Mettl3* deletion is early embryonic lethal. This is due to the ability of METTL3-mediated m^6A to promote either mRNA turnover, such as degradation, during development. Knockout of *METTL3* from both human and mouse embryonic stem cells results in an increased transcript half-life (decreases mRNA degradation) of key pluripotency regulators such Nanog, Sox2, and Klf4. By increasing the transcript half-life of these pluripotency regulators, it improves self-renewal and proliferative abilities, plus prevents differentiation from naïve pluripotency into downstream lineages (*95, 96*).

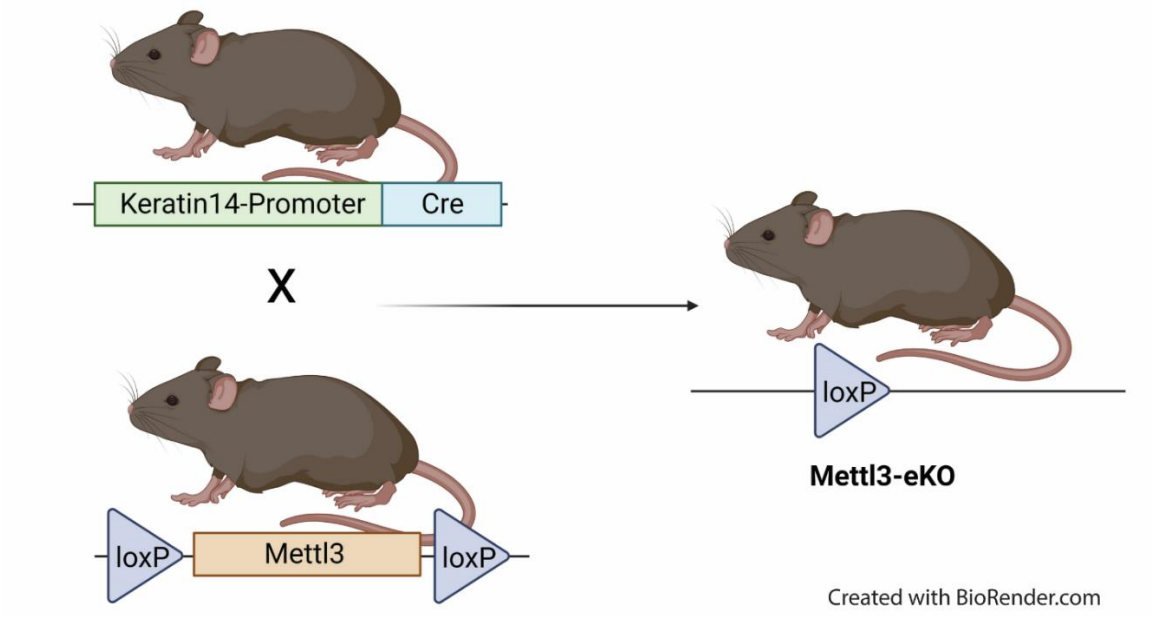

Figure 5. Generation of Mettl3-eKO mouse model.

Generation of epidermal-specific knockout mice using the Cre-loxP system. In the Cre mouse line, the expression of Cre is under the control of a Keratin 14 (*K14*) promoter. The floxed target gene of *Mettl3* mouse line contains loxP sites (▶) in the first and the last introns of the gene thus flanking the region of 9 out of the 11 exons of *Mettl3* to be deleted. When the two mouse lines are bred together, the Cre enzyme recognizes the loxP sites and deletes the *Mettl3* DNA sequence only in basal keratinocytes where the *K14*-Cre is expressed.

2.1. Continued…

In the epithelial development epitranscriptomics field, there has been two studies already published (mentioned above) but none of them have tackled what happens when *Mettl3* is deleted and how it affects the development and differentiation of the interfollicular epidermis (IFE) as well as the implications that m^6A has in epithelial epigenetics.

2.2. Results

2.2.1. Mouse model

Interestingly, even when trying to get around the embryonic lethality of the full-body *Mettl3* knockout by creating an epithelial-specific deletion of *Mettl*3, the *Mettl3*-eKO mice did not survive past one week of age, thus we harvested them for our experimental purposes on postnatal day 5 or 6 (P5 or P6) which recapitulated the two studies that have used similar conditional knockout models for studying the tongue in most of them survived by P4 and few could survive by P7 (*90*) and to study the hair follicle in which the mice could not survive beyond P6 (*88*). Phenotypically, *Mettl3*-eKO mice displayed pink skin at P5 and P6 that was strikingly different in comparison to control mice (*Mettl3*$^{fl/fl}$ or *K14*-Cre; *Mettl3*$^{+/+}$ or *Mettl3*$^{+/+}$), (Fig. 6A), suggesting a potential failure to enter anagen, the period of active hair growth from postnatal days 1 to day 12 (*97-99*). Furthermore, *Mettl3*-eKO mice were also about half the size of control littermates (Fig. 6A).

Additionally, we observed that *Mettl3* heterozygotes (*K14*-Cre; *Mettl3*$^{+/fl}$ or "*Mettl3*-Hets"), weighed more than *Mettl3*-eKO mice, but less than wildtype (*K14*-Cre; *Mettl3*$^{+/+}$ or *Mettl3*$^{+/+}$) control mice, suggesting that there is a correlation between weight loss with the loss of each allele of *Mettl3* (Fig. 6B, S1). Together, these gross observations underscored how critical Mettl3 is for proper epithelial development. We next examined the epidermal tissues for the *Mettl3* knockout. Immunohistochemistry (IHC) and western blotting (WB) confirmed a complete loss of Mettl3 throughout the mouse epidermis of *Mettl3*-eKO mice (Fig. 6C and 13A).

2.2.2. Abnormalities in epithelia (skin and tongue)

Now that we confirmed the knockout, we used hematoxylin & eosin (H&E) staining to examine the skin and tongue epithelial tissues histologically. The skin of control mice has normally formed epidermal layers with fully developed hair follicles and visible hair growth compared to the *Mettl3*-eKO skin. The *Mettl3*-eKO epidermis has several morphological abnormalities such as that the keratinocyte nuclei at the basal layer of the interfollicular epidermis were not parallel to each other and displayed a loss of cell polarity. This loss of cell polarity suggests potential defects in cell adhesion to the basement membrane (*67*) and proliferation (*100*).

Beyond the basal layer of the interfollicular epidermis, the clear separation that is typically observed between K14 and K10 layers of the interfollicular epidermis was unclear, suggesting potential dysregulation of the differentiation process (Fig. S2A). Furthermore, the suprabasal interfollicular epidermis displayed increased thickness of the stratum granulosum and the stratum corneum (Figs. 6D and S2B). For instance, while overall expression of the stratum corneum protein filaggrin did not appear to change in the *Mettl3*-eKO epidermis, there is a clear thickened stratum granulosum layer below the stratum corneum (Fig. S2B). Consistent with a previous study, we observed striking abnormalities in hair follicle morphogenesis (Figs. 6D and S3A) (*88*).

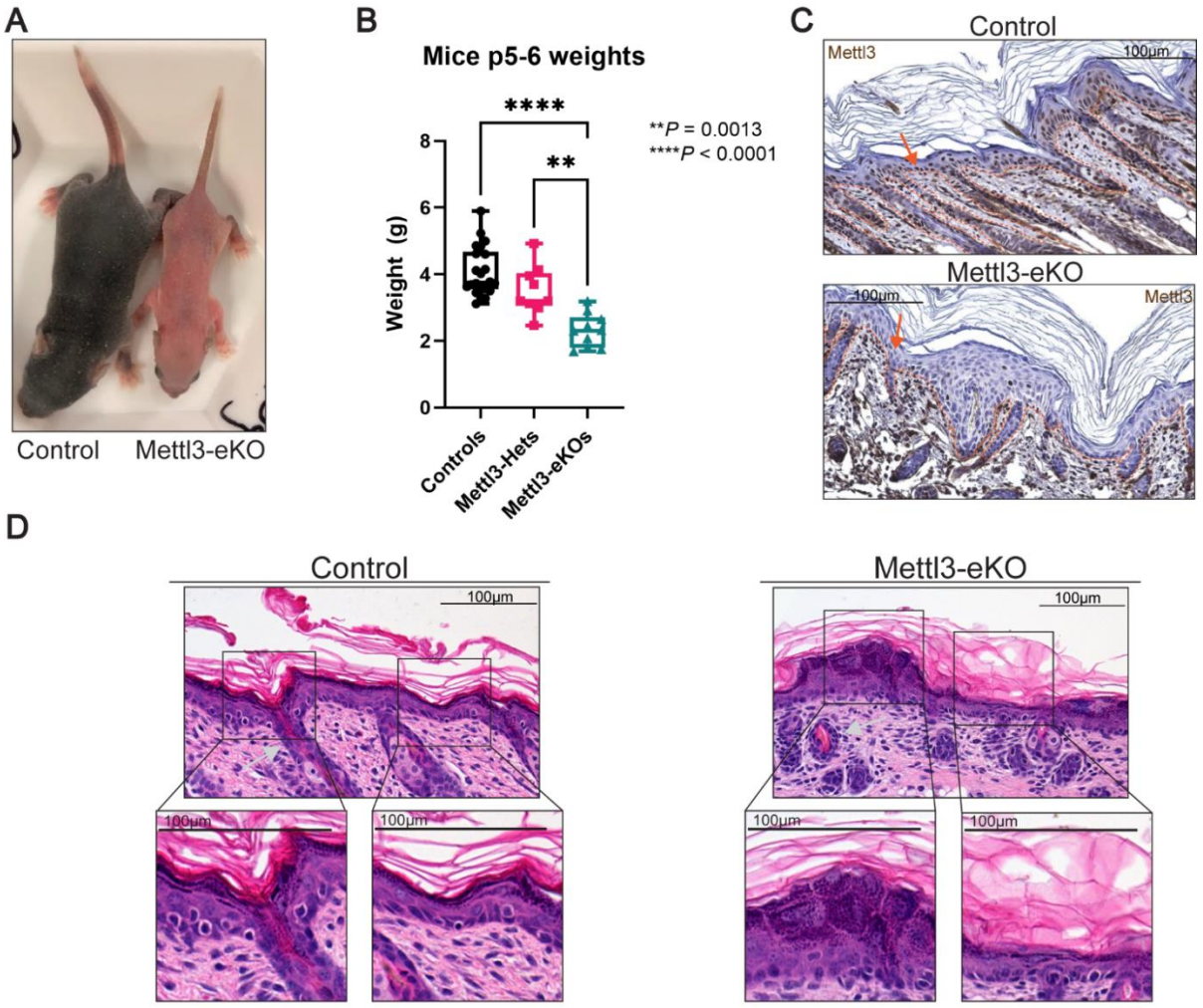

Figure 6. Loss of Mettl3 leads to grossly abnormal epidermal development.

(A) Postnatal day 6 (P6) *Mettl3*-eKO mice display a complete absence of hair and are half the size of WT control littermates. (B) *Mettl3*-eKO mice weigh less than controls and *Mettl3*-heterozygotes ("Hets"). (C) IHC of murine dorsal skin, the dotted orange line demarcates the epidermis-dermis junction. The orange arrow signals the nucleus of the keratinocyte in which Mettl3 is found. Controls have Mettl3 present throughout the epidermis, but the staining is gone in the *Mettl3*-eKO

epidermis. (D) *Mettl3*-eKO skin displays malformed hair follicles (silver arrows), as well as loss of cell polarity in the basal epidermal cells along with thicker granular and cornified layers.

2.2.2. Continued…

Since the *K14*-Cre system used for knocking out *Mettl3* from the epidermis also deletes *Mettl3* in the oral epithelium (*101*), we examined the murine tongue. While control tongues demonstrated a normal dorsal lingual epithelium with developed taste buds and filiform papillae, *Mettl3*-eKO mice displayed severely impaired development of these features (Fig. 7A). This is consistent with previous work mention above which shows that loss of Mettl3 led to severe defects in taste bud development and abnormal epithelial thickening (*90*). More surprisingly, however, we observed that 80% of *Mettl3*-eKO mice were found to have full thickness ulcerations in the posterior part of the tongue, while none were present in WT controls, nor in *Mettl3*-Hets (Fig. 7B). This ulceration suggests that the *Mettl3*-eKO mice had impaired cell adhesion. Together, these results from the mouse epidermis and tongue have demonstrated that Mettl3 is a critical regulator of normal epithelial development and homeostasis.

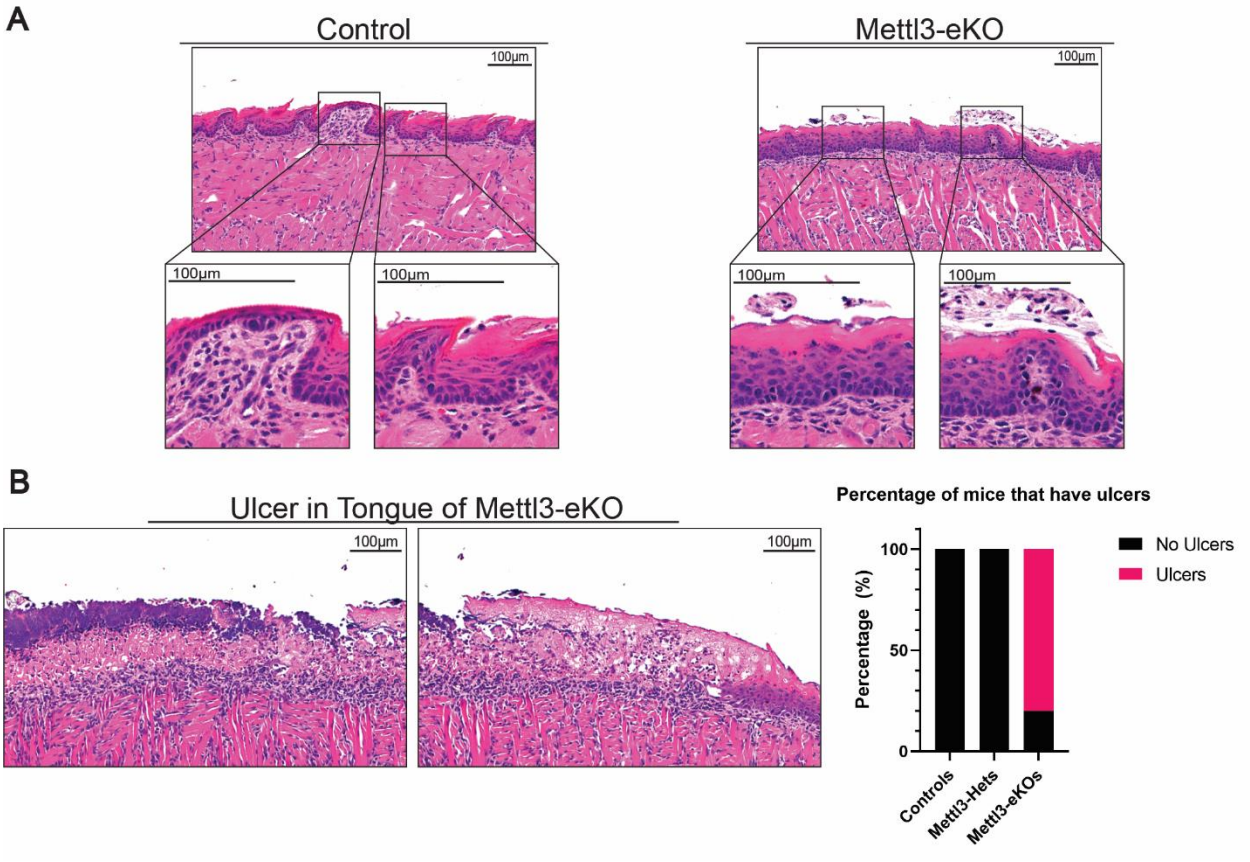

Figure 7. Loss of Mettl3 leads to grossly abnormal tongue development.

(A) *Mettl3*-eKO oral epithelium of the tongue has malformed filiform papillae and tastebuds. (B) *Mettl3*-eKO tongues also display large ulcers in the posterior dorsal aspect.

2.2.3. Transcriptional analysis

Since we see these dramatic phenotypic changes, we next performed RNA-seq from the dissected epidermis of *Mettl3*-eKO mice in comparison with their control littermates to begin to address the mechanisms behind how Mettl3 loss drove these changes. Consistent with Mettl3's established role in mRNA transcript turnover regulation, *Mettl3*-eKO mice epidermis displayed profound transcriptional dysregulation, with almost 4,000 genes displaying significant differential

expression upon *Mettl3* deletion (Fig. 8A). When we compare what we see phenotypically with the transcriptional data, we see correlations**.** With the increased epidermal thickening we observe in the *Mettl3*-eKO mice, Gene Ontology (GO) analysis of upregulated genes identified categories such as "Keratinization" and "Keratinocyte Differentiation", along with specific transcripts like *Krt6a, Krt6b, Krt16,* and *Krt17* (Fig. 8B, C). All these keratins are associated with thickened acral skin such as the human palm or sole, as well as in wounded and/or stressed keratinocytes after injury. Additionally, numerous other transcripts associated with keratinocyte terminal differentiation were significantly upregulated, including pro-differentiation transcription factors (*Grhl3*) (Fig. S4A), several small proline rich (SPRR) protein (*Sprr1a, Sprr2b, Sprr2d, Sprr2f, Sprr2g*) genes (SPRR proteins are markers of epidermal terminal differentiation that function as crosslinking substrates of transglutaminase in the cornified layer (*69, 102*)) and several late cornified envelope (*Lce3a, Lce3b, Lce3d, Lce3f*) genes (*103*), as well as *Tgm1* and *Sfn* (Transglutamerase 1 functions in the formation of the cornified layer (*104*) and Stratifin which affects barrier function and dermal fibroblasts in photoaging skin (*105*)**)**. However, even though not all canonical epidermal differentiation genes seemed altered, like filaggrin (Fig. S2B, S4A), these results suggest that Mettl3 loss is not simply "turning on" genes of differentiation, but rather dysregulating them.

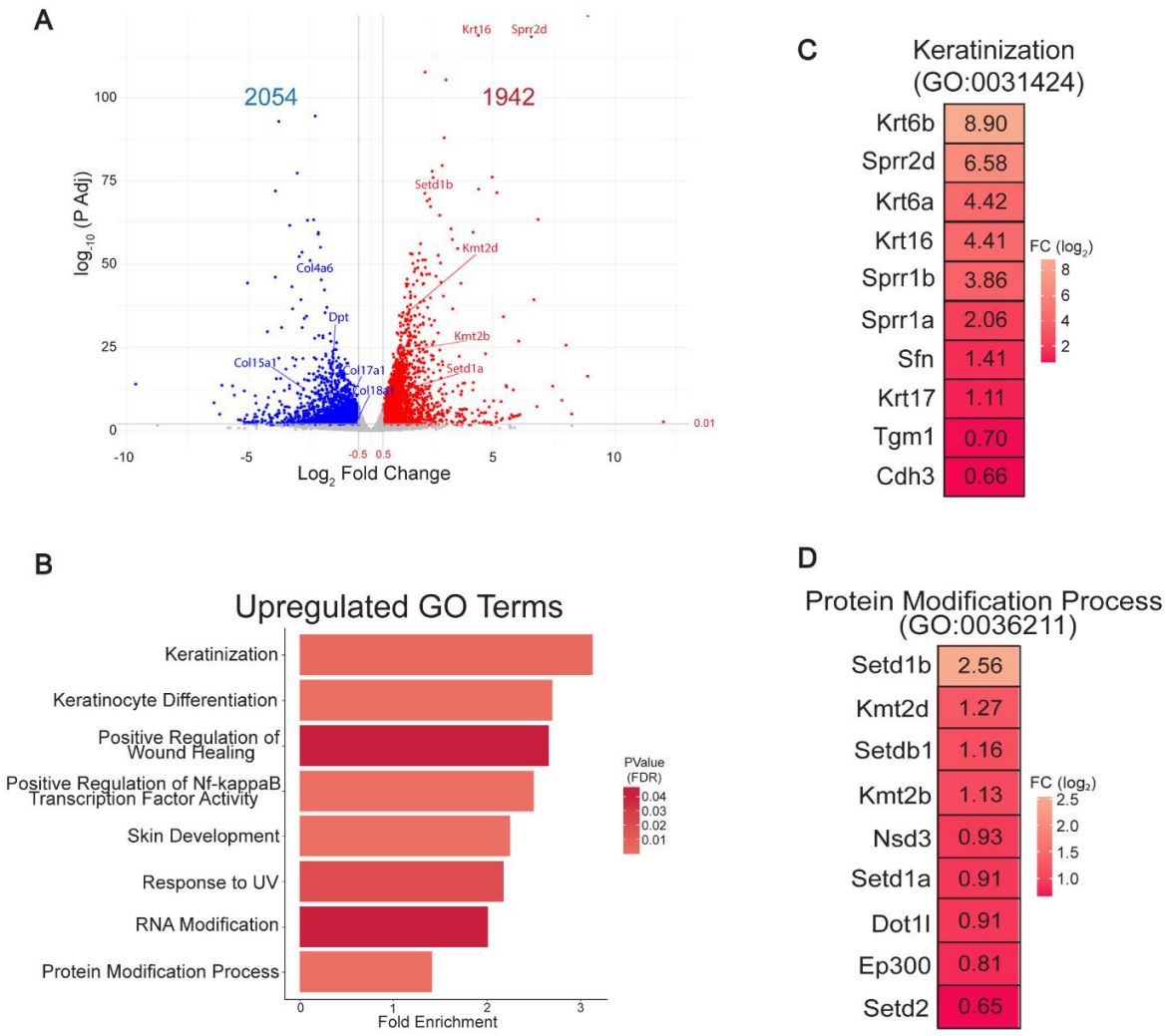

Figure 8. Mettl3 loss promotes dramatic transcriptional upregulation.

(A) RNA-seq was performed on epidermis from *Mettl3*-eKO P6 mice (n = 3) vs control littermates (n=3). A log2 Fold Change of ± 0.5 and an adjusted p-value of <0.01 was done to visualize the significant changes. (B) Biological Process Terms Gene Ontology (GO:BP) analysis of upregulated transcripts in *Mettl3*-eKO mice. (C) Highly significant upregulated transcripts in *Mettl3*-eKO mice from the "Keratinization" category. (D) Highly significant transcripts from the upregulated "Protein Modification Process" category.

2.2.3. Continued…

Next, we performed GO analysis on the downregulated transcripts. Downregulated transcripts were enriched for pathways and categories typically associated with epithelial progenitor cells and developmental pathways. The downregulated GO categories include "Regulation of non-canonical Wnt signaling", "Epithelial Cell Proliferation", "Extracellular Matrix (ECM) Organization", "Collagen Fibril Organization", "Cell Adhesion", and "Pattern Specification Process" (Fig. 9A). All these GO categories are known to be important for the development and establishment of the basal layer of epithelial surface tissues like the epidermis and oral epithelium as well as hair follicle morphogenesis. For example, we saw that numerous collagen genes were downregulated in these GO categories (Fig. 9B), one of which is *Col17a1* (collagen XVII) (Fig. S5A, S5B). Col17a1 facilitates epidermal-dermal attachment (the attachment between the basal layer of the epidermis to the basement membrane) and regulates the proliferation of keratinocyte stem cells at the interfollicular epidermis (*106*). Interestingly, mutations in human *COL17A1* are associated with junctional epidermolysis bullosa, a genetic blistering disease of the skin (*107, 108*). Additionally, autoantibodies against COL17A1 are also known to be the primary cause of mucous membrane pemphigoid, a mucous membrane-dominated autoimmune subepithelial blistering disease that causes oral epithelial blistering (*109*).

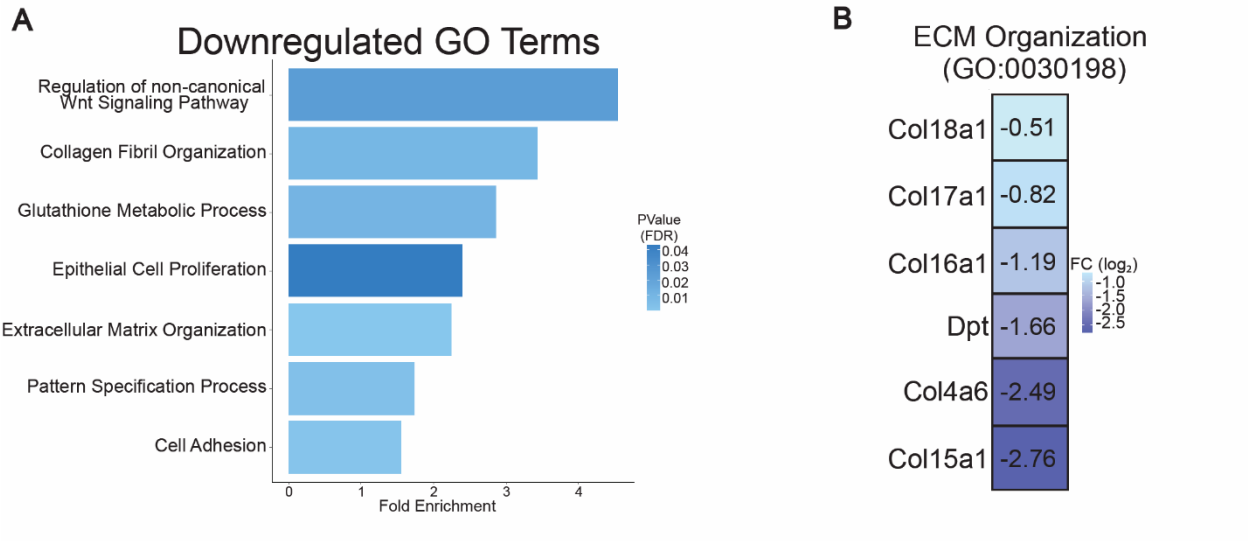

Figure 9. Mettl3 loss promotes dramatic transcriptional downregulation.

(A) GO:BP Analysis of downregulated transcripts in *Mettl3*-eKO mice. (B) Highly significant downregulated transcripts of the downregulated extracellular matrix (ECM) organization category.

2.3. Discussion

Altogether, this phenotypic characterization and transcriptional data present an overall picture where loss of Mettl3-dependent m^6A in skin and oral epithelial tissues promotes a more differentiated, less progenitor stem cell-like phenotype. While the upregulation of numerous terminal differentiation transcripts may explain the phenotype of the thickened outer layers of the epidermis, the loss of transcripts involved in cell-to-cell adhesion and adhesion to the epithelial basement membrane, may offer insight into the loss of polarity observed in the epidermis, as well as the ulcerations observed in the tongue.

2.4. Supplemental information

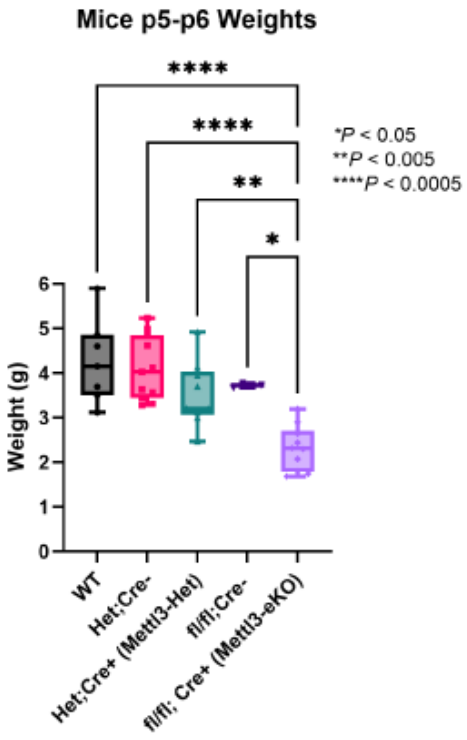

Figure S1. Weight loss correlates with loss of *Mettl3* alleles.

Wildtype (WT), *Mettl3*-heterozygotes without *K14*-Cre (Het;Cre-), and *Mettl3*-floxed/floxed without *K14*-Cre ($^{fl/fl}$;Cre-) genotypes serve as control mice. *Mettl3*-eKO mice weigh less than all genotype controls and *Mettl3*-heterozygotes with *K14*-Cre (*Mettl3*-Het).

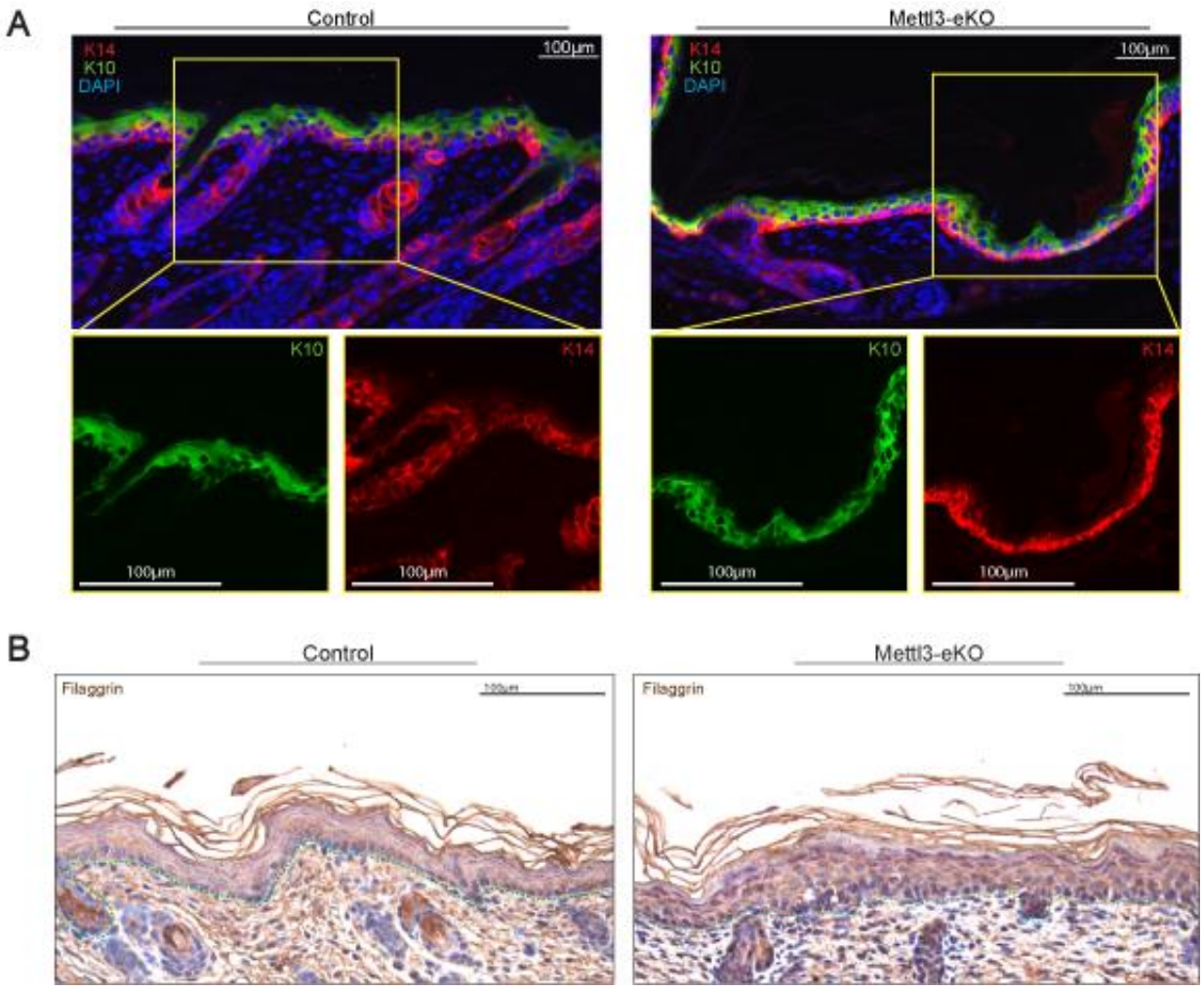

Figure S2. Histological analysis of Mettl3-eKO skin layers.

(A) IF of murine dorsal skin of cytokeratin 14 (K14) in the basal layer and cytokeratin 10 (K10) at the suprabasal layer. Controls have distinct basal and suprabasal layers, while there is overlapping staining of both K14 and K10 in the *Mettl3*-eKO epidermis. (B) IHC of murine dorsal skin, the dotted green line demarcates the epidermis-dermis junction. Filaggrin is present normally in control and in *Mettl3*-eKO epidermis.

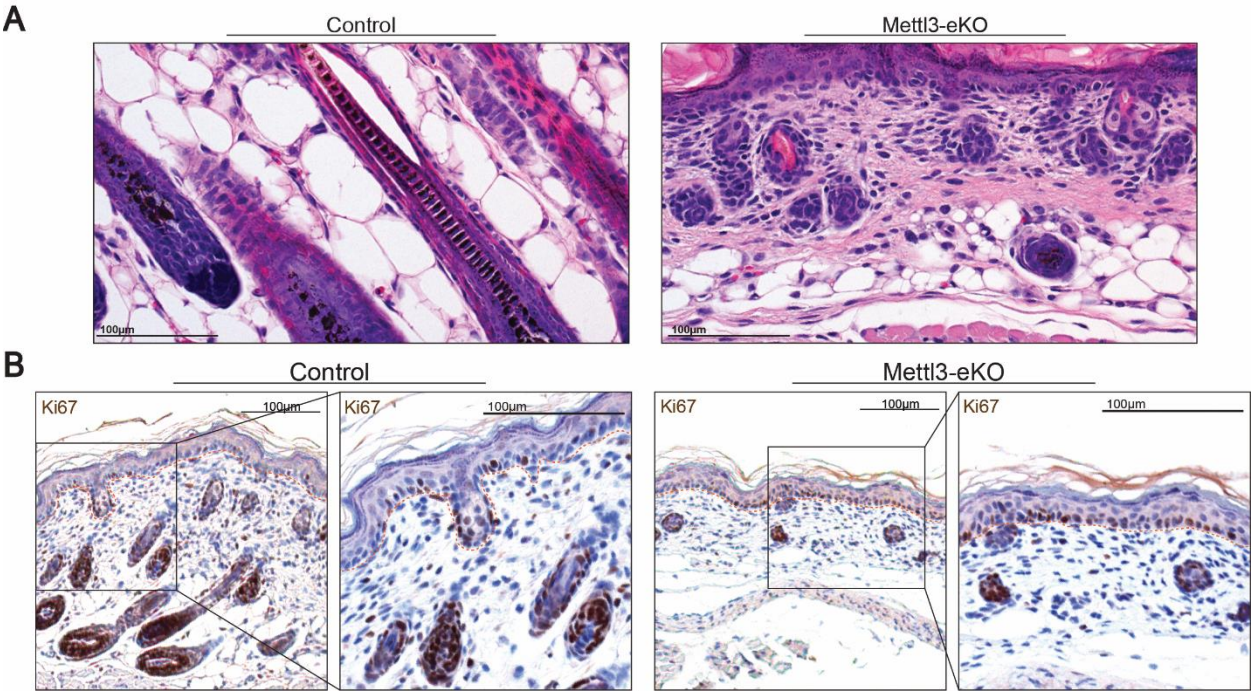

Figure S3. Histological analysis of Mettl3-eKO murine skin.

(A) *Mettl3*-eKO skin displays underdeveloped, malformed hair follicles. (B) Ki67 IHC of murine dorsal skin, the dotted orange line demarcates the epidermis-dermis junction. *Mettl3*-eKO epidermis have more positive Ki67-positive staining cells in both the basal and suprabasal transit-amplifying cells in *Mettl3*-eKO mice in comparison to WT mice, suggestive of potentially accelerated transition of basal progenitors to the suprabasal layers.

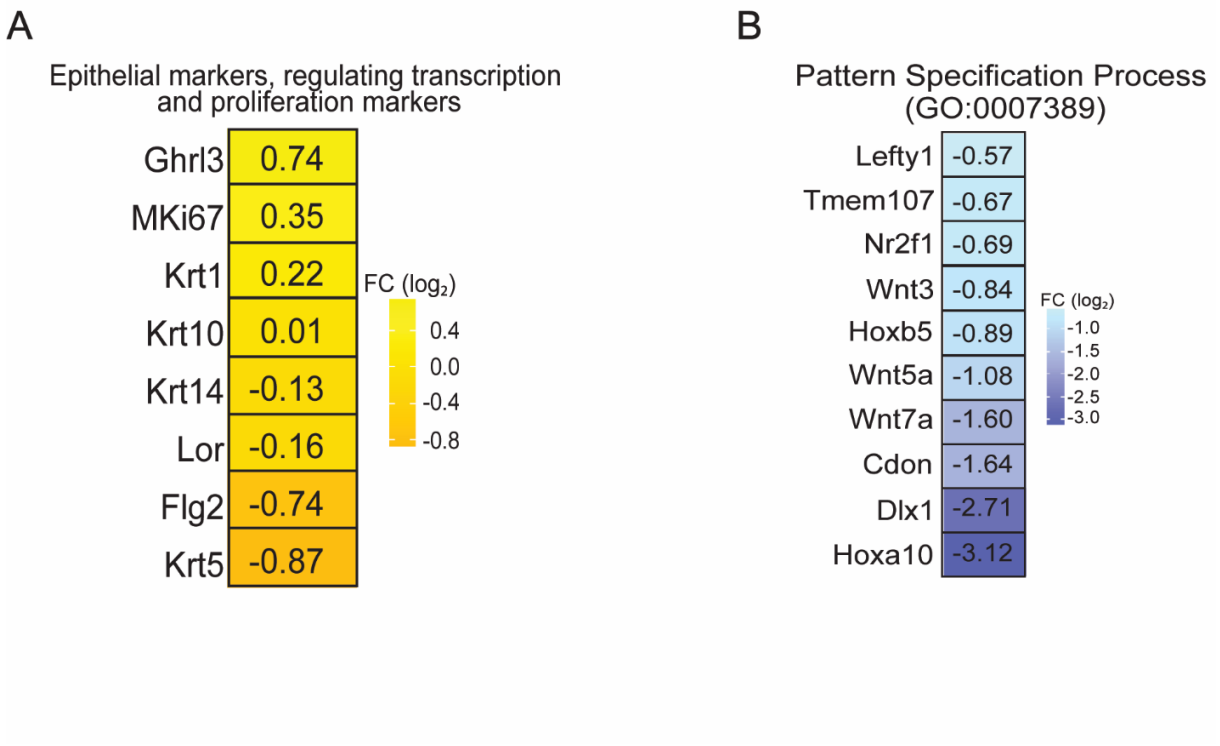

Figure S4. Bulk RNA-seq additional data.

(A) Representative makers of epithelial stemness and differentiation and their changes in gene expression by RNA-seq in *Mettl3*-eKO mice epidermis in comparison to WT mice. (B) Highly significant downregulated transcripts of the downregulated pattern specification process category.

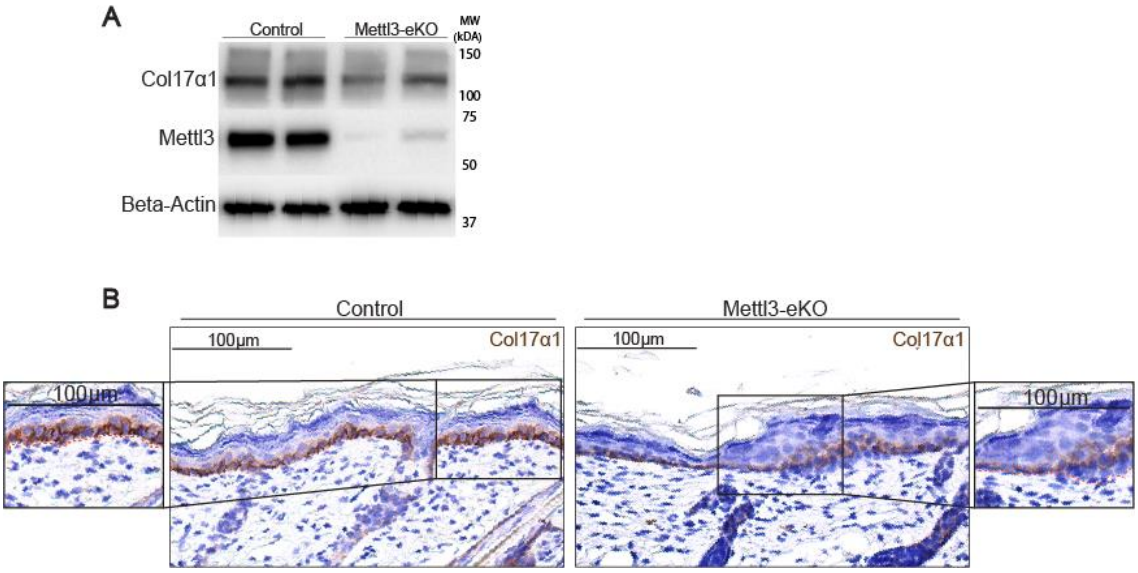

Figure S5. Continued: Collagen 17 alpha 1 is decreased with deletion of Mettl3.

(A) Western blot for Col17a1 in P6 mice epidermis. (B) IHC for Col17a1 in P6 mice epidermis

2.5. Materials and Methods

Mice

Animal protocols were reviewed and approved by the Institutional Animal Care and Use Committee (IACUC) of the University of Pennsylvania. Mice were maintained on a C57BL/6 background. Mice carrying *Mettl3* floxed alleles crossed with *K14*-Cre transgenic mice. *K14*-Cre; *Mettl3*$^{fl/fl}$ (*Mettl3*-eKO) were considered mutants. Unless noted otherwise, littermates homozygous for the *Mettl3* alleles of interest lacking *K14*-Cre were used as controls. The generation of *Mettl3*$^{fl/fl}$ mice has been described elsewhere (*110*).

Genotyping

Polymerase chain reaction (PCR) was done using a Thermo Phire Animal Tissue PCR kit (F140WH). All experimental mice were an equal mix of males and females. The number of animals used per experiment is stated in the figure legends.

Weight collection

Before euthanasia, mice at 6 days of age were measured for total body weight. Data figures are the composite of multiple litters of *Mettl3*-eKO, littermate controls or *Mettl3*-Hets (mice heterozygous for *Mettl3*: *K14*-Cre; $Mettl3^{+/fl}$). A one-way analysis of variance (ANOVA) was used to calculate the significance between groups when considered for genotype. All P are noted in figure legends and were considered significant if $P < 0.05$ and nonsignificant (NS) if $P > 0.05$.

Mice RNA and protein extraction

Murine epidermis was dissociated from the dermis before the isolation of bulk RNA and protein. Following the euthanasia of 6-day-old mice, the skin was dissected, and the underlying fat pad was removed using a scalpel. The resulting tissue was floated dermis side down in dispase (5 U/ml; Corning) in PBS for 40 min at 37°C. The epidermis was then removed using a scalpel, and for RNA, the epidermis was flash-frozen in TRIzol and stored at −80°C until RNA isolation. RNA was extracted using a RNeasy kit (#74104, QIAGEN) at the same time and date for all mice belonging to a single experimental cohort (i.e., RNA-seq) regardless of the date of murine euthanasia to reduce batch effects and stored at −80°C. For protein, the epidermis was placed directly into cold PBS and centrifuged at 4°C for 5 min at 2500 rpm. To the resulting pellet, protein

lysis buffer (Cell Signaling Technology) containing a protease inhibitor cocktail was added, and the mixture was homogenized, sonicated, rotated at 4°C for 10 min, and then centrifuged at 4°C at full speed for 10 min. Lysates were quantified using the Bradford assay. Frozen lysates were stored at −80°C.

Bulk RNA-seq

Total RNA was extracted using the Qiagen RNeasy Mini kit (Cat No./ID: 74104). The following protocol was performed with 1ug of total RNA. mRNA was purified using the NEBNext poly(A) mRNA magnetic isolation module. RNA-seq libraries were prepared using NEBNext Ultra Directional RNA library preparation kit for Illumina (NEB #E7760). Library quality was checked by Agilent BioAnalyzer 2100 using the DNA 1000 kit (Part number 5067-1504) and libraries were quantified using the Library Quant Kit for Illumina (NEB #7630). Libraries were then sequenced using a NextSeq500 platform (75-base-pair (bp) single-end reads).

RNA-seq data processing

All RNA-seq was aligned using RNA STAR (*111*) under default settings to Mus musculus GRCm38. FPKM (fragments per kilobase per million mapped fragments) generation and differential expression analysis were performed using DESeq2 (*112*). Statistical significance was obtained using an adjusted p value (padj) generated by DESeq2 of less than 0.01.

Gene Ontology (GO) analyses

All GO analyses were performed using PANTHER at http://pantherdb.org/ to determine statistically overrepresented GO terms using Fisher's exact test under the category "biological process." P values for GO terms are false discovery rate statistics. GO term figures are generated using ggplot2.

Immunoblotting

Samples were separated by electrophoresis in 4 to 20% SDS–polyacrylamide gel electrophoresis gels with 30 ug per lane, transferred to a polyvinylidene difluoride membrane, and blotted with antibodies. Secondary horseradish peroxidase–conjugated secondary antibodies (Santa Cruz Biotechnology) and Amersham ECL Prime Western Blotting Detection Reagents (catalog no. RPN2232, GE Healthcare) were used for detection.

Histology

Mouse dorsal and ventral skin tissues were processed for histological examination by Core A - Cutaneous Phenomics and Transcriptomics (CPAT) Core of the Penn Skin Biology and Diseases Resource-based Center (NIH P30-AR069589) and mounted on frost-free slides. H&E staining was processed by Penn Skin Biology and Disease Resource-based Center Core A. A Leica DM6 B microscope was used to observe and capture representative images. Exposure times and microscope intensity were kept constant for all human samples and across mouse littermate comparisons.

Immunohistochemistry

Tissue slides were baked for 1 hour at 65°C, deparaffinized in xylene, and rehydrated through a series of graded alcohols. After diH2O washes, slides were treated with antigen unmasking solution (1:100; SKU H-3300-250, Vector Laboratories) at 95°C for 12 min according to the manufacturer's protocol. Hydrogen peroxide, blocking, primary antibody binding, HRP conjugated secondary antibody and 3, 3'-diaminobenzidine (DAB) were done using the Mouse and Rabbit Specific HRP/DAB IHC Detection Kit - Micro-polymer (ab236466, Abcam). Before the protein block, tissues were treated with 0.1% Triton X-100 diluted in 1X TBS for 5 minutes to unmask the antigens expressed in the nucleus. After overnight primary antibody incubation at 4°C and endogenous treatment with secondary anti-rabbit antibody at RT for 20 min, the staining was visualized with DAB with exposure times synchronized throughout all tissue samples within an antibody group for the exact same time. All slides were counterstained with hematoxylin (Hematoxylin QS, H-3404, Vector Laboratories) for 20s at RT, dehydrated in ethanol, cleared in xylene, and mounted with VectaMount (permanent mounting medium, H-5000, Vector Laboratories).

Immunofluorescence

Tissue slides were baked for 1 hour at 65°C, deparaffinized in xylene, and rehydrated through a series of graded alcohols. After diH2O washes, slides were treated with antigen unmasking solution (1:100; SKU H-3300-250, Vector Laboratories) at 95°C for 12 min according to the manufacturer's protocol. Hydrogen peroxide, blocking, primary antibody binding and

secondary antibody binding were done using the Mouse and Rabbit Specific HRP/DAB IHC Detection Kit - Micro-polymer (ab236466, Abcam). Before the protein block, tissues were treated with 0.1% Triton X-100 diluted in 1X TBS for 5 minutes to unmask the antigens expressed in the nucleus. After overnight primary antibody incubation at 4°C and endogenous treatment with secondary fluorescent antibodies at RT for 1hr. All slides are mounted with ProLong Gold antifade reagent with DAPI (P36935, Invitrogen).

Statistical analyses

All statistical analyses were performed using R or GraphPad Prism 10. Details of each statistical test are included in Materials and Methods. Sample sizes and P values are included in the figure legends or main figures. Investigators were not blinded during experiments or outcome assessment.

Table 1. Antibodies utilized in this thesis.

Antibody	Company	Catalog Number	Application
Mettl3	Abcam	ab195352	Immunoblot, IHC
Setd1a	Invitrogen	PA5-78298	Immunoblot, IHC
H3K4me2	Abcam	ab7766	IHC
H3K4me3	Abcam	ab8580	IHC
Cytokeratin 14 (K14)	Abcam	ab7800	ICC, IF
Cytokeratin 10 (K10)	Abcam	Ab76318	IF
Ki67	Abcam	Ab15580	IHC
Filaggrin	Abcam	Ab81468	IHC

Beta-Actin	Cell Signaling	4970S	Immunoblot
Collagen XVII	Novus Biologicals	NBP2-67316	Immunoblot, IHC
m^6A	Synaptic Systems	202003	ICC
Alexa Fluor 555	Invitrogen	A31570	ICC, IF
Alexa Fluor 488	Invitrogen	A21206	ICC, IF
Rb IgG HRP Linked	Cell Signaling	7074S	Immunblot

CHAPTER 3: M^{6}A REGULATES THE CHROMATIN MODIFIERS IN THE EPIDERMIS

This chapter includes work adapted from a previously published manuscript: Maldonado López, A.M., Ko, E.K., Huang, S., Pacella G., Kuprasertkul, N., D'souza, C., Reyes Hueros, R.A., Shen, H., Stoute, J., Elashal, H., Sinkfield, M., Anderson, A., Prouty, S., Li, H., Seykora, J.T., Liu, K.F., Capell, B. C. (2023) Mettl3-catalyzed m6A regulates histone modifier and modification expression in self-renewing somatic tissue. *Science Advances* DOI: 10.1126/sciadv.adg5234.

3.1. Introduction

Due to the limitations of the lethality of the *Mettl3*-eKO mice, we decided to continue to gain further insight into the underlying mechanisms Mettl3 and m^{6}A function in epithelial tissues by using human skin epidermis and an *in vitro* model of primary normal human epidermal keratinocytes (NHEKs). In the histology of human skin, we observed that METTL3 is present in the nuclei of keratinocytes, and its abundance decreased gradually from the basal stem-like progenitors to the terminally differentiated cornified layer (Fig. 10A). We also found that the global amount of m^{6}A present in mRNAs of differentiated keratinocytes was reduced when compared to the basal stem-like progenitors upon *in vitro* differentiation of NHEKs (Fig. 10B). Taking both results together, they suggest that higher levels of expression of METTL3 and m^{6}A are associated with a more stem-like progenitor cell state in keratinocytes, while reduced levels of both correlate with the more differentiated epidermal cells and layers. This is consistent with our *Mettl3*-eKO bulk RNA-seq data which suggested that *in vivo* deletion of *Mettl3* promoted a more differentiated and less progenitor-like transcriptional phenotype.

3.2. Results

3.2.1. Transcriptional analysis

We decided to look further into the GO analysis of the *Mettl3*-eKO mice bulk RNA-seq to see if we could elucidate a Mettl3-m^{6}A mechanism by which we are seeing such a dysregulation of epithelial tissues. To our surprise, the GO categories of "RNA Modification" and "Protein Modification Process" were upregulated **(**Fig 8B**)**. This was intriguing due to the emerging role of Mettl3 and m^{6}A being shown to play in the regulation of epigenetic modifiers in a context-specific fashion (*57*) (also mentioned above in 1.2.4.).

In the "Protein Modification Process" category, transcripts of numerous chromatin modifiers, and in particular, histone methyltransferases (writers) were abundant (Fig 8D**)**. These included four transcripts of H3K4 methyltransferases, *Setd1a*, *Setd1b*, *Kmt2b* (*Mll2*) and Kmt2d (*Mll4*), as well as transcripts of methyltransferases for H3K36 (*Setd2*), H3K9 (*Setdb1*), and H3K79 (*Dot1l*) (Fig. 8D). This was particularly interesting, since it has been shown that reduction of H3K4me3 by KMT2B knockdown could reduce *TGM1* in primary normal human epidermal keratinocytes (NHEKs). Additionally, KMT2D knockdown caused a reduction of *SPRR2B*, suggesting that these H3K4 methyltransferases may activate many genes involved in different stages of keratinocyte differentiation (*113*). Supporting this hypothesis on how H3K4 methyltransferases affect epidermal differentiation, a study has demonstrated the importance of Kmt2d (Mll4) in promoting epidermal differentiation and tumor suppression *in vivo* (*114*), while on the other hand, enzymes that remove H3K4 methylation (erasers) can suppress the expression of terminal epidermal differentiation genes (*115*). Finally, this wide-ranging upregulation of

numerous chromatin modifying enzymes and histone methyltransferases demonstrated that a loss of Mettl3 may function to promote extensive gene expression alterations, and consequently gross phenotypic abnormalities, through extensive disruption of chromatin and epigenetic state.

Next, we used the NHEK cell model and performed m^6A-sequencing (m^6A-seq) to map m^6A across all the mRNAs in the transcriptome. As previously reported in other cell systems, m^6A in the epidermal transcriptome is enriched in DRACH motifs (Fig. S8A). After calling common m^6A peaks across all human donor samples, we performed GO analysis to identify any enriched categories of m^6A-modified mRNAs within the epidermal progenitors. Interestingly, just like in the bulk RNA-seq data in our mice, our human model m^6A-seq was enriched in categories representing epigenetic modifications, such as “Peptidyl-lysine Modification”, “Macromolecule methylation”, “Histone Modification”, and “Chromatin Organization” (Fig. 10C). Within these GO categories we found many of the same H3K4 methyltransferase (writer) transcripts as the bulk RNA-seq, such as *SETD1A*, *SETD1B*, *KMT2B*, and *KMT2D* (Fig. 10D).

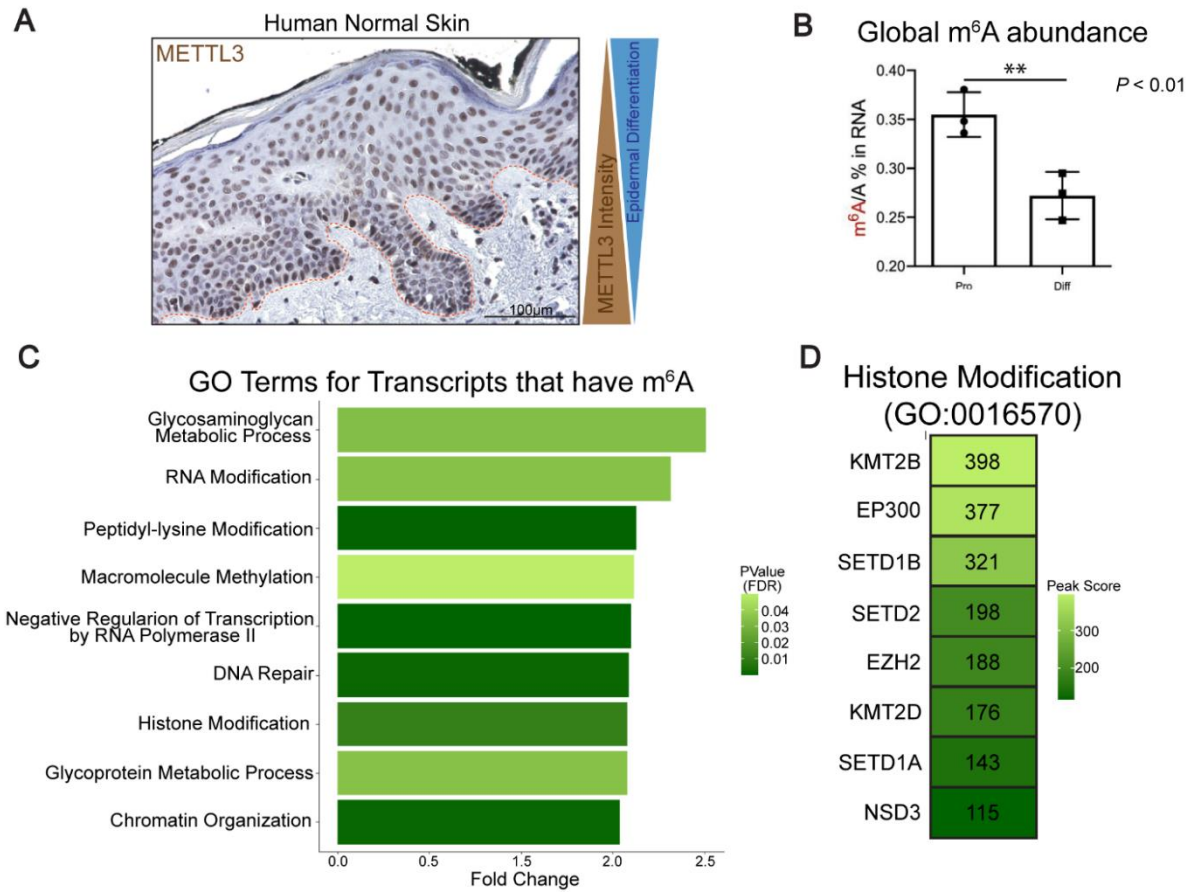

Figure 10. METTL3-mediated m^{6}A is present in epidermal mRNAs.

(A) IHC of METTL3 in normal human skin, where above the dotted line is the epidermis. (B) Quantitative analysis of the m^{6}A level by LC-MS/MS done in proliferating vs differentiated neonatal human epidermal keratinocytes (NHEKs) demonstrates reduced global m^{6}A with differentiation. (C) METTL3 siRNA reduces visible m^{6}A in NHEKs. (D) GO analysis of transcripts which contain m^{6}A peaks enriched in epidermal progenitors.

3.2.1. Continued…

To continue with our quest to elucidate a METTL3-m^{6}A mechanism we knocked down *METTL3* in keratinocytes via siRNA since a full knockout made the cells die due to it being embryonic lethal (*94*)**.** When we confirmed that *METTL3* knockdown in keratinocytes displayed global reductions in METTL3 and m^{6}A (Fig. 11A**,** S8B), we did an m^{6}A-seq to further explore which epidermal transcripts lose m^{6}A upon METTL3 depletion. By performing GO analysis on transcripts that displayed a significant reduction in m^{6}A with siRNA *METTL3* knockdown, we saw once again that mRNAs pertaining to the biological process GO categories of "Histone Methylation", "Histone Modification", and "Chromatin organization" were particularly enriched for a loss of m^{6}A (Fig. 11B). Remarkably, all these epigenetic modifiers were amongst the 377 transcripts that displayed both reduced m^{6}A and increased mRNA abundance with METTL3 depletion (Fig. 11C). On the other hand, only 152 transcripts that lost m^{6}A also showed reduced mRNA expression (Fig. S8C). When doing looking directly at the UCSC tracks of these m^{6}A changes, it was demonstrated that the intensity of m^{6}A enrichment had decreased substantially in the transcripts of *SETD1A, SETD1B, KMT2B* and *KMT2D* in long internal exons, stop codons and/or 3'UTRs (Fig. 11D). This data suggests that METTL3-mediated m^{6}A is directly regulating the abundance of these H3K4 methyltransferase (writer) mRNAs. In contrast, canonical keratinocyte genes associated with either the progenitor state (for example *COL17A1*) or the differentiated state that were dysregulated with *Mettl3* deletion did not display m^{6}A enrichment or loss (Fig. S9). Leading us to think that their dysregulation is a secondary effect of the epigenetic dysregulation in the epidermal keratinocytes.

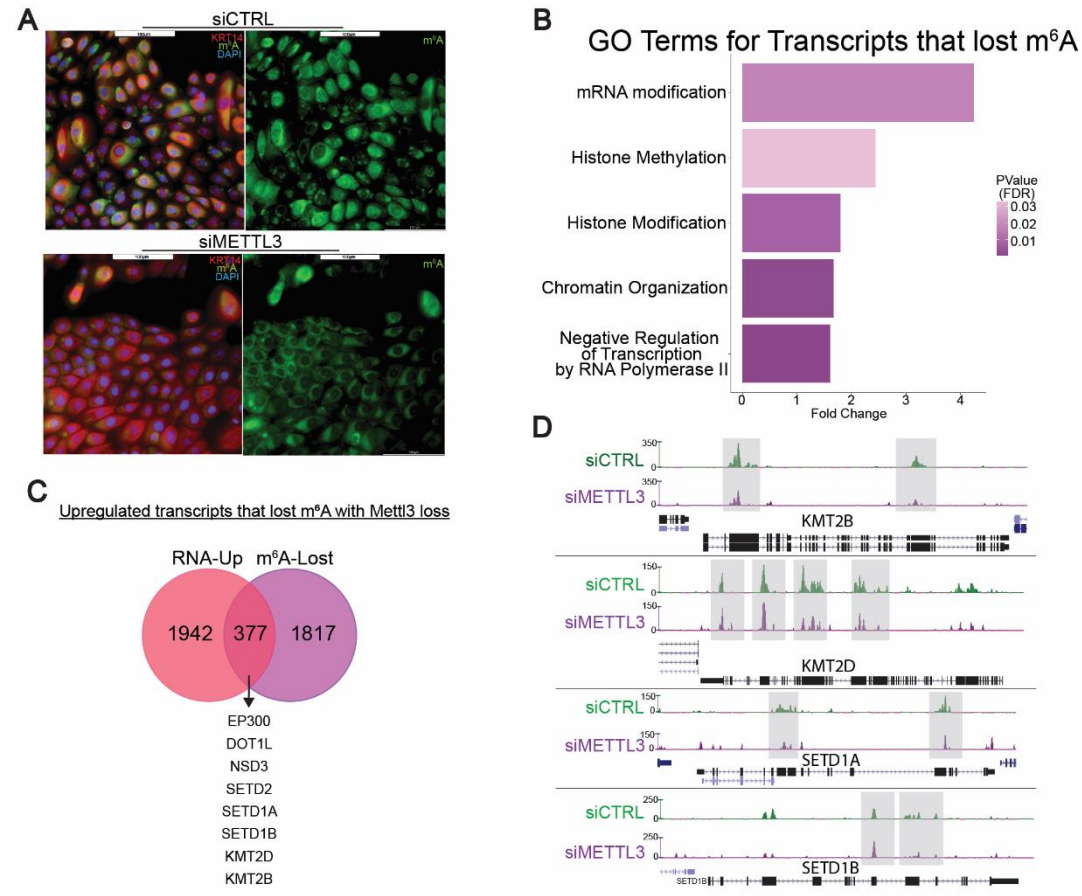

Figure 11. METTL3-mediated m^{6}A dynamically regulates chromatin modifier mRNAs in epithelia.

(A) Representative transcripts of the "Histone Modification" GO:BP category. (B) GO analysis of transcripts which contain m^{6}A peaks which are lost with siRNA depletion of METTL3. (C) Overlap of the upregulated transcripts by RNA-seq (pink) and transcripts that lost m^{6}A peaks with METTL3 depletion (purple). (D) UCSC Genome Browser on Human (GRCh37/hg19) tracks from the m^{6}A-seq analysis to visualize the decrease of m^{6}A peaks in representative "Histone Modification" transcripts in control (green) and METTL3-depleted NHEKs (purple).

3.2.2. mRNA degradation assays

Given our m^6A-seq and bulk RNA-seq data demonstrating that a loss of METTL3-mediated m^6A on chromatin modifying enzyme transcripts was associated with the mRNA's increased expression, we wanted to test whether METTL3 depletion was affecting the degradation of these transcripts since m^6A destabilizes and promotes the degradation of the mRNA via its readers (*46-49*). To do this, we utilized an mRNA turnover assay (*116*), which measures mRNA stability following the inhibition of transcription by Actinomycin D. Inhibiting the synthesis of new mRNA allows researchers to measure of mRNA decay by measuring mRNA abundance (*117*). Using this approach, we measured the mRNA half-life of the *KMT2B*, *KMT2D*, *SETD1A* and *SETD1B* transcripts in *METTL3* knocked down epidermal progenitors by siRNA for a transient knockdown and by shRNA for a more constitutive one. Additionally, to test whether the dysregulation of these H3K4 methyltransferases (writers) were due directly to the depletion of m^6A over these transcripts (in contrast to some other non-catalytic function of METTL3, like the one proposed in chronic myeloid leukemic cells in which METTL3 goes to the cytoplasm and regulates ribosome levels and translation indirectly (*118*)), we used a highly specific catalytic inhibitor of METTL3 (STM2457). STM2457 showed no evidence of disrupting the METTL3/METTL14 complex. STM2457 is highly specific for METTL3 and showed no inhibition of other RNA methyltransferases (*119*). Upon treating HEK293T and HeLa with the METTL3 inhibitor, there is drastic reduction in the overall m^6A methylation level of the transcriptome (*120*). (Fig. S10).

STM2457 potently and significantly reduced global m^6A levels and generally recapitulated the gene expression changes observed in our *Mettl3*-eKO mouse model in the epidermal progenitors following just 48 hours of exposure (Figs. S11A and S11B). Upon METTL3-mediated m^6A inhibition, we observed that *KMT2B, KMT2D*, *SETD1B* and *SETD1A* transcripts have evidence of a longer mRNA half-life (Figs. 12 and S11). Similar trends were observed using the genetic Metttl3 knockdown studies with both siRNAs and shRNAs (Figs. S12A and S12B). While not all results reached statistical significance in every case, the trends were consistent across the differing systems and contrasted sharply with other dysregulated transcript that did not display similar patterns, such as collagen genes that lost expression in the *Mettl3*-eKO mice. These results suggest that a complete depletion of m^6A is needed to observe the enhanced stability of H3K4 methyltransferases (writers) in epidermal keratinocytes. Collectively, these data supported a model whereby the loss of METTL3-mediated m^6A is leading to reduced degradation of chromatin modifier mRNA transcripts.

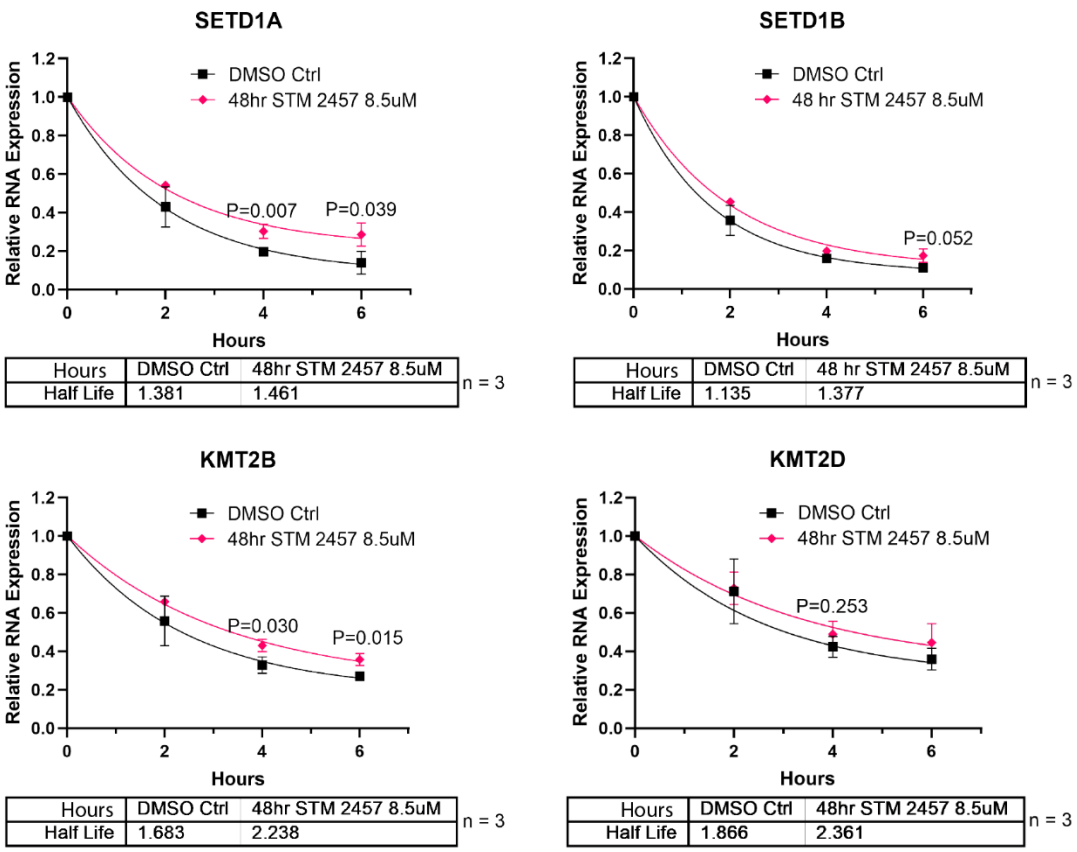

Figure 12. METTL3 loss increases mRNA half-life of chromatin modifiers.

mRNA turnover assay to measure the mRNA half-life transcripts in epidermal progenitors demonstrates prolonged half-life of *SETD1A*, *SETD1B*, and *KMT2B* transcripts with METTL3 depletion. *KMT2D* transcript shows a trend of prolonged half-life with METTL3 depletion. Transcripts were normalized by *GAPDH*.

3.2.3. Protein analysis

Given the longer half-life mRNA of the H3K4 methyltransferases, we next asked whether these increases in transcript levels are also seen at the protein level due to the reduced mRNA degradation. We examined Setd1a (also known as Kmt2f) given its abundant expression in human skin as per the Human Protein Atlas (Fig. S13), as well as its essentiality for early mouse embryonic development (*121*). High molecular western blotting shows an upregulation of Setd1a protein levels in *Mettl3*-eKO mice in comparison to littermate controls (Fig 13A, B). Subsequently, we stained the skin of the mice to see the expression of Setd1a. Intriguingly, the epidermis of *Mettl3*-eKO mice confirmed the increased expression of Setd1a, but also noted that it was particularly enriched in the basal epidermal progenitors of the *Mettl3*-eKO mice, while in littermates Setd1a is largely absent from the basal keratinocytes (Fig 13C).

Since Setd1a is one of the major H3K4me1/2/3 methyltransferases in mammals (*122*), we next interrogated levels of H3K4me2 (which marks the gene body for activation) and H3K4me3 (which primarily marks transcription start sites) (*123, 124*). Consistent with the increased expression of multiple H3K4 methyltransferases mRNAs including the Setd1a transcript and protein, we found increased levels of both (H3K4me2 and me3) modifications throughout the epidermis in *Mettl3*-eKO mice compared to littermate controls (Figs. 13D, E). Interestingly, similar to the Setd1a expression in *Mettl3*-eKO mice, we saw a particular enrichment of the modifications in the basal epidermal keratinocytes in comparison to littermate controls (Figs. 13D, E).

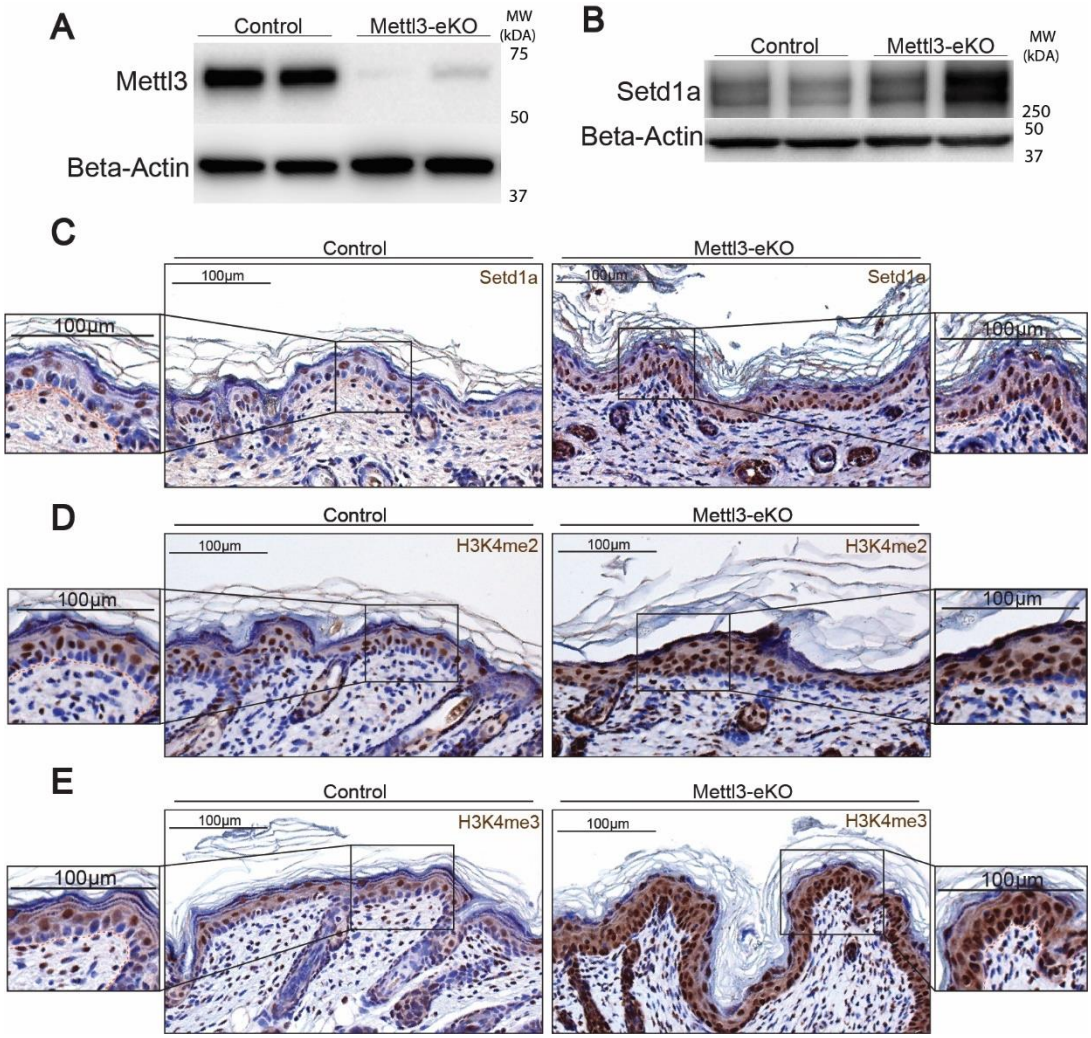

Figure 13. METTL3 loss increases expression of chromatin modifiers and their histone modifications.

(A) Immunoblotting of Mettl3 in control vs *Mettl3*-eKO P6 mouse epidermis. (B) High molecular western blot for Setd1a in P6 mice epidermis. (C) IHC for Setd1a in P6 mice epidermis. (D) IHC for H3K4me2 in P6 mice epidermis. (E) IHC for H3K4me3 in P6 mice epidermis.

3.3. Discussion

All together, these data suggest a model whereby METTL3-catalyzed m^6A on H3K4 methyltransferase transcripts promotes their degradation. When METTL3 is absent, m^6A is lost on these mRNAs and their reduced degradation and longer half-life leads to their increased transcript levels possibly leading to increased levels in protein abundance. This increase in H3K4 methyltransferase mRNAs and protein levels ultimately results in both extensive epigenetic and phenotypic dysregulation (Fig. 14). Remarkably, enzymes that remove H3K4 methylation (i.e. histone demethylase or eraser: LSD1) have been shown to repress differentiation (*115*), while enzymes that catalyze H3K4 methylation (i.e. KMT2D/MLL4) have been shown to promote epidermal differentiation (*113, 114, 125*). The increased expression of these chromatin modifiers and the resulting increased H3K4 methylations in basal epidermal keratinocytes can promote an atypical activation of terminal differentiation genes and thus consequently losing the progenitor state. This model is consistent with the emerging data of recent studies demonstrating the existence of extensive crosstalk between epitranscriptomics and epigenetics (*57*).

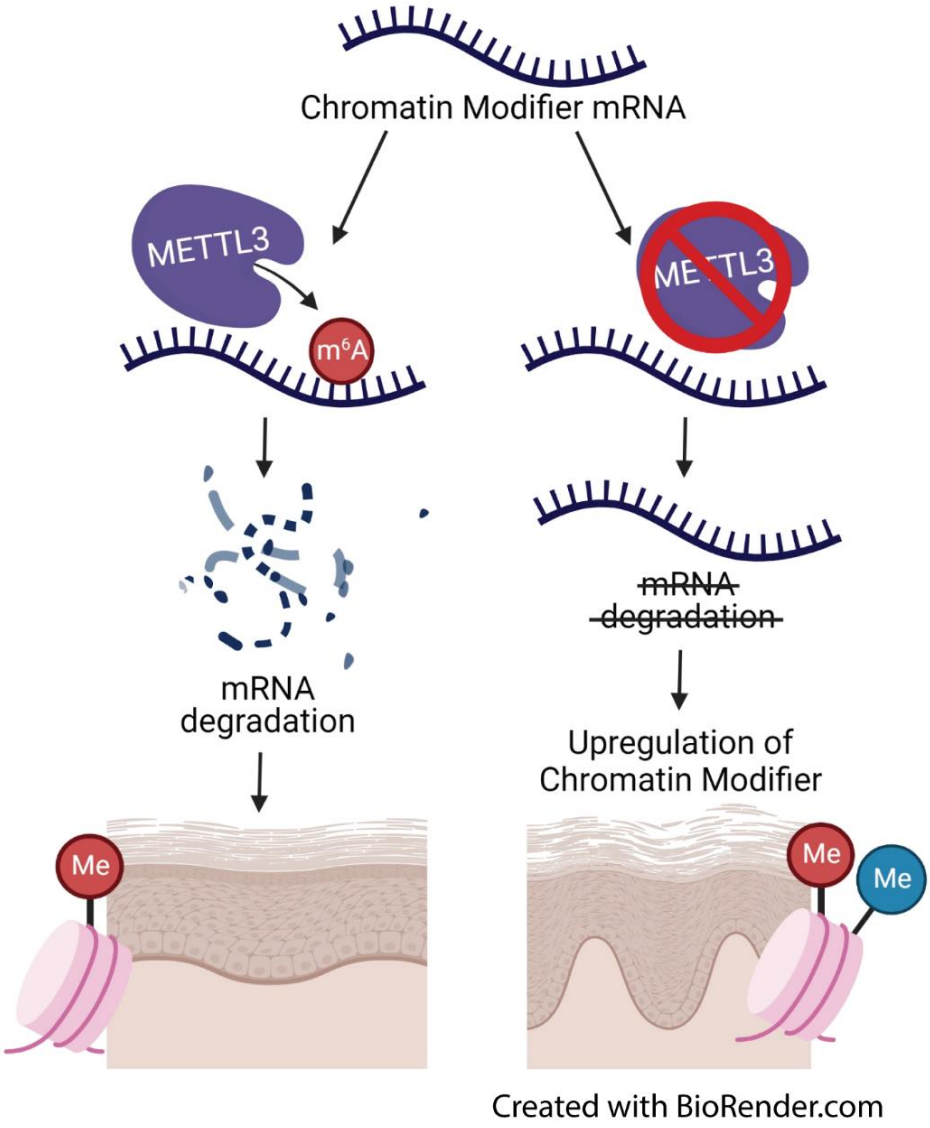

Figure 14. Schematic of METTL3-mediated m^{6}A gene regulation in self-renewing stratifying epithelial tissues.

Loss of the METTL3-m^{6}A epitranscriptome promotes the upregulation of chromatin modifiers by increasing their mRNA half-life and enhancing their transcripts' translation. This upregulation of chromatin modifiers, and thus histone modifications, in turn, deregulate proper epidermal development and differentiation.

3.4. Supplemental information

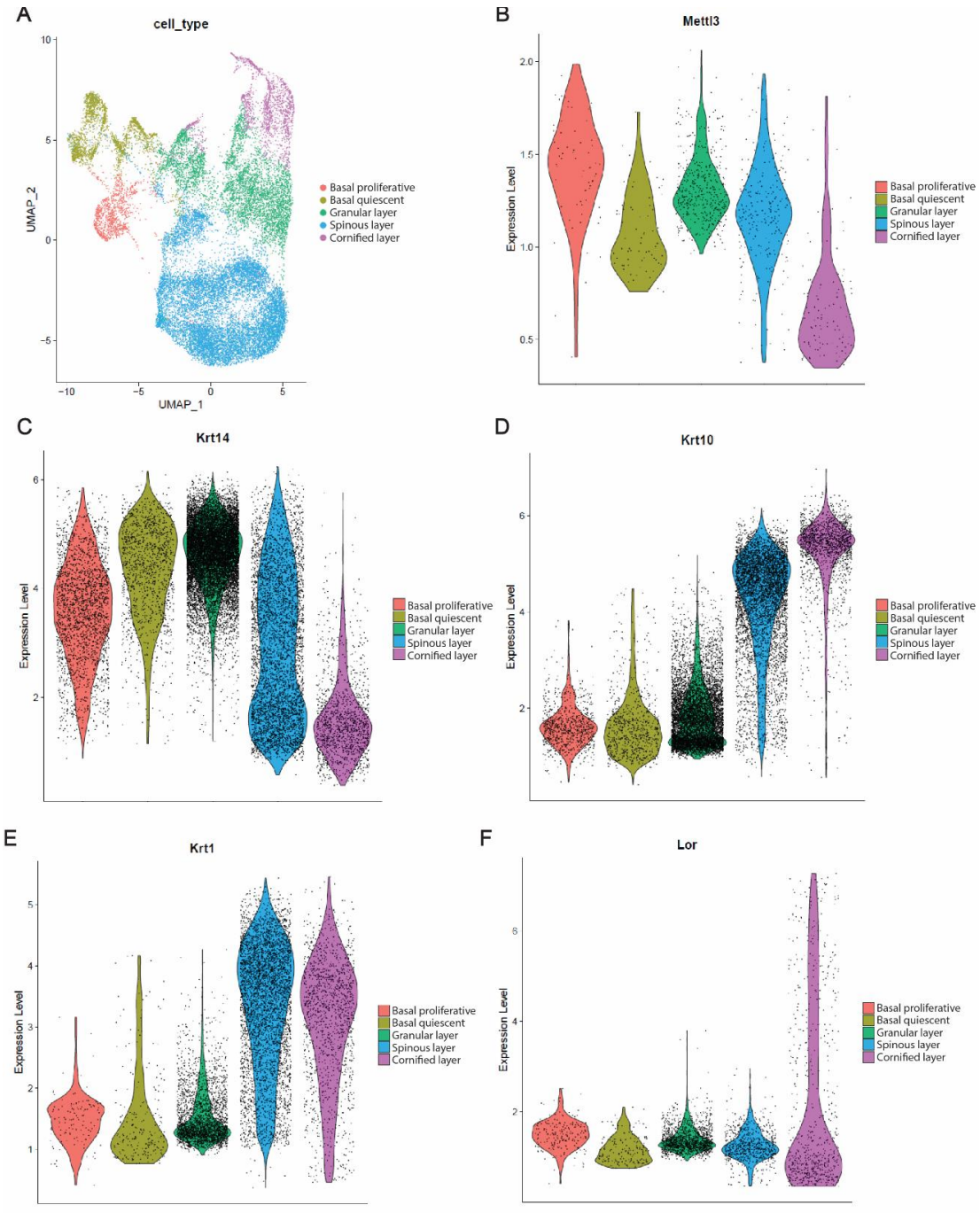

Figure S6. *Mettl3* distribution in murine epidermal keratinocytes.

(A) Epidermal cell types identified in mice in a UMAP projection of public scRNA-seq data. (B-D) Violin plots show gene expression in cells on the single-cell level. Each dot represents a single mouse keratinocyte. Statistically significant gene expression is observed only if a violin-shaped fitting area can be calculated. (B) *Mettl3* expression is reduced in the more differentiated cornified layer in comparison to the basal and suprabasal layers of the epidermis. (C) *K14* is expressed on all basal and suprabasal layers of the epidermis. (D) *K10* expression is increased with differentiation. (E) *K1* expression is increased with epidermal differentiation. (F) *Lor* is present in the most differentiated layer of the skin, the cornified layer.

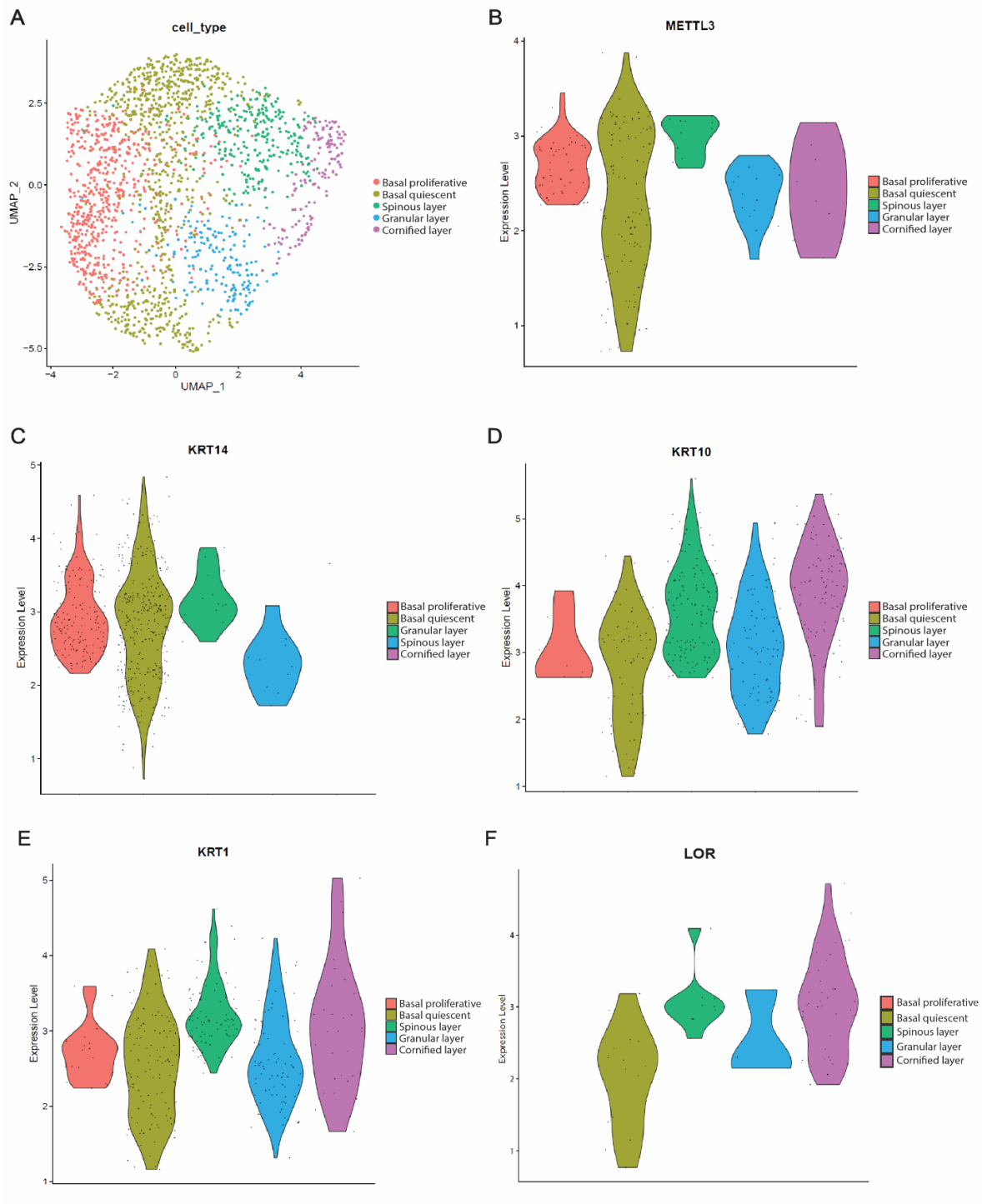

Fig. S7. *METTL3* distribution in human epidermal keratinocytes.

(A) Human epidermal cell types identified in a UMAP projection of public scRNA-seq data. (B-D) Violin plots show gene expression in cells on the single-cell level. Each dot represents a single human keratinocyte. Statistically significant gene expression is observed only if a violin-shaped fitting area can be calculated. (B) *METTLl3* expression is reduced in the more differentiated cornified layer in comparison to the basal and suprabasal layers of the epidermis. (C) *K14* is expressed on all basal and suprabasal layers of the epidermis. (D) *K10* expression is increased with differentiation. (E) *K1* expression is increased with epidermal differentiation. (F) *LOR* is present in the most differentiated layer of the skin, the cornified layer.

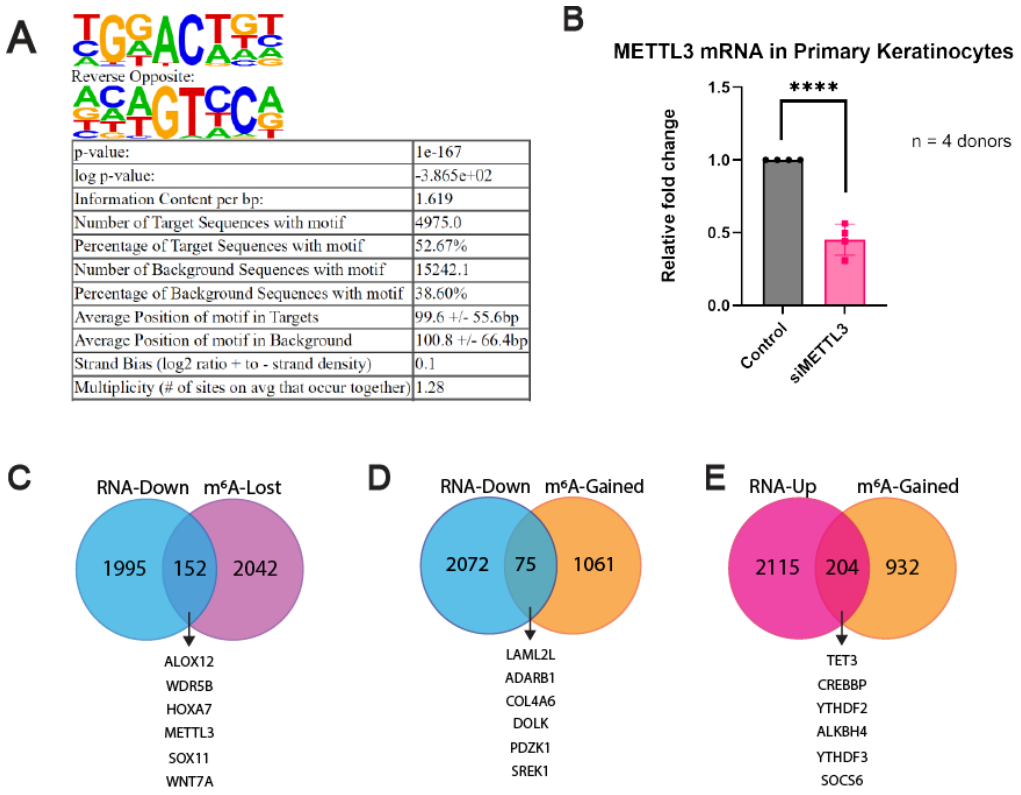

p-value:	1e-167
log p-value:	-3.865e+02
Information Content per bp:	1.619
Number of Target Sequences with motif	4975.0
Percentage of Target Sequences with motif	52.67%
Number of Background Sequences with motif	15242.1
Percentage of Background Sequences with motif	38.60%
Average Position of motif in Targets	99.6 +/- 55.6bp
Average Position of motif in Background	100.8 +/- 66.4bp
Strand Bias (log2 ratio + to - strand density)	0.1
Multiplicity (# of sites on avg that occur together)	1.28

Figure S8. METTL3-m^{6}A dynamics in epidermal keratinocytes.

(A) HOMER-identified enriched motifs for m6 A peaks in proliferating epidermal progenitors (normal human epidermal keratinocytes, or NHEKs). (B) RT-qPCR for *METTL3* demonstrating knockdown with siMETTL3 treatment. (C) Overlap of transcripts that demonstrate a concomitant loss of mRNA expression by RNA-seq (blue) as well as a significant reduction in m^{6}A enrichment by m^{6}A-seq (purple) with depletion of METTL3. (D) Overlap of transcripts that demonstrate a concomitant loss of mRNA expression by RNA-seq (blue) as well as a significant gain in m^{6}A enrichment by m^{6}A-seq (orange) with depletion of METTL3. (E) Overlap of transcripts that

demonstrate a concomitant gain of mRNA expression by RNA-seq (pink) as well as a significant gain in m^{6}A enrichment by m^{6}A-seq (orange) with depletion of METTL3.

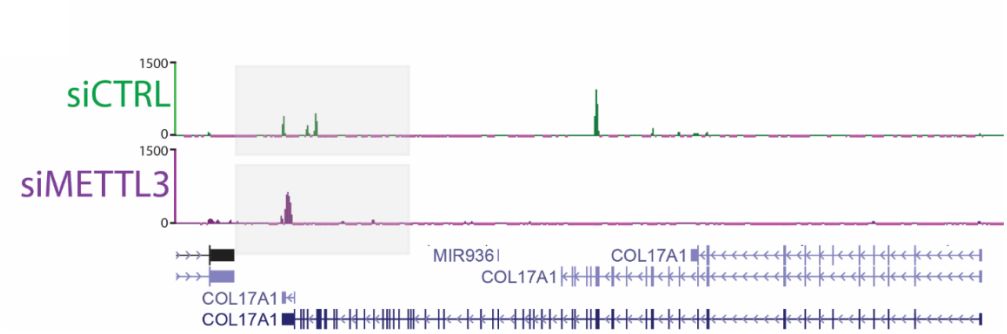

Figure S9. METTL3-dependent m^{6}A does not affect the regulation of *COL17A1*.

UCSC Genome Browser on Human (GRCh37/hg19) tracks from the m^{6}A-seq analysis to visualize the m^{6}A peaks in the *COL17A1* transcript in control (green) and METTL3-depleted NHEKs (purple).

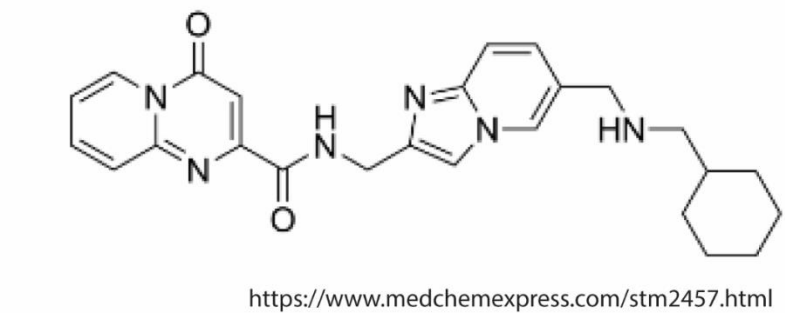

Figure S10. Chemical structure of STM2457.

STM2457 is a potent inhibitor of METTL3/METTL14 catalytic activity. It works by doing a co-factor competitive binding to the SAM binding site of the METTL3/METTL14 heterodimer in the

METTL3 catalytic enzyme. STM2457 is highly specific for METTL3 and showed no inhibition of other RNA methyltransferases (*119*).

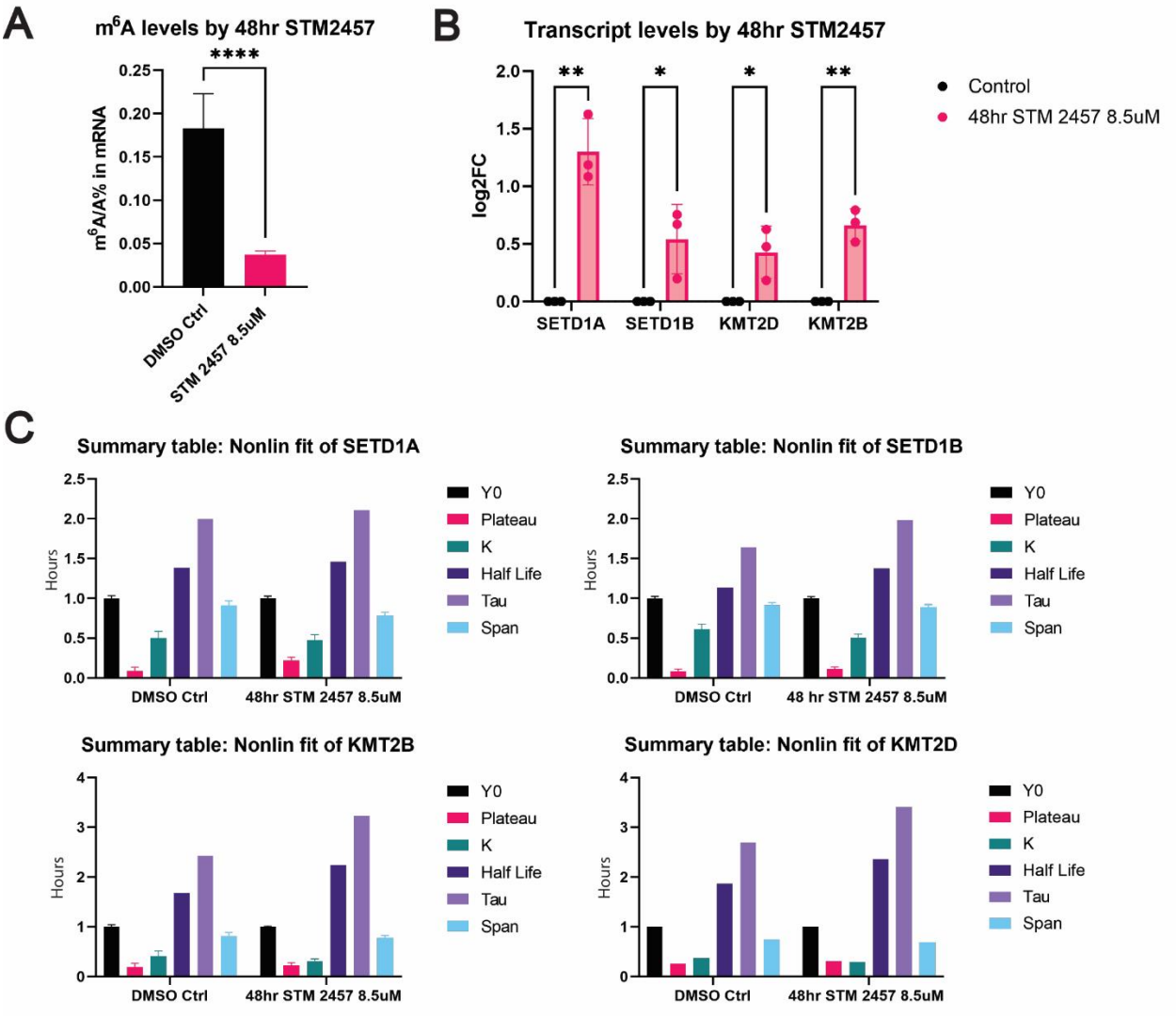

Figure S11. H3K4 methyltransferases' mRNA half-life are dysregulated with METTL3 loss.

(A) Quantitative analysis of the m^6A level by LC-MS/MS done in NHEKs demonstrates reduced global m6A with METTL3 catalytic inhibition by STM2457 treatment. (B) RT-qPCR was done in

STM2457-treated NHEKs vs. DMSO vehicle control at the 6hr timepoint. A log2 Fold Change of ± 0.5 and an adjusted p-value of <0.05 was done to visualize the significant changes that recapitulate what is seen in the bulk RNA-seq done in *Mettl3*-eKO epidermis. Transcripts were normalized by *GAPDH*. (C) Non-linear, one phase decay fit summary that was used to calculate mRNA half-life (t1/2) of *SETD1A*, *SETD1B*, *KMT2B* and *KMT2D*. (D) RT-qPCR for METTL3 shows METTL3 knockdown when treated with siRNA or shRNA treatment (siMETTL3 KD and shMETTL3 KD were added to make METTL3-KD).

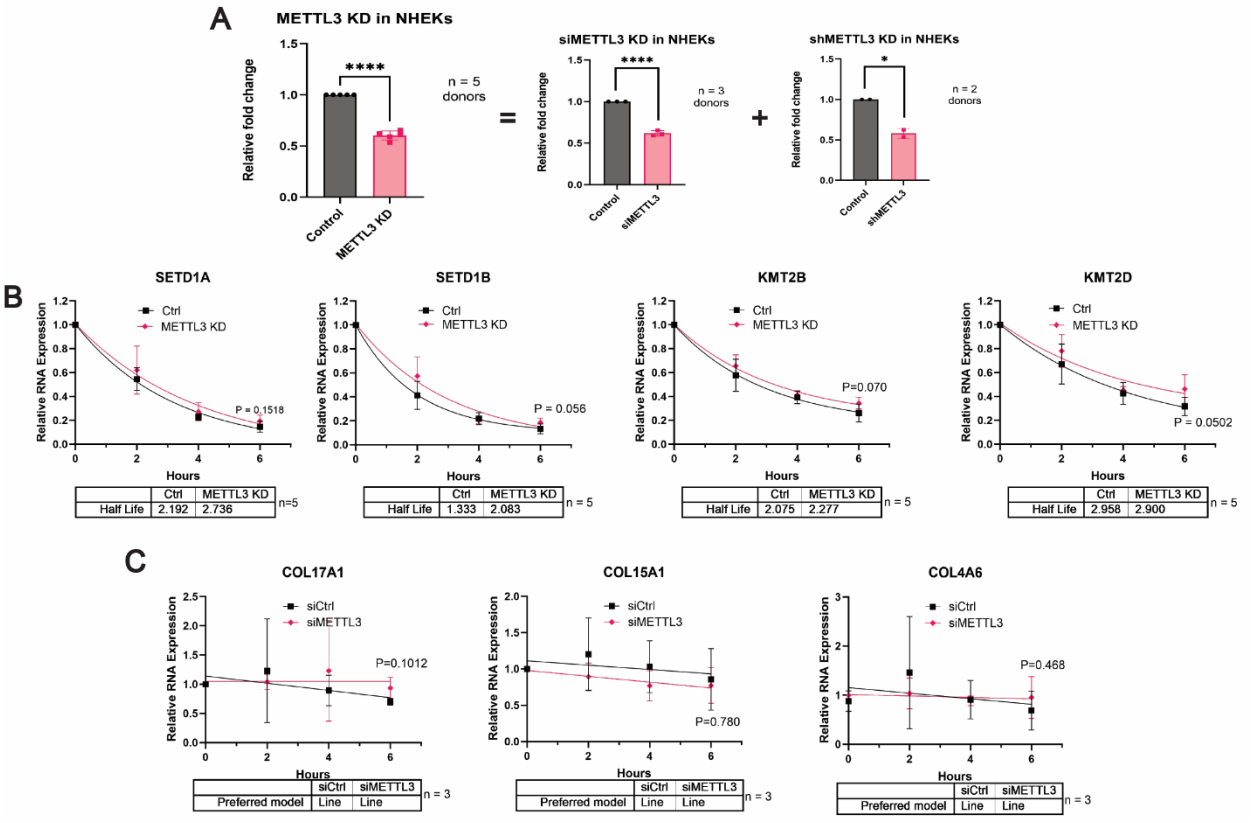

Figure S12. mRNA half-life is dysregulated with METTL3 loss.

(A) RT-qPCR for METTL3 shows METTL3 knockdown when treated with siRNA or shRNA treatment (siMETTL3 KD and shMETTL3 KD were added to make METTL3-KD). (B) mRNA turnover assay to measure the mRNA half-life transcripts in epidermal progenitors demonstrates a trend in prolonged half-life of *SETD1A, SETD1B, KMT2B* and *KMT2D* transcripts with METTL3 depletion. Transcripts were normalized by *GAPDH*. (C) mRNA turnover assay to measure the mRNA half-life transcripts of *COL17A1*, *COL15A1* and *COL4A6* in NHEKs with METTL3 depletion show that the transcripts follow a linear model instead of a one phase decay model, meaning that the transcripts are stable and not undergoing mRNA degradation. Transcripts were normalized by *GAPDH*.

Figure S13. SETD1A distribution in human epidermis.

IHC staining of H3K4 methyltransferase SETD1A enzyme in human epidermis obtained from the Human Protein Atlas.

3.5. Materials and Methods

2D Cell Culture

Proliferating primary Normal Human Epidermal Keratinocytes (NHEKs, or epidermal progenitors) cells were isolated from de-identified discarded neonatal foreskin provided by Core B - Skin Translational Research Core (STaR) of the Penn Skin Biology and Diseases Resource-based Center (NIH P30-AR069589). NHEK medium: filtered 50:50 mix of 1x keratinocyte serum-free medium (keratinocyte-SFM) supplemented with human recombinant epidermal growth factor and pituitary extract combined with medium 154 supplemented with human keratinocyte growth supplement (HKGS) and 1% 10,000 U/mL penicillin-streptomycin. Incubator: 37°C with 5% CO2. Proliferating NHEKs were cultured in NHEK medium under normal incubating conditions. Differentiating NHEKs arise from seeding proliferating NHEKs in NHEK medium for the first 24 hours after seeding and then changing the NHEK medium containing 1.22mM Calcium chloride (CaCl2) for 72 hours.

siRNAs

Proliferating NHEKs cells cultured in penicillin-streptomycin free NHEK media and 24 hours later add the scrambled control siRNAs (siCTRL) or the siRNAs against *METTL3* (siMETTL3) at 500nM dose for 72 hours under normal incubation conditions, changing to fresh penicillin-streptomycin free medium at 48 hours to prevent cell differentiation. Cells were harvested 72 hours after transfection.

RT-qPCR

Complementary DNA was obtained using a high-capacity RNA-to- DNA kit (#4368814, Thermo Fisher Scientific). For quantitative real-time PCR, Power SYBR Green PCR Master Mix (#4367659, Thermo Fisher Scientific) was used. Quantitative real-time PCR data analysis was performed by first obtaining the normalized cycle threshold (CT) values (normalized to beta-actin and gapdh RNA), and the $2 - Ct$ method was applied to calculate the relative gene expression. ViiA 7 Real-Time PCR System was used to perform the reaction (Applied Biosystems). The average and SDs were assessed for significance using a Student's t test. All P are noted in the figure legends and were considered significant if $P < 0.05$ and nonsignificant (NS) if $P > 0.05$.

shRNAs

We generated stable fresh *METTL3* knock down in proliferating NHEKs cell-lines and, after 2 or 3 passages to avoid compensatory mechanisms of loss of knockdown, we performed experiments.

mRNA turnover assay

To assess the half-life of mRNA, Actinomycin D was used to treat the proliferating NHEK cells after shRNA knockdown. After the treatment, mRNA expression level at 0, 2, 4 and 6 h was analyzed via RT-qPCR following. Half-life statistics were done by doing non-linear analysis of a one phase decay model (*116*).

Quantitative analysis of the m^6A level via LC-MS/MS

The PolyA+ RNA was extracted from total RNA using the Dynabeads mRNA Purification Kit (Ambion) following the manufacturer's instructions. Purified RNA was digested and dephosphorylated to single nucleosides using Nucleoside Digestion Mix (NEB, M0649S) at 37 °C for 1 h. The detailed procedure was as previously described (*126*). The nucleosides were quantified using retention time and the nucleoside-to-base ion mass transitions of 282.1 to 150.1 (m^6A) and 268.0 to 136.0 (A). All quantifications were performed by converting the peak area from the LC-MS/MS to moles using the standard curve obtained from pure nucleoside standards running with the same group of samples. Then, the percentage ratio of m^6A to A was used to compare the different modification levels.

m^6A-seq

Total RNA was extracted using the Qiagen RNeasy Mini kit (Cat No./ID: 74104). The following protocol was performed with 35-50ug of total RNA. mRNA was purified with Dynabeads mRNA purification kit (Invitrogen Catalog No. 61006). Fragmentation of the mRNA was performed using the Ambion RNA fragmentation reagents (Catalog #: AM8740). Then subjected to the RNA Clean and Concentrator-5 (Catalog No. R1013 from Zymo Research). mRNA quality was checked by Aligent BioAnalyzer 2100 using the RNA 6000 Pico Kit (Part number 5067-1513). One round of m^6A immunoprecipitation was performed using the EpiMark *N6*-Methyladenosine Enrichment Kit (NEB #E1610S) and protocol. m^6A-seq libraries were prepared using the NEBNext Ultra Directional RNA library preparation kit for Illumina (NEB

#E7760). Library quality was checked by Agilent BioAnalyzer 2100 using the High Sensitivity DNA kit (Part number 5067-4626) and libraries were quantified using the Library Quant Kit for Illumina (NEB #7630). Libraries were then sequenced using a NextSeq500 platform (75-base-pair (bp) single-end reads). All kits were used following the manufacturer's instructions.

m^6A-seq data processing

First, sequence quality was verified using fastqc. We used bowtie2 to map reads to the human genome (hg38) with default parameters. Then, bedtools were used to remove the reads that contained low quality bases (MAPQ < 10) and undetermined bases. Mapped reads of IP and input libraries were processed by macs2 callpeak function, which identifies m^6A peaks with bed or bam format that can be adapted for visualization on the UCSC genome browser. We called the peaks using the threshold of FDR < 0.05, no shifting model building, extension-size of 200bp and the removal of duplicates. HOMER is used for both the annotation of the called peaks and the de novo and known motif finding followed by localization of the motif with respect to peak summit. The differentially expressed peaks were selected with an absolute value of a fold change > 2 (and P < 0.05) by R package deseq2 (*112*). Specifically for the motif analysis, HOMER was used for the de novo and known motif finding by perl scripts. In particular, we specified the motif finding size parameter in findMotifsGenome.pl to 200 bp. We sorted the predicted motif in the Supplementary Fig. S8B. According to the p-value, the smaller the p-value, the higher the rank. The most reported motif structures are RRACH (where R = A or G, H = A, C or U). The differential m6A peaks were characterized by the GGACT motif, which is the first rank motif structure from the merged prosiCtrl sample.

Gene Ontology (GO) analyses

All GO analyses were performed using PANTHER at http://pantherdb.org/ to determine statistically overrepresented GO terms using Fisher's exact test under the category "biological process." P values for GO terms are false discovery rate statistics. GO term figures are generated using ggplot2.

Immunoblotting

Samples were separated by electrophoresis in 4 to 20% SDS–polyacrylamide gel electrophoresis gels with 30 ug per lane, transferred to a polyvinylidene difluoride membrane, and blotted with antibodies. Secondary horseradish peroxidase–conjugated secondary antibodies (Santa Cruz Biotechnology) and Amersham ECL Prime Western Blotting Detection Reagents (catalog no. RPN2232, GE Healthcare) were used for detection.

High molecular weight immunoblotting

Samples were separated by electrophoresis in 3 to 18% Tris-Acetate gel electrophoresis gels with 30 ug per lane, transferred to a polyvinylidene difluoride membrane, and blotted with antibodies. Secondary horseradish peroxidase–conjugated secondary antibodies (Santa Cruz Biotechnology) and Amersham ECL Prime Western Blotting Detection Reagents (catalog no. RPN2232, GE Healthcare) were used for detection.

STM2547 treatment

Proliferating NHEKs cells cultured in NHEK media and 24 hours later DMSO (vehicle control) or STM2457 (Selleck, #S9870) at 8.5uM was added for 48 hours under normal incubation conditions. Cells were harvested 48 hours to investigate METTL3 catalytic inhibition.

Publicly available data

Human protein atlas IHC data derived from the Human Protein Atlas can be found at www.proteinatlas.org/. scRNA-seq data from the mice keratinocytes was derived from the Gene Expression Omnibus at https://www.ncbi.nlm.nih.gov/geo/. Mouse data was downloaded from GSE154679. Human scRNA-seq data used for the analyses described in this manuscript were obtained from the GTEx Portal dbGaP accession number phs000424.v9.

scRNA-seq analysis and filtering

scRNA-seq (*127*) datasets of human (*128*) and mouse (*129*) epidermis were previously published. Each dataset was individually filtered based on standard filtering before combining them using Seurat V4 62. First, exclusion of poorly sequenced cells with a low number of genes detected. Additionally, removal of cells that were likely to be doublets, characterized by a high number of genes was done by. Additional removal of doublets was done with a doublet finder (scDblFinder) to further filter doublets (*130*). Each individual dataset was then normalized, filtered for epidermal keratinocytes, and visualized with FindVariableFeatures, ScaleData and RunPCA. This was followed by RunUMAP (performing reductions with Harmony that significantly improve

batch effects (*131*), FindNeighbors, and FindClusters. Finally, selection and visualization via violin plots was conducted of *METTL3/Mettl3, K14, K10, K1* and *LOR/Lor* transcripts.

Statistical analyses

All statistical analyses were performed using R or GraphPad Prism 10. Details of each statistical test are included in Materials and Methods. Sample sizes and P values are included in the figure legends or main figures. Investigators were not blinded during experiments or outcome assessment.

Table 2. siRNAs, shRNAs and inhibitor utilized in this thesis.

Accell Human METTL3 siRNA -SMARTpool	Catalog ID: E-005170-00-0020
Accell Non-targeting siRNA #1	Catalog ID: D-001910-01-20
Sigma METTL3 shRNA	SKU: TRCN0000034717
Sigma pLKO.1-puro Non-Mammalian shRNA Control Plasmid DNA	SKU: SHC002
STM2457 - Selleck Chem	Catalog No: S9870

Table 3. Primers utilized for genotyping and RT-PCR in this thesis.

Mettl3 (mouse)	F' 5-AAGTGCTGCCATGTGAATGA-3 R' 5-TAAAGTGGAAAGGGTCAGTC-3
Keratin 14-Cre (mouse)	F' 5-GAACCTGATGGACATGG-3 R' 5-AGTGCGTTCGAACGCTAGAGCCTGT-3
METTL3 (human)	F' 5-CAAGCTGCACTTCAGACGAA-3 R' 5-GCTTGGCGTGTGGTCTTT-3

SETD1A (human)	F’ 5-TTGCCATGTCAGGTCCAAAAA-3 R’ 5-CGTACTTACGGCACATATCCTTC-3
SETD1B (human)	F’ 5-AGCGAGCTCCAGAACATGAC-3 R’ 5-ATGGGTGTGAGGCATCTGTG-3
KMT2D (human)	F’ 5-ATCCTGGAGACACCCATCAG-3 R’ 5-GACAGGCTCAGGGTCAGTG-3
KMT2B (human)	F’ 5-GGAGGAAGCAGCAAGCAGTA-3 R’ 5-GCTCAGGTTTGGGGATTGT-3
COL17A1 (human)	F’ 5-GCAGAGCTGAGTAGTCGCAT-3 R’ 5-AATTCAGACCCTCGCAGCAA-3
COL15A1 (human)	F’ 5-CTGGGAGTCCAGAGCTCATC-3 R’ 5-ATCAAGTGGAGGACCTGGTG-3
COL4A6 (human)	F’ 5-AAAGGAGCCAGAGGAGATCG-3 R’ 5-GAGGCCTCGAGACCCTTTAG-3
Beta-Actin (human)	F’ 5-TGAAGTGTGACGTGGACATC-3 R’ 5-GCAGGAGCAATGATCTTGAT-3
GAPDH (human)	F’ 5-ATCATCCCTGCCTCTACTGG-3 R’ 5-GTCAGGTCCACCACTGACAC-3

CHAPTER 4: CONCLUSIONS AND FUTURE DIRECTIONS

4.1. Conclusions and Future Directions, Chapter 2

In chapter 2, we studied the effect of *Mettl3* deletion in the epithelial tissues of the epidermis and filiform papillae in postnatal mice. Here, we discuss two major conclusions from this work, summarize their impact, as well as discuss future directions. Firstly, we see a major dysregulation in the development and differentiation of the epidermis. We did a bulk RNA-seq of the P6 *Mettl3*-eKO epidermis where we saw upregulation of keratinization transcripts such as *Krt6b, Sprr2d, Krt6a, Krt16, Krt17* and *Tgm1*, although this data could not tell us precisely in what layer of the epidermis they might be increasing. Even though single-cell RNA sequencing (scRNA-seq) allows researchers to study heterogeneity and dynamic change in eukaryotic cells, it doesn't provide information of transcriptional patterning and regulation in tissues that spatial transcriptomics would give (*132*). That is why we would benefit from doing spatial transcriptomics to dive deeper into the dysregulation of epidermal differentiation that Mettl3 depletion drives.

Our *Mettl3*-eKO mouse model, as well as in other *Mettl3* conditional knockout mice using a *K14*-Cre driver in past studies (*88, 90*), the mice also did not survive past a week of age. Therefore, the ability to inducibly delete Mettl3 in adult mice after development would be critical to further study potential alterations in keratinocyte differentiation. Notably, we have tried to develop a tamoxifen-inducible *K14*-CreERT^{tam} model (*92, 133*) to induce deletion of *Mettl3* in adulthood, but we have been unsuccessful. Even after trying different doses, timelines, and methods of tamoxifen delivery (topical, intraperitoneal [IP] injections, and diets) we were unable to observe more than 15% of *Mettl3* deletion in the epidermis. Our hypothesis is that basal cells

that are successfully floxing out *Mettl3* are being outcompeted by the cells that are not deleting *Mettl3* since the ones that can are differentiating prematurely and not proliferating enough to compete with cells that are able to maintain Mettl3 expression. A future direction would be to develop a new inducible model using a *K5*-CreERT^{tam} model instead of the *K14*-CreERT^{tam} because keratin 5 (K5) is a member of type II keratins and is expressed with its type I keratin partner K14 in the basal layer of stratified squamous epithelium which will recapitulate the progenitor populations that give rise to the suprabasal differentiated cells of stratified epithelia (*134*). Another alternative would be to switch our *Mettl3*$^{fl/fl}$ model to one that does not delete the whole *Mettl3* gene but only partially by only floxing out the fourth exon of the *Mettl3* gene (*88, 135*) or by floxing exons 2 and 3 of the *Mettl3* gene (*94*), as it has been shown that the Cre-loxP recombination efficiency decreases with increased size between loxP sites (*136, 137*)**.**

Building on this, the second conclusion is that the reason behind this postnatal death has not been explored. We did not see any obvious signs of trans-epidermal water loss (TEWL) nor any other defect in the epidermal permeability barrier that may be leading to premature death (*138*). Thus, we hypothesize that the cause of death is due to the dysregulated development of major epithelial tissues needed for survival such as the tongue since where we saw severe ulcerations in the *Mettl3*-eKO mice.

As discussed in Chapter 2, the dorsal lingual epithelium in *Mettl3*-eKO mice displayed severely impaired development of filiform papillae, as well as abnormal epithelial thickening which has been studied before (*90*). The novelty in our mouse model is that we observed that 80% of *Mettl3*-eKO mice were found to have full thickness ulcerations in the posterior part of the

tongue. Our hypothesis is that since there is a homeostatic dysregulation of the lingual epithelium that includes impaired expression of numerous cell adhesion genes, when the postnatal mice go to their mother to feed, the mechanical force of the feeding mechanism creates painful ulcerations in the tongue that incapacitate the pups from nursing and thus they die of malnutrition. Consistent with this, the histology shows an underdevelopment in the keratinization of the filiform papillae that is needed to withstand strong physical force (*139*). Therefore, to begin to investigate if the pups are nursing properly, we can consider examining all mice for the presence of a bright abdominal milk spot which indicates normal suckling behavior and nursing (*140*). If an absence of milk spot is encountered, an alternative approach to feeding would need to be implemented with new pups to study these mice beyond 6-7 days of life. For example, using cotton balls or covers soaked with milk could be a good alternative so the neonates can acquire their nutrients at least in an involuntary fashion (*141*). By using milk-soaked cotton balls, the pups would not have to go through the normal suckling behavior and thus avoid any mechanical ulcerations, potentially surviving past the first week of life. If the pups survive more than seven days, we could then start characterizing lingual and epidermal development and differentiation past the neonatal stage.

Together, these observations and proposed *in vivo* experiments call for a more comprehensive understanding and characterization of the role of Mettl3 during epidermal development and homeostasis in postnatal and adult mice.

4.2. Conclusions and Future Directions, Chapter 3

In chapter 3, we studied the effect of *METTL3* knockdown, and subsequent m^6A loss, in regulating chromatin modifiers. Here, we discuss two major conclusions from this work,

summarize their impact, as well as discuss future directions. Firstly, H3K4 methyltransferase transcripts are more stable and degrade at a lower rate when m^6A is depleted from proliferating keratinocytes**.** By doing genetic knockdown of *METTL3* as well as a catalytic inhibition of METTL3 *in vitro* for our mRNA degradation assays, we are confident that the destabilization of histone modifiers is due to m^6A that is written by METTL3 instead of through an alternative non-catalytic mechanism of METTL3. Due to this increased stabilization of the H3K4 methyltransferase transcripts and the increased staining of the SETD1A protein and its subsequent histone marks in the *Mettl3*-eKO mouse epidermis, we conclude that m^6A plays a role in the degradation of the methyltransferases demonstrating the regulation of the histone modifiers. Nevertheless, we know from the m^6A epitranscriptome that not only does m^6A play a role in mRNA stabilization by regulating its degradation, but also it regulates its translation. To demonstrate that this increase in SETD1A staining in *Mettl3*-eKO epidermis is due to mRNA stabilization by a decrease in mRNA degradation and subsequent increase in mRNA translation we can perform polysome profiling analysis. By performing polysome profiling of the H3K4 methyltransferase mRNAs we will study their ribosome occupancy and translation efficiency as it can provide an estimation of the ribosome occupancy on all the transcripts expressed in the cell. This offers a readout of ribosome density (the number of ribosomes associated with an mRNA molecule) that highly correlates with protein production from which the translational efficiency of H3K4 methyltransferases can be calculated from these results (*142-144*).

This first conclusion leads us to our second one. We saw that METTL3-dependent m^6A also regulates other chromatin modifiers such as DOT1L, NSD3, SETD2 and EP300. DOT1L is a

writer for H3K79me1/me2/me3 (*145, 146*), modifications present in coding regions of active genes (*147, 148*). NSD3 is a histone methyltransferase that catalyzes H3K36me1/me2 while SETD2 writes H3K36me3 (*149*). Interestingly, the generation of H3K36me3 by SETD2 is not dependent on the presence of H3K36me2 (*150*) but all these modifications influence transcriptional activation. Even more intriguing, as said earlier in *1.2*, H3K36me3 was recently shown to be recognized and bound directly by METTL14 (*17*). EP300 (or P300) is a histone acetyltransferase that installs H3K27ac at promoters and enhancers leading to transcriptional activation of genes (*151, 152*) with a potential crosstalk between the histone mark and H3K4me3 (*153*). Given the importance of these chromatin modifiers and their modification in epigenetic regulation, it will be interesting to dive deeper into how METTL3-dependent m^6A is regulating their mRNA stability. To do this mRNA degradation assays and polysome profiling analysis needs to be done in proliferating keratinocytes with *METTL3* knockdown and with METTL3 catalytic inhibitor STM2457, as well as western blotting and IHC for the chromatin modifiers and their modifications. Furthermore, histone modifications will be examined via ChIP-seq or Cut&Run to see how the chromatin and epigenome is disrupted via m^6A disruption.

Table 4. Histone Modifiers that are regulated by m^6A.

Chromatin Modifier	Histone Modification Written	Epigenetic Regulation
SETD1A	H3K4me2/me3	me2 marks the gene body for activation and me3 primarily marks transcription start sites.
SETD1B	H3K4me2/me3	me2 marks the gene body for activation and me3 primarily marks transcription start sites.

KMT2D	H3K4me1	me1 marks gene enhancers for activation.
KMT2B	H3K4me3	Primarily marks transcription start sites.
DOT1L	H3K79me1/me2/me3	In coding regions of active genes.
NSD3	H3K36me1/me2	Transcriptional activation.
SETD2	H3K36me3	Transcriptional activation and bind METTL14.
EP300	H3K27ac	In promoters and enhancers leading to transcriptional activation of genes.

4.2. Continued…

Altogether, these data and proposed *in vitro* experiments will investigate in depth the role of the m^6A epitranscriptome and how it regulates important histone modifiers during epidermal development and homeostasis.

4.3. Future Directions, METTL3-m^6A in epithelial carcinogenesis

4.3.1. Introduction and preliminary data

This subchapter includes work adapted from a previously published manuscript: Maldonado López, A., & Capell, B. C. (2021). The METTL3-m^6A Epitranscriptome: Dynamic Regulator of Epithelial Development, Differentiation, and Cancer. *Genes*, *12*(7), 1019. https://doi.org/10.3390/genes12071019.

No other area of disease has been better studied than cancer in the epitranscriptomics field (*2, 154, 155*). In a variety of different cancers such as acute myeloid leukemia (*156*) and cutaneous

squamous cell carcinoma (*89*), METTL3-mediated m^{6}A is thought to impair differentiation and promote carcinogenesis (*157*). Intriguingly for our studies in the lab, RNA epigenetics, but more importantly METTL3 and m^{6}A, have been implicated in numerous aspects of epithelial cancer biology (Fig. 15).

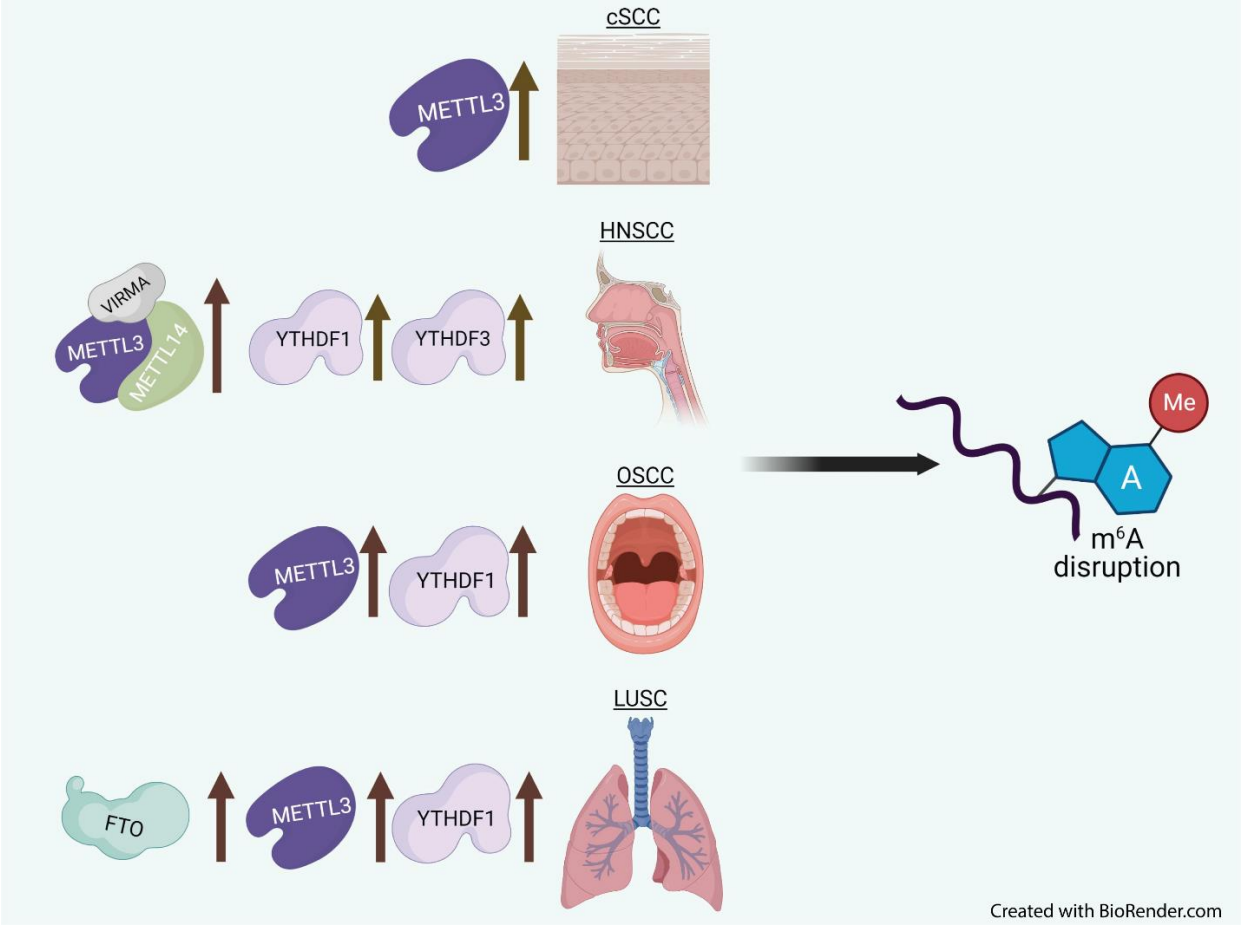

Figure 15. m^{6}A dysregulation in epithelial cancers.

Epithelial cancers, and SCCs, share numerous common biological underpinnings, including dysregulation of the METTL3-m^{6}A epitranscriptome. Studies have demonstrated consistent overexpression of METTL3 across these cancers. As detailed further in the text, depending upon

the cancer, other writers, readers, erasers, and adaptors have been shown to display dysregulated expression or activity, ultimately driving m^6A disruption and carcinogenesis through diverse mechanisms, such as oncogene activation or therapy resistance. Cancers listed include cutaneous SCC (cSCC), head and neck SCC (HNSCC), oral SCC (OSCC), and lung SCC (LUSC).

4.3.1. Continued…

Several squamous cell carcinomas (SCCs) are that share numerous common biological bases (*158, 159*), in which the disruption of METTL3 and m^6A function can promote similar broad effects (Figure 15 and Table 1). Cutaneous squamous cell carcinoma (cSCC) originates in the epidermis and is the second most common of all human cancers with increasing incidence with the aging of the population. Even though cSCCs are typically treatable with surgery, up to 5000–8000 people die every year in the United States (U.S.) due to metastatic cSCC (*160*), numbers rivaling that of melanoma deaths. Recently, a study demonstrated that METTL3 is frequently overexpressed in cSCC patient samples (*89*) and mentioned in 1.3.4.

Head and neck squamous cell carcinoma (HNSCC) is the sixth most common cancer worldwide, and despite advances in cancer therapies, it continues to have a relatively poor prognosis and high rate of morbidity and mortality (*161*). HNSCC entails malignant tumors that develop on the mucosal surfaces of the upper respiratory digestive tract which encompasses the nasal cavity, paranasal sinuses, nasopharynx, hypopharynx, larynx, trachea, oropharynx and the oral cavity. Due to this extensiveness, several studies have been performed to examine epitranscriptomic regulators in hopes of identifying potential biomarkers in HNSCC and

treatments. A recent study examined data from The Cancer Genome Atlas (TCGA) to explore relationships between expression levels of m^6A regulatory genes (m^6A writers, readers and erasers) and the survival rate of HNSCC patients (*162*). A broad upregulation of these genes in HNSCC tumor samples were identified when compared to normal tissues. The significant increases were in METTL3, METTL14, KIAA1429 (VIRMA), YTHDF1, YTHDF2, ALKBH5, FTO, WTAP, RBM15, and HNRNPC. On the other hand, the reader YTHDC2 was significantly downregulated and patients with higher YTHDC2 expression showed greater overall survival (*162*).

Another study performed a similar analysis and found that the adaptor VIRMA was the most frequently altered m^6A regulatory gene, followed by the YTHDF1 and YTHDF3 readers, and the writer METTL3. The increased expression of VIRMA is associated with higher cancer stages, tumor grade, and nodal metastasis, suggesting that its dysregulation plays an important part in the initiation and progression of HNSCC (*163*). Another research group also investigated TCGA data to focus on how the expression of long non-coding RNAs (lncRNAs) may impact HNSCC tumorigenesis. They identified that the lncRNA LNCAROD plays a potentially oncogenic role in HNSCC (*164*). Even more interesting, they found that mechanistically METTL3/14-mediated m^6A enhanced the stability of LNCAROD, which then protected the oncogenic protein YBX1 from proteasomal degradation to promote HNSCC cell proliferation and mobility *in vitro* and tumorigenic ability *in vivo* (*164*). Furthermore, in the nasopharyngeal form of HNSCC, m^6A was shown to reduce the expression of ZNF750, an important pro-differentiation tumor suppressor (*165*).

Oral squamous cell carcinoma (OSCC), a form of HNSCC, is the major subtype of oral cancer, responsible for approximately 90% of oral tumors (*161*) and is characterized by a high rate of recurrence and metastasis, as well as a poor response to clinical therapies. Several studies have shown that METTL3 is significantly upregulated in human OSCC tissues and cells. One of these studies showed that METTL3 mediates the stabilization of the *MYC* mRNA by 3'UTR m^6A methylation in a YTHDF1-dependent manner (*166*). Depleting METTL3 leads to reduced c-Myc protein levels and reduced proliferation and migration of OSCC cells *in vitro* and tumorigenicity *in vivo* (*166*). Another study found similar results upon *METTL3* knockdown, but they observed that METTL3-mediated m^6A methylation of BMI1 promoted its translation in conjunction with IGF2BP1 and thus inhibited the development of OSCC upon carcinogen exposure *in vivo* (*167*).

Finally, another type of epithelial cancer is the principal cause of cancer-related death with an approximate 5-year survival rate of 16.6%, lung cancer (*168*). There are two main types of lung cancers: non-small-cell lung cancer (NSCLC) and small-cell lung cancer (SCLC). NSCLCs account for 80% of lung cancers and within them there are two major subtypes which are lung adenocarcinoma (LUAD) and lung squamous cell carcinoma (LUSC). These two are responsible for 50–60%, and 30% of lung cancer cases, respectively. A recent study analyzed the correlation between m^6A regulatory genes and patient prognosis utilizing TCGA data. This analysis revealed that higher FTO (eraser) expression was associated with a poor prognosis in LUSC patients. The authors found that FTO significantly increased MZF1 expression in LUSC by reducing its m^6A levels and in turn increasing its mRNA stability and translation (*169*). Another study identified

that knockdown of YTHDF1 dramatically stunted tumor formation, tumor weights, and volumes in a NSCLC xenograft model (*170*). Surprisingly, when looking at human patient data it was observed that high YTHDF1 expression was associated with improved clinical outcomes, as reduced YTHDF1 impaired responses the chemotherapy (*170*). Finally, in lung adenocarcinoma, METTL3 has been reported to be upregulated and play an oncogenic role in promoting the growth, survival, and invasion of human lung cancer cells by promoting the translation of certain mRNAs, such as *EGFR, TAZ*, and *BRD4* (*12, 45*).

A few small molecules that act as METTL3 inhibitors have been discovered in the past couple of years (*171*) along with the investment of numerous start-up companies in developing inhibitors against RNA modifiers as a new therapeutic strategy for several diseases including cancer. Some of these companies have already started human clinical trials using a METTL3 inhibitor. For example, STORM Therapeutics LTD started in November of 2022 a phase 1 clinical trial study (clinical trial NCT05584111) to evaluate an oral METTL3 inhibitor (STC-15) in patients with advanced solid tumors (*172*). An earlier compound of STC-15 is STM2457, which has been shown to inhibit osteosarcoma cell growth and induced osteosarcoma cell apoptosis (*173*), improve the immunotherapy benefits based on PD-L1 upregulation in non-small cell lung cancer (*174*), reverse small cell lung cancer chemoresistance (*175*), and by working together with anti-PD-1showed antitumor efficacy against cervical squamous cell carcinoma (*176*) and colorectal cancer (*177*). But the METTL3 inhibitors haven’t been studied in the context of epidermal cancers, such as cutaneous squamous cell carcinoma in which we see the overexpression of METTL3 (*89*).

We examined gene expression data from TCGA and intriguingly, consistent with our results in the *Mettl3*-eKO mice and in the in NHEK *in vitro* model, we found an inverse correlation between METTL3 expression and the expression of histone methyltransferases in the two epithelial cancers of HNSCC and LUSC (Figs. 16A, B). This suggests that the gene regulatory relationships observed in our self-renewing epithelia model systems under homeostatic conditions might also be reflective of what is occurring in diverse disease states.

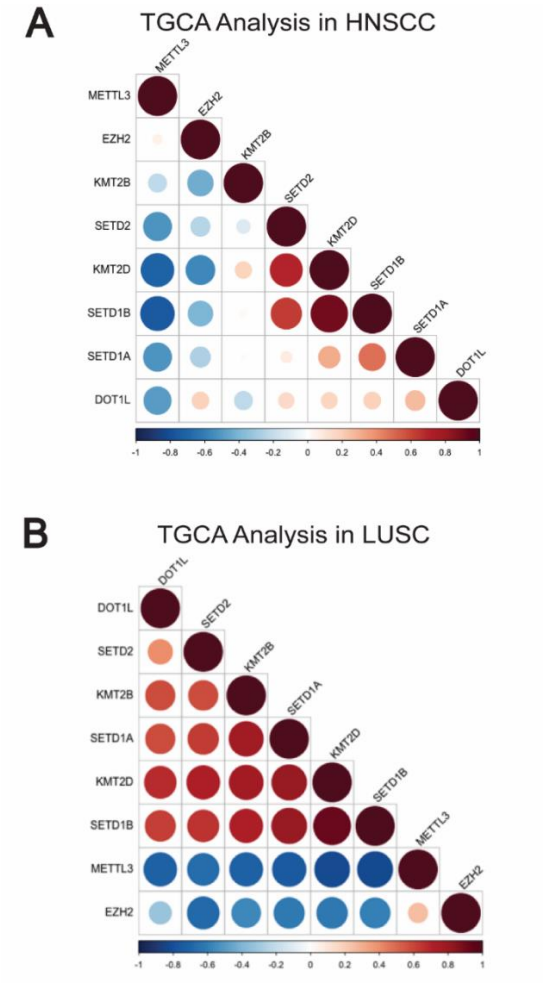

Figure 16. METTL3-m^{6}A dynamics in epithelial SCCs.

TCGA analysis of Head and Neck Squamous Cell Carcinoma (HNSCC) (A) and Lung Squamous Cell Carcinoma (LUSC) (B) showing the inverse correlation of METTL3 expression and multiple histone methyltransferases.

4.3.2. Proposed experiments

As described above, STM2457 has been shown to effectively show antitumor efficacy against several cancers. Since METTL3 inhibitors have not been studied in the context of epidermal cancers, such as cutaneous squamous cell carcinoma in which we see the overexpression of METTL3 (*89*), this makes it an interesting and important future direction for the overall study of m^6A. To find the correct dose that would be effective against cSCC and not affect the normal surrounding epidermis an IC50 dosage analysis will be done in NHEKs and cSCC cell lines such as IC1 (*178*). With an anticipation that the IC50 of STM2457 in cSCC cells will be significantly lower than in NHEKs we will start experiments to evaluate the effectiveness of the METTL3 inhibitor as a potential anti-cancer drug before proceeding to study it in a mouse model by doing proliferation, migration and invasion assays (*179*).

Once we have established the efficacy of the STM2457 treatment *in vitro* in inhibiting cSCC cell proliferation/migration/invasion, we will translate the METTL3 inhibitor dosage into an *in vivo* model. Athymic nude mice has been one of the primary models used in cancer research by their lack of thymus making them immunocompromised allowing the engraftment of a desired type of tumor by simply injecting the cancer cells into the mouse (*180*). For the purpose of the project, we would use the subcutaneous heterotopic model, in which cSCC cells in suspension will be injected into a the right or left flank of mice. After two to six weeks the cSCC tumor becomes

visible and measurable (*181*, *182*) and will be ready for treatment. The STM2457 dose selected from the *in vitro* studies will be diluted in DMSO cream to create a topical treatment. DMSO without the inhibitor will be used as sham control. The growth of the cSCC xenograft will be measured 2 or 3-times a week by a caliper (*183*) by measuring the width (w) and a length (l). These parameters measure the tumor surface area (l x w) (*184*). By the end of treatment with the inhibitor we expect the cSCC tumors to have shrink/resolve in comparison to the control treated tumors (Fig. 17). After, the mice are sacrificed, tumors are extracted and weighed (*183*, *185*) to evaluate the potential anticancer activity of a of the inhibitor. By doing these experiments we will explore METTL3 inhibitor STM2457 as a potential therapeutic for cSCC.

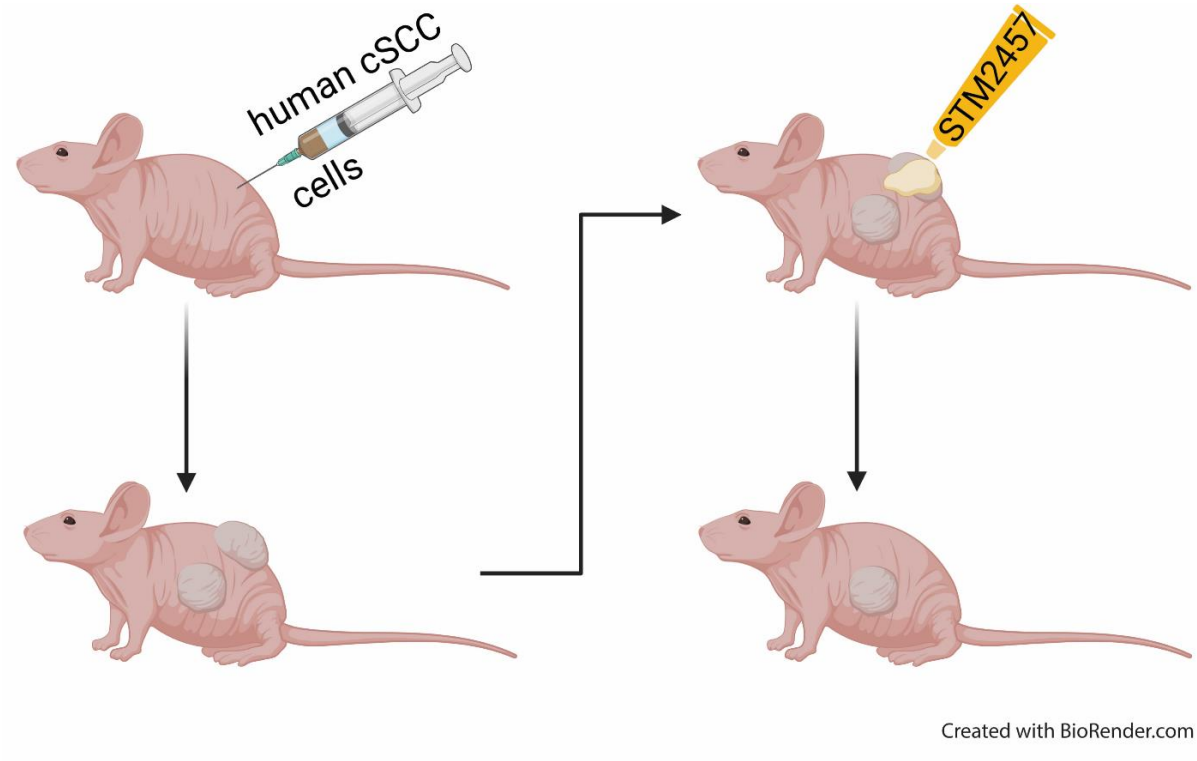

Figure 17. Humanized xenograft and STM2457 cancer treatment model.

Nude mice are injected subcutaneously with human cutaneous squamous cell carcinoma (cSCC) cells. After letting the injected cells grow into visible tumors, the tumors will be treated with the STM2457 dose decided by an IC50 curve done in the same cSCC cells *in vitro*. The control will be DMSO cream in which the STM2457 inhibitor will be diluted in. The expected results are that the STM2457 treated cSCC tumors shrink in size/disappear in comparison to the DMSO control treated cSCC tumors.

4.3.2. Continued…

An additional mouse model to investigate STM2457's efficacy as a therapeutic for cSCCs are mice that express a constitutively active form of Fyn under the control of the *K14* promoter: the *K14-Fyn* Y528F transgenic mice model (*186, 187*). Fyn is part of the Src family tyrosine kinases (SFK), known oncogenes, and plays a significant role regulating keratinocyte proliferation. Activation of SFK family members leads to activation of the oncogenic Ras/MEK/ERK signaling pathway and the *K14-Fyn* Y528F mouse model exhibit constitutive activation of this pathway. Activating and amplifying mutations in RAS have been found in human actinic keratoses (AK) and cSCC lesions (*188-190*). At 4-5 weeks, these mice spontaneously form punctate keratotic lesions, scaly plaques, and large tumors resembling actinic keratoses (AKs), carcinoma in situ (SCIS), and SCCs that resemble human cSCCs at the molecular level (*186*).

A genetic knockout alternative approach can also be used to study the effects of m^6A depletion in cutaneous tumors. For this we need to successfully deplete Mettl3 in adult mice as described in section 4.1 (*Mettl3*-eKO-ERT). Since chronic UVR (primarily UVB) from sunlight

is the leading driver of skin cancer (*191*), exposing *Mettl3*-eKO-ERT mice to chronic ultraviolet radiation will provide insight of the role of Mettl3-mediated m^6A methylation in UVR-induced carcinogenesis. The shaved dorsal skin of *Mettl3*-eKO-ERT mice and wildtype (WT) mice that will serve as controls will be exposed to chronic UVB UV-irradiated skin (*192-194*) with sham treatment (non-UVR exposure) cohorts of *Mettl3*-eKO-ERT and WT mice as additional controls. Based on previous studies (*195*), 75% of C57BL/6 wildtype mice that undergo a UV-induced protocol developed tumors; with more than 50% of the cases being cSCC (*196*). Given this, our hypothesis is that tumor penetrance will be significantly reduced in UVR-irradiated *Mettl3*-eKO-ERT mice epidermis in comparison to the WT cohort. Another way to induce carcinogenesis is by using a faster alternative of the chemical carcinogens DMBA/TPA. This approach also is advantageous since it recapitulates the stepwise progression of human cSCC with the initial formation of hyperplastic epidermis and papillomas (*197-200*). Additionally, by studying the effects of STM2457 treatments in carcinogen mouse models, it can lead to examining whether it enhances the model's immune response, thus translating the treatment for immunotherapy.

Epitranscriptomics, more specifically m^6A epitranscriptomics, provides for an entirely new layer of gene regulation, offering an intriguing new complexity that needs to be investigated in the regulation of dynamic tissues, such as the epidermis. Given the ability to target epitranscriptomic writer and erasers pharmacologically, there is significant potential of epitranscriptome-targeting drugs used as new-age therapeutics to treat disease, as shown to by the significant number of companies that have jumped at the opportunity to develop these compounds.

4.4. Concluding Remarks

The data collected from transgenic mice, next-generation sequencing experiments, human skin cell models, catalytic inhibition assays and genetic knockdowns in human cells during the past five years of this thesis project has revealed critical functions of how epitranscriptomics regulates histone epigenetics in self-renewing epithelia, thus contributing to the knowledge of this exciting new area of gene regulation.

Even though a great deal remains to be done, these findings lay the foundation for novel clinical approaches to maintain skin homeostasis and treat benign and malignant skin diseases with the goal of delivering therapeutic benefits to patients.

BIBLIOGRAPHY

1. S. Zaccara, R. J. Ries, S. R. Jaffrey, Reading, writing and erasing mRNA methylation. *Nat Rev Mol Cell Biol* **20**, 608-624 (2019).
2. H. Huang, H. Weng, J. Chen, m(6)A Modification in Coding and Non-coding RNAs: Roles and Therapeutic Implications in Cancer. *Cancer Cell* **37**, 270-288 (2020).
3. B. S. Zhao, I. A. Roundtree, C. He, Post-transcriptional gene regulation by mRNA modifications. *Nat Rev Mol Cell Biol* **18**, 31-42 (2017).
4. S. Kumar, T. Mohapatra, Deciphering Epitranscriptome: Modification of mRNA Bases Provides a New Perspective for Post-transcriptional Regulation of Gene Expression. *Front Cell Dev Biol* **9**, 628415 (2021).
5. F. F. Davis, F. W. Allen, Ribonucleic acids from yeast which contain a fifth nucleotide. *J Biol Chem* **227**, 907-915 (1957).
6. M. Frye, B. T. Harada, M. Behm, C. He, RNA modifications modulate gene expression during development. *Science* **361**, 1346-1349 (2018).
7. H. Shi, J. Wei, C. He, Where, When, and How: Context-Dependent Functions of RNA Methylation Writers, Readers, and Erasers. *Mol Cell* **74**, 640-650 (2019).
8. D. Wiener, S. Schwartz, The epitranscriptome beyond m(6)A. *Nat Rev Genet* **22**, 119-131 (2021).
9. G. Jia *et al.*, N6-methyladenosine in nuclear RNA is a major substrate of the obesity-associated FTO. *Nat Chem Biol* **7**, 885-887 (2011).
10. J. Liu *et al.*, Landscape and Regulation of m(6)A and m(6)Am Methylome across Human and Mouse Tissues. *Mol Cell* **77**, 426-440 e426 (2020).
11. R. J. Ries *et al.*, m(6)A enhances the phase separation potential of mRNA. *Nature* **571**, 424-428 (2019).
12. S. Lin, J. Choe, P. Du, R. Triboulet, R. I. Gregory, The m(6)A Methyltransferase METTL3 Promotes Translation in Human Cancer Cells. *Mol Cell* **62**, 335-345 (2016).
13. B. Slobodin *et al.*, Transcription Impacts the Efficiency of mRNA Translation via Co-transcriptional N6-adenosine Methylation. *Cell* **169**, 326-337 e312 (2017).
14. J. Zhou *et al.*, N(6)-Methyladenosine Guides mRNA Alternative Translation during Integrated Stress Response. *Mol Cell* **69**, 636-647 e637 (2018).
15. D. Dominissini *et al.*, Topology of the human and mouse m6A RNA methylomes revealed by m6A-seq. *Nature* **485**, 201-206 (2012).
16. K. D. Meyer *et al.*, Comprehensive analysis of mRNA methylation reveals enrichment in 3' UTRs and near stop codons. *Cell* **149**, 1635-1646 (2012).
17. H. Huang *et al.*, Histone H3 trimethylation at lysine 36 guides m(6)A RNA modification co-transcriptionally. *Nature* **567**, 414-419 (2019).
18. K. I. Zhou *et al.*, Regulation of Co-transcriptional Pre-mRNA Splicing by m(6)A through the Low-Complexity Protein hnRNPG. *Mol Cell* **76**, 70-81 e79 (2019).
19. A. M. Heck, C. J. Wilusz, Small changes, big implications: The impact of m(6)A RNA methylation on gene expression in pluripotency and development. *Biochim Biophys Acta Gene Regul Mech* **1862**, 194402 (2019).
20. S. Ke *et al.*, m(6)A mRNA modifications are deposited in nascent pre-mRNA and are not required for splicing but do specify cytoplasmic turnover. *Genes Dev* **31**, 990-1006 (2017).

21. S. Wang *et al.*, Dynamic regulation and functions of mRNA m6A modification. *Cancer Cell Int* **22**, 48 (2022).
22. S. Adhikari, W. Xiao, Y. L. Zhao, Y. G. Yang, m(6)A: Signaling for mRNA splicing. *RNA Biol* **13**, 756-759 (2016).
23. P. C. He, C. He, m(6) A RNA methylation: from mechanisms to therapeutic potential. *EMBO J* **40**, e105977 (2021).
24. P. Sledz, M. Jinek, Structural insights into the molecular mechanism of the m(6)A writer complex. *Elife* **5**, (2016).
25. P. Wang, K. A. Doxtader, Y. Nam, Structural Basis for Cooperative Function of Mettl3 and Mettl14 Methyltransferases. *Mol Cell* **63**, 306-317 (2016).
26. X. Wang *et al.*, Structural basis of N(6)-adenosine methylation by the METTL3-METTL14 complex. *Nature* **534**, 575-578 (2016).
27. H. Huang, H. Weng, J. Chen, The Biogenesis and Precise Control of RNA m(6)A Methylation. *Trends Genet* **36**, 44-52 (2020).
28. Y. Xu *et al.*, Novel insights into the METTL3-METTL14 complex in musculoskeletal diseases. *Cell Death Discov* **9**, 170 (2023).
29. K. E. Pendleton *et al.*, The U6 snRNA m(6)A Methyltransferase METTL16 Regulates SAM Synthetase Intron Retention. *Cell* **169**, 824-835 e814 (2017).
30. E. M. Turkalj, C. Vissers, The emerging importance of METTL5-mediated ribosomal RNA methylation. *Exp Mol Med* **54**, 1617-1625 (2022).
31. H. Ma *et al.*, N(6-)Methyladenosine methyltransferase ZCCHC4 mediates ribosomal RNA methylation. *Nat Chem Biol* **15**, 88-94 (2019).
32. X. L. Ping *et al.*, Mammalian WTAP is a regulatory subunit of the RNA N6-methyladenosine methyltransferase. *Cell Res* **24**, 177-189 (2014).
33. E. Scholler *et al.*, Interactions, localization, and phosphorylation of the m(6)A generating METTL3-METTL14-WTAP complex. *RNA* **24**, 499-512 (2018).
34. Y. Yue *et al.*, VIRMA mediates preferential m(6)A mRNA methylation in 3'UTR and near stop codon and associates with alternative polyadenylation. *Cell Discov* **4**, 10 (2018).
35. J. Wen *et al.*, Zc3h13 Regulates Nuclear RNA m(6)A Methylation and Mouse Embryonic Stem Cell Self-Renewal. *Mol Cell* **69**, 1028-1038 e1026 (2018).
36. D. P. Patil *et al.*, m(6)A RNA methylation promotes XIST-mediated transcriptional repression. *Nature* **537**, 369-373 (2016).
37. P. Knuckles *et al.*, Zc3h13/Flacc is required for adenosine methylation by bridging the mRNA-binding factor Rbm15/Spenito to the m(6)A machinery component Wtap/Fl(2)d. *Genes Dev* **32**, 415-429 (2018).
38. T. Gerken *et al.*, The obesity-associated FTO gene encodes a 2-oxoglutarate-dependent nucleic acid demethylase. *Science* **318**, 1469-1472 (2007).
39. J. Mauer *et al.*, Reversible methylation of m(6)A(m) in the 5' cap controls mRNA stability. *Nature* **541**, 371-375 (2017).
40. J. Mauer *et al.*, FTO controls reversible m(6)Am RNA methylation during snRNA biogenesis. *Nat Chem Biol* **15**, 340-347 (2019).
41. G. Zheng *et al.*, ALKBH5 is a mammalian RNA demethylase that impacts RNA metabolism and mouse fertility. *Mol Cell* **49**, 18-29 (2013).
42. W. Xiao *et al.*, Nuclear m(6)A Reader YTHDC1 Regulates mRNA Splicing. *Mol Cell* **61**, 507-519 (2016).

43. I. A. Roundtree *et al.*, YTHDC1 mediates nuclear export of N(6)-methyladenosine methylated mRNAs. *Elife* **6**, (2017).
44. Y. Saito *et al.*, YTHDC2 control of gametogenesis requires helicase activity but not m(6)A binding. *Genes Dev* **36**, 180-194 (2022).
45. J. Choe *et al.*, mRNA circularization by METTL3-eIF3h enhances translation and promotes oncogenesis. *Nature* **561**, 556-560 (2018).
46. X. Wang *et al.*, N(6)-methyladenosine Modulates Messenger RNA Translation Efficiency. *Cell* **161**, 1388-1399 (2015).
47. A. Li *et al.*, Cytoplasmic m(6)A reader YTHDF3 promotes mRNA translation. *Cell Res* **27**, 444-447 (2017).
48. L. Lasman *et al.*, Context-dependent functional compensation between Ythdf m(6)A reader proteins. *Genes Dev* **34**, 1373-1391 (2020).
49. S. Zaccara, S. R. Jaffrey, A Unified Model for the Function of YTHDF Proteins in Regulating m(6)A-Modified mRNA. *Cell* **181**, 1582-1595 e1518 (2020).
50. B. Shi *et al.*, Phase separation of Ddx3xb helicase regulates maternal-to-zygotic transition in zebrafish. *Cell Res* **32**, 715-728 (2022).
51. J. Y. Kang *et al.*, LLPS of FXR1 drives spermiogenesis by activating translation of stored mRNAs. *Science* **377**, eabj6647 (2022).
52. N. Liu *et al.*, N6-methyladenosine alters RNA structure to regulate binding of a low-complexity protein. *Nucleic Acids Res* **45**, 6051-6063 (2017).
53. N. Liu *et al.*, N(6)-methyladenosine-dependent RNA structural switches regulate RNA-protein interactions. *Nature* **518**, 560-564 (2015).
54. C. R. Alarcon *et al.*, HNRNPA2B1 Is a Mediator of m(6)A-Dependent Nuclear RNA Processing Events. *Cell* **162**, 1299-1308 (2015).
55. H. Huang *et al.*, Recognition of RNA N(6)-methyladenosine by IGF2BP proteins enhances mRNA stability and translation. *Nat Cell Biol* **20**, 285-295 (2018).
56. D. Ramesh-Kumar, S. Guil, The IGF2BP family of RNA binding proteins links epitranscriptomics to cancer. *Semin Cancer Biol* **86**, 18-31 (2022).
57. R. L. Kan, J. Chen, T. Sallam, Crosstalk between epitranscriptomic and epigenetic mechanisms in gene regulation. *Trends Genet* **38**, 182-193 (2022).
58. I. Barbieri *et al.*, Promoter-bound METTL3 maintains myeloid leukaemia by m(6)A-dependent translation control. *Nature* **552**, 126-131 (2017).
59. Y. Wang *et al.*, N(6)-methyladenosine RNA modification regulates embryonic neural stem cell self-renewal through histone modifications. *Nat Neurosci* **21**, 195-206 (2018).
60. C. Wu *et al.*, Interplay of m(6)A and H3K27 trimethylation restrains inflammation during bacterial infection. *Sci Adv* **6**, eaba0647 (2020).
61. Y. Li *et al.*, N(6)-Methyladenosine co-transcriptionally directs the demethylation of histone H3K9me2. *Nat Genet* **52**, 870-877 (2020).
62. J. Liu *et al.*, N (6)-methyladenosine of chromosome-associated regulatory RNA regulates chromatin state and transcription. *Science* **367**, 580-586 (2020).
63. T. Ganz, Epithelia: not just physical barriers. *Proc Natl Acad Sci U S A* **99**, 3357-3358 (2002).
64. Y. Guan, Y. J. Yang, P. Nagarajan, Y. Ge, Transcriptional and signalling regulation of skin epithelial stem cells in homeostasis, wounds and cancer. *Exp Dermatol* **30**, 529-545 (2021).

65. H. H. Bragulla, D. G. Homberger, Structure and functions of keratin proteins in simple, stratified, keratinized and cornified epithelia. *J Anat* **214**, 516-559 (2009).
66. A. Baroni *et al.*, Structure and function of the epidermis related to barrier properties. *Clin Dermatol* **30**, 257-262 (2012).
67. K. A. U. Gonzales, E. Fuchs, Skin and Its Regenerative Powers: An Alliance between Stem Cells and Their Niche. *Dev Cell* **43**, 387-401 (2017).
68. N. Roberts, V. Horsley, Developing stratified epithelia: lessons from the epidermis and thymus. *Wiley Interdiscip Rev Dev Biol* **3**, 389-402 (2014).
69. E. Candi, R. Schmidt, G. Melino, The cornified envelope: a model of cell death in the skin. *Nat Rev Mol Cell Biol* **6**, 328-340 (2005).
70. H. Yousef, M. Alhajj, S. Sharma, in *StatPearls*. (Treasure Island (FL), 2023).
71. A. Avgustinova, S. A. Benitah, Epigenetic control of adult stem cell function. *Nat Rev Mol Cell Biol* **17**, 643-658 (2016).
72. C. Blanpain, E. Fuchs, Epidermal homeostasis: a balancing act of stem cells in the skin. *Nat Rev Mol Cell Biol* **10**, 207-217 (2009).
73. K. M. Halprin, Epidermal "turnover time"--a re-examination. *Br J Dermatol* **86**, 14-19 (1972).
74. S. Gelfant, The cell cycle in psoriasis: a reappraisal. *Br J Dermatol* **95**, 577-590 (1976).
75. C. S. Potten, R. Saffhill, H. I. Maibach, Measurement of the transit time for cells through the epidermis and stratum corneum of the mouse and guinea-pig. *Cell Tissue Kinet* **20**, 461-472 (1987).
76. M. I. Koster, Making an epidermis. *Ann N Y Acad Sci* **1170**, 7-10 (2009).
77. Y. A. Miroshnikova, I. Cohen, E. Ezhkova, S. A. Wickstrom, Epigenetic gene regulation, chromatin structure, and force-induced chromatin remodelling in epidermal development and homeostasis. *Curr Opin Genet Dev* **55**, 46-51 (2019).
78. P. Rousselle , E. Gentilhomme, Y. Neveux, *Markers of Epidermal Proliferation and Differentiation. in Agache's Measuring the Skin, pp. 397-405*. (Springer International Publishing., 2016).
79. E. Soares, H. Zhou, Master regulatory role of p63 in epidermal development and disease. *Cell Mol Life Sci* **75**, 1179-1190 (2018).
80. Y. Kajee, J. P. Pelteret, B. D. Reddy, The biomechanics of the human tongue. *Int J Numer Method Biomed Eng* **29**, 492-514 (2013).
81. K. Arvidson, U. Friberg, Human taste: response and taste bud number in fungiform papillae. *Science* **209**, 807-808 (1980).
82. E. J. Golden *et al.*, Onset of taste bud cell renewal starts at birth and coincides with a shift in SHH function. *Elife* **10**, (2021).
83. D. Gaillard, M. Xu, F. Liu, S. E. Millar, L. A. Barlow, beta-Catenin Signaling Biases Multipotent Lingual Epithelial Progenitors to Differentiate and Acquire Specific Taste Cell Fates. *PLoS Genet* **11**, e1005208 (2015).
84. T. Okubo, L. H. Pevny, B. L. Hogan, Sox2 is required for development of taste bud sensory cells. *Genes Dev* **20**, 2654-2659 (2006).
85. D. Castillo-Azofeifa *et al.*, Sonic hedgehog from both nerves and epithelium is a key trophic factor for taste bud maintenance. *Development* **144**, 3054-3065 (2017).
86. R. F. Bloomquist *et al.*, Developmental plasticity of epithelial stem cells in tooth and taste bud renewal. *Proc Natl Acad Sci U S A* **116**, 17858-17866 (2019).

87. J. Lee *et al.*, N(6) -methyladenosine modification of lncRNA Pvt1 governs epidermal stemness. *EMBO J* **40**, e106276 (2021).
88. L. Xi *et al.*, m6A RNA methylation impacts fate choices during skin morphogenesis. *Elife* **9**, (2020).
89. R. Zhou *et al.*, METTL3 mediated m(6)A modification plays an oncogenic role in cutaneous squamous cell carcinoma by regulating DeltaNp63. *Biochem Biophys Res Commun* **515**, 310-317 (2019).
90. Q. Xiong *et al.*, METTL3-mediated m(6)A RNA methylation regulates dorsal lingual epithelium homeostasis. *Int J Oral Sci* **14**, 26 (2022).
91. J. J. S. Ji Won Son, Min-Gyu Kim, Jaehyung Kim & Sang Wook Son, Keratinocyte-specific knockout mice models via Cre–loxP recombination system . *Mol. Cell. Toxicol* **17**, 15-27 (2021).
92. H. Kim, M. Kim, S. K. Im, S. Fang, Mouse Cre-LoxP system: general principles to determine tissue-specific roles of target genes. *Lab Anim Res* **34**, 147-159 (2018).
93. B. Hall, A. Limaye, A. B. Kulkarni, Overview: generation of gene knockout mice. *Curr Protoc Cell Biol* **Chapter 19**, Unit 19 12 19 12 11-17 (2009).
94. Y. Wu *et al.*, Mettl3-mediated m(6)A RNA methylation regulates the fate of bone marrow mesenchymal stem cells and osteoporosis. *Nat Commun* **9**, 4772 (2018).
95. S. Geula *et al.*, Stem cells. m6A mRNA methylation facilitates resolution of naive pluripotency toward differentiation. *Science* **347**, 1002-1006 (2015).
96. P. J. Batista *et al.*, m(6)A RNA modification controls cell fate transition in mammalian embryonic stem cells. *Cell Stem Cell* **15**, 707-719 (2014).
97. R. Paus, Principles of hair cycle control. *J Dermatol* **25**, 793-802 (1998).
98. E. Fuchs, B. J. Merrill, C. Jamora, R. DasGupta, At the roots of a never-ending cycle. *Dev Cell* **1**, 13-25 (2001).
99. M. V. Plikus, C. M. Chuong, Complex hair cycle domain patterns and regenerative hair waves in living rodents. *J Invest Dermatol* **128**, 1071-1080 (2008).
100. M. Watanabe *et al.*, Type XVII collagen coordinates proliferation in the interfollicular epidermis. *Elife* **6**, (2017).
101. L. Su, P. R. Morgan, J. A. Thomas, E. B. Lane, Expression of keratin 14 and 19 mRNA and protein in normal oral epithelia, hairy leukoplakia, tongue biting and white sponge nevus. *J Oral Pathol Med* **22**, 183-189 (1993).
102. A. Cabral *et al.*, Structural organization and regulation of the small proline-rich family of cornified envelope precursors suggest a role in adaptive barrier function. *J Biol Chem* **276**, 19231-19237 (2001).
103. B. Jackson *et al.*, Late cornified envelope family in differentiating epithelia--response to calcium and ultraviolet irradiation. *J Invest Dermatol* **124**, 1062-1070 (2005).
104. K. M. Boeshans, T. C. Mueser, B. Ahvazi, A three-dimensional model of the human transglutaminase 1: insights into the understanding of lamellar ichthyosis. *J Mol Model* **13**, 233-246 (2007).
105. H. Adachi, Y. Murakami, H. Tanaka, S. Nakata, Increase of stratifin triggered by ultraviolet irradiation is possibly related to premature aging of human skin. *Exp Dermatol* **23 Suppl 1**, 32-36 (2014).
106. K. Natsuga, M. Watanabe, W. Nishie, H. Shimizu, Life before and beyond blistering: The role of collagen XVII in epidermal physiology. *Exp Dermatol* **28**, 1135-1141 (2019).

107. T. J. Sproule *et al.*, Molecular identification of collagen 17a1 as a major genetic modifier of laminin gamma 2 mutation-induced junctional epidermolysis bullosa in mice. *PLoS Genet* **10**, e1004068 (2014).
108. J. Hoffmann *et al.*, A Silent COL17A1 Variant Alters Splicing and Causes Junctional Epidermolysis Bullosa. *Acta Derm Venereol* **99**, 460-461 (2019).
109. H. H. Xu, V. P. Werth, E. Parisi, T. P. Sollecito, Mucous membrane pemphigoid. *Dent Clin North Am* **57**, 611-630 (2013).
110. H. B. Li *et al.*, m(6)A mRNA methylation controls T cell homeostasis by targeting the IL-7/STAT5/SOCS pathways. *Nature* **548**, 338-342 (2017).
111. A. Dobin *et al.*, STAR: ultrafast universal RNA-seq aligner. *Bioinformatics* **29**, 15-21 (2013).
112. M. I. Love, W. Huber, S. Anders, Moderated estimation of fold change and dispersion for RNA-seq data with DESeq2. *Genome Biol* **15**, 550 (2014).
113. A. S. Hopkin *et al.*, GRHL3/GET1 and trithorax group members collaborate to activate the epidermal progenitor differentiation program. *PLoS Genet* **8**, e1002829 (2012).
114. S. Egolf *et al.*, MLL4 mediates differentiation and tumor suppression through ferroptosis. *Sci Adv* **7**, eabj9141 (2021).
115. S. Egolf *et al.*, LSD1 Inhibition Promotes Epithelial Differentiation through Derepression of Fate-Determining Transcription Factors. *Cell Rep* **28**, 1981-1992 e1987 (2019).
116. M. Ratnadiwakara, M. L. Anko, mRNA Stability Assay Using transcription inhibition by Actinomycin D in Mouse Pluripotent Stem Cells. *Bio Protoc* **8**, e3072 (2018).
117. C. Y. Chen, N. Ezzeddine, A. B. Shyu, Messenger RNA half-life measurements in mammalian cells. *Methods Enzymol* **448**, 335-357 (2008).
118. Z. Ianniello *et al.*, New insight into the catalytic -dependent and -independent roles of METTL3 in sustaining aberrant translation in chronic myeloid leukemia. *Cell Death Dis* **12**, 870 (2021).
119. E. Yankova *et al.*, Small-molecule inhibition of METTL3 as a strategy against myeloid leukaemia. *Nature* **593**, 597-601 (2021).
120. C. Liu *et al.*, Absolute quantification of single-base m(6)A methylation in the mammalian transcriptome using GLORI. *Nat Biotechnol* **41**, 355-366 (2023).
121. A. S. Bledau *et al.*, The H3K4 methyltransferase Setd1a is first required at the epiblast stage, whereas Setd1b becomes essential after gastrulation. *Development* **141**, 1022-1035 (2014).
122. S. Wang *et al.*, SETD1A Mediated H3K4 Methylation and Its Role in Neurodevelopmental and Neuropsychiatric Disorders. *Front Mol Neurosci* **14**, 772000 (2021).
123. N. D. Heintzman *et al.*, Histone modifications at human enhancers reflect global cell-type-specific gene expression. *Nature* **459**, 108-112 (2009).
124. A. Kranz, K. Anastassiadis, The role of SETD1A and SETD1B in development and disease. *Biochim Biophys Acta Gene Regul Mech* **1863**, 194578 (2020).
125. E. Lin-Shiao *et al.*, KMT2D regulates p63 target enhancers to coordinate epithelial homeostasis. *Genes Dev* **32**, 181-193 (2018).
126. R. J. Ontiveros *et al.*, Coordination of mRNA and tRNA methylations by TRMT10A. *Proc Natl Acad Sci U S A* **117**, 7782-7791 (2020).
127. M. P. Polito, G. Marini, M. Palamenghi, E. Enzo, Decoding the Human Epidermal Complexity at Single-Cell Resolution. *Int J Mol Sci* **24**, (2023).

128. G. Eraslan *et al.*, Single-nucleus cross-tissue molecular reference maps toward understanding disease gene function. *Science* **376**, eabl4290 (2022).
129. R. Ruiz-Vega *et al.*, Dynamics of nevus development implicate cell cooperation in the growth arrest of transformed melanocytes. *Elife* **9**, (2020).
130. P. L. Germain, A. Lun, C. Garcia Meixide, W. Macnair, M. D. Robinson, Doublet identification in single-cell sequencing data using scDblFinder. *F1000Res* **10**, 979 (2021).
131. I. Korsunsky *et al.*, Fast, sensitive and accurate integration of single-cell data with Harmony. *Nat Methods* **16**, 1289-1296 (2019).
132. C. G. Williams, H. J. Lee, T. Asatsuma, R. Vento-Tormo, A. Haque, An introduction to spatial transcriptomics for biomedical research. *Genome Med* **14**, 68 (2022).
133. V. Vasioukhin, L. Degenstein, B. Wise, E. Fuchs, The magical touch: genome targeting in epidermal stem cells induced by tamoxifen application to mouse skin. *Proc Natl Acad Sci U S A* **96**, 8551-8556 (1999).
134. C. C. Liang, L. R. You, J. L. Chang, T. F. Tsai, C. M. Chen, Transgenic mice exhibiting inducible and spontaneous Cre activities driven by a bovine keratin 5 promoter that can be used for the conditional analysis of basal epithelial cells in multiple organs. *J Biomed Sci* **16**, 2 (2009).
135. S. Nachtergaele, Enzymes flying under the radar: Cryptic METTL3 can persist in knockout cells. *PLoS Biol* **20**, e3001717 (2022).
136. B. Zheng, M. Sage, E. A. Sheppeard, V. Jurecic, A. Bradley, Engineering mouse chromosomes with Cre-loxP: range, efficiency, and somatic applications. *Mol Cell Biol* **20**, 648-655 (2000).
137. H. X. Poh, A. H. Mirza, B. F. Pickering, S. R. Jaffrey, Alternative splicing of METTL3 explains apparently METTL3-independent m6A modifications in mRNA. *PLoS Biol* **20**, e3001683 (2022).
138. A. K. Indra, M. Leid, Epidermal permeability barrier measurement in mammalian skin. *Methods Mol Biol* **763**, 73-81 (2011).
139. S. Iwasaki, Evolution of the structure and function of the vertebrate tongue. *J Anat* **201**, 1-13 (2002).
140. B. Fehlhaber *et al.*, A sensitive scoring system for the longitudinal clinical evaluation and prediction of lethal disease outcomes in newborn mice. *Sci Rep* **9**, 5919 (2019).
141. C. Kreikemeier-Bower, P. Polepole, K. Pinkerton, L. Zhang, A simple method for short-term maintenance of neonatal mice without foster mothers. *J Biol Methods* **7**, e126 (2020).
142. H. Y. Jin, C. Xiao, An Integrated Polysome Profiling and Ribosome Profiling Method to Investigate In Vivo Translatome. *Methods Mol Biol* **1712**, 1-18 (2018).
143. I. T. Pereira *et al.*, Polysome profiling followed by RNA-seq of cardiac differentiation stages in hESCs. *Sci Data* **5**, 180287 (2018).
144. H. Yoshikawa *et al.*, Efficient analysis of mammalian polysomes in cells and tissues using Ribo Mega-SEC. *Elife* **7**, (2018).
145. J. Min, Q. Feng, Z. Li, Y. Zhang, R. M. Xu, Structure of the catalytic domain of human DOT1L, a non-SET domain nucleosomal histone methyltransferase. *Cell* **112**, 711-723 (2003).
146. K. Wood, M. Tellier, S. Murphy, DOT1L and H3K79 Methylation in Transcription and Genomic Stability. *Biomolecules* **8**, (2018).
147. Z. Wang *et al.*, Combinatorial patterns of histone acetylations and methylations in the human genome. *Nat Genet* **40**, 897-903 (2008).

148. A. Kouskouti, I. Talianidis, Histone modifications defining active genes persist after transcriptional and mitotic inactivation. *EMBO J* **24**, 347-357 (2005).
149. U. T. F. Lam, B. K. Y. Tan, J. J. X. Poh, E. S. Chen, Structural and functional specificity of H3K36 methylation. *Epigenetics Chromatin* **15**, 17 (2022).
150. J. W. Edmunds, L. C. Mahadevan, A. L. Clayton, Dynamic histone H3 methylation during gene induction: HYPB/Setd2 mediates all H3K36 trimethylation. *EMBO J* **27**, 406-420 (2008).
151. Y. Zhang *et al.*, The ZZ domain of p300 mediates specificity of the adjacent HAT domain for histone H3. *Nat Struct Mol Biol* **25**, 841-849 (2018).
152. I. B. Hilton *et al.*, Epigenome editing by a CRISPR-Cas9-based acetyltransferase activates genes from promoters and enhancers. *Nat Biotechnol* **33**, 510-517 (2015).
153. W. Zhao *et al.*, Investigating crosstalk between H3K27 acetylation and H3K4 trimethylation in CRISPR/dCas-based epigenome editing and gene activation. *Sci Rep* **11**, 15912 (2021).
154. I. Barbieri, T. Kouzarides, Role of RNA modifications in cancer. *Nat Rev Cancer* **20**, 303-322 (2020).
155. Q. Lan *et al.*, The Critical Role of RNA m(6)A Methylation in Cancer. *Cancer Res* **79**, 1285-1292 (2019).
156. L. P. Vu *et al.*, The N(6)-methyladenosine (m(6)A)-forming enzyme METTL3 controls myeloid differentiation of normal hematopoietic and leukemia cells. *Nat Med* **23**, 1369-1376 (2017).
157. S. Liu *et al.*, METTL3 plays multiple functions in biological processes. *Am J Cancer Res* **10**, 1631-1646 (2020).
158. J. D. Campbell *et al.*, Genomic, Pathway Network, and Immunologic Features Distinguishing Squamous Carcinomas. *Cell Rep* **23**, 194-212 e196 (2018).
159. G. P. Dotto, A. K. Rustgi, Squamous Cell Cancers: A Unified Perspective on Biology and Genetics. *Cancer Cell* **29**, 622-637 (2016).
160. K. S. Nehal, C. K. Bichakjian, Update on Keratinocyte Carcinomas. *N Engl J Med* **379**, 363-374 (2018).
161. D. E. Johnson *et al.*, Author Correction: Head and neck squamous cell carcinoma. *Nat Rev Dis Primers* **9**, 4 (2023).
162. X. Zhao, L. Cui, Development and validation of a m(6)A RNA methylation regulators-based signature for predicting the prognosis of head and neck squamous cell carcinoma. *Am J Cancer Res* **9**, 2156-2169 (2019).
163. P. Arumugam, R. George, V. P. Jayaseelan, Aberrations of m6A regulators are associated with tumorigenesis and metastasis in head and neck squamous cell carcinoma. *Arch Oral Biol* **122**, 105030 (2021).
164. Y. Ban *et al.*, LNCAROD is stabilized by m6A methylation and promotes cancer progression via forming a ternary complex with HSPA1A and YBX1 in head and neck squamous cell carcinoma. *Mol Oncol* **14**, 1282-1296 (2020).
165. P. Zhang *et al.*, Correction: m(6)A-mediated ZNF750 repression facilitates nasopharyngeal carcinoma progression. *Cell Death Dis* **13**, 83 (2022).
166. W. Zhao *et al.*, METTL3 Facilitates Oral Squamous Cell Carcinoma Tumorigenesis by Enhancing c-Myc Stability via YTHDF1-Mediated m(6)A Modification. *Mol Ther Nucleic Acids* **20**, 1-12 (2020).

167. L. Liu *et al.*, METTL3 Promotes Tumorigenesis and Metastasis through BMI1 m(6)A Methylation in Oral Squamous Cell Carcinoma. *Mol Ther* **28**, 2177-2190 (2020).
168. D. R. Gandara, P. S. Hammerman, M. L. Sos, P. N. Lara, Jr., F. R. Hirsch, Squamous cell lung cancer: from tumor genomics to cancer therapeutics. *Clin Cancer Res* **21**, 2236-2243 (2015).
169. J. Liu *et al.*, m(6)A demethylase FTO facilitates tumor progression in lung squamous cell carcinoma by regulating MZF1 expression. *Biochem Biophys Res Commun* **502**, 456-464 (2018).
170. Y. Shi *et al.*, YTHDF1 links hypoxia adaptation and non-small cell lung cancer progression. *Nat Commun* **10**, 4892 (2019).
171. Y. Du *et al.*, Discovery of METTL3 Small Molecule Inhibitors by Virtual Screening of Natural Products. *Front Pharmacol* **13**, 878135 (2022).
172. ClinicalTrials.gov*,* N. L. o. Medicine, Ed. (2023).
173. X. An *et al.*, ZBTB7C m6A modification incurred by METTL3 aberration promotes osteosarcoma progression. *Transl Res*, (2023).
174. H. Xiao, Zhaou, R., Meng, W., Liao, Y., Effects and translatomics characteristics of a small-molecule inhibitor of METTL3 against non-small cell lung cancer. *Journal of Pharmaceutical Analysis*, (2023).
175. Y. Sun *et al.*, METTL3 promotes chemoresistance in small cell lung cancer by inducing mitophagy. *J Exp Clin Cancer Res* **42**, 65 (2023).
176. R. Yu *et al.*, Integrative Analyses of m6A Regulators Identify that METTL3 is Associated with HPV Status and Immunosuppressive Microenvironment in HPV-related Cancers. *Int J Biol Sci* **18**, 3874-3887 (2022).
177. H. Chen *et al.*, METTL3 Inhibits Antitumor Immunity by Targeting m(6)A-BHLHE41-CXCL1/CXCR2 Axis to Promote Colorectal Cancer. *Gastroenterology* **163**, 891-907 (2022).
178. S. Hassan *et al.*, A Unique Panel of Patient-Derived Cutaneous Squamous Cell Carcinoma Cell Lines Provides a Preclinical Pathway for Therapeutic Testing. *Int J Mol Sci* **20**, (2019).
179. S. Martinez-Pacheco, L. O'Driscoll, Pre-Clinical In Vitro Models Used in Cancer Research: Results of a Worldwide Survey. *Cancers (Basel)* **13**, (2021).
180. I. Szadvari, O. Krizanova, P. Babula, Athymic nude mice as an experimental model for cancer treatment. *Physiol Res* **65**, S441-S453 (2016).
181. J. C. Schuh, Trials, tribulations, and trends in tumor modeling in mice. *Toxicol Pathol* **32 Suppl 1**, 53-66 (2004).
182. L. P. Dipersio, Regional growth differences of human tumour xenografts in nude mice. *Lab Anim* **15**, 179-180 (1981).
183. P. Workman *et al.*, Guidelines for the welfare and use of animals in cancer research. *Br J Cancer* **102**, 1555-1577 (2010).
184. M. M. Tomayko, C. P. Reynolds, Determination of subcutaneous tumor size in athymic (nude) mice. *Cancer Chemother Pharmacol* **24**, 148-154 (1989).
185. T. C. Haddad, D. Yee, Of mice and (wo)men: is this any way to test a new drug? *J Clin Oncol* **26**, 830-832 (2008).
186. L. Zhao *et al.*, Srcasm inhibits Fyn-induced cutaneous carcinogenesis with modulation of Notch1 and p53. *Cancer Res* **69**, 9439-9447 (2009).

187. M. D. Gober, H. M. Bashir, J. T. Seykora, Reconstructing skin cancers using animal models. *Cancer Metastasis Rev* **32**, 123-128 (2013).
188. P. A. Khavari, Modelling cancer in human skin tissue. *Nat Rev Cancer* **6**, 270-280 (2006).
189. W. E. Pierceall, L. H. Goldberg, M. A. Tainsky, T. Mukhopadhyay, H. N. Ananthaswamy, Ras gene mutation and amplification in human nonmelanoma skin cancers. *Mol Carcinog* **4**, 196-202 (1991).
190. J. M. Spencer, S. M. Kahn, W. Jiang, V. A. DeLeo, I. B. Weinstein, Activated ras genes occur in human actinic keratoses, premalignant precursors to squamous cell carcinomas. *Arch Dermatol* **131**, 796-800 (1995).
191. D. L. Narayanan, R. N. Saladi, J. L. Fox, Ultraviolet radiation and skin cancer. *Int J Dermatol* **49**, 978-986 (2010).
192. R. Casagrande *et al.*, Protective effect of topical formulations containing quercetin against UVB-induced oxidative stress in hairless mice. *J Photochem Photobiol B* **84**, 21-27 (2006).
193. C. F. Hung, C. L. Fang, S. A. Al-Suwayeh, S. Y. Yang, J. Y. Fang, Evaluation of drug and sunscreen permeation via skin irradiated with UVA and UVB: comparisons of normal skin and chronologically aged skin. *J Dermatol Sci* **68**, 135-148 (2012).
194. A. R. Svobodova *et al.*, DNA damage after acute exposure of mice skin to physiological doses of UVB and UVA light. *Arch Dermatol Res* **304**, 407-412 (2012).
195. M. L. Kripke, Experimental ultraviolet carcinogenesis. *Recent Results Cancer Res* **128**, 269-274 (1993).
196. S. Kimeswenger *et al.*, Impact of infrared radiation on UVB-induced skin tumourigenesis in wild type C57BL/6 mice. *Photochem Photobiol Sci* **18**, 129-139 (2019).
197. Y. H. Kong, S. P. Xu, Salidroside prevents skin carcinogenesis induced by DMBA/TPA in a mouse model through suppression of inflammation and promotion of apoptosis. *Oncol Rep* **39**, 2513-2526 (2018).
198. E. L. Abel, J. M. Angel, K. Kiguchi, J. DiGiovanni, Multi-stage chemical carcinogenesis in mouse skin: fundamentals and applications. *Nat Protoc* **4**, 1350-1362 (2009).
199. M. Neagu *et al.*, Chemically induced skin carcinogenesis: Updates in experimental models (Review). *Oncol Rep* **35**, 2516-2528 (2016).
200. A. Y. Yang *et al.*, Genome-wide analysis of DNA methylation in UVB- and DMBA/TPA-induced mouse skin cancer models. *Life Sci* **113**, 45-54 (2014).